Nonlinear Behavior of Cylinder-Plate Junction of Tensionless Elastic Subgrade

by

Hassan Aly Hassan Waly

A Thesis Presented to the

FACULTY OF THE COLLEGE OF GRADUATE STUDIES

KING FAHD UNIVERSITY OF PETROLEUM & MINERALS

DHAHRAN, SAUDI ARABIA

In Partial Fulfillment of the
Requirements for the Degree of

MASTER OF SCIENCE

In

CIVIL ENGINEERING

January, 1992

Order Number 1354048

Nonlinear behavior of cylinder-plate junction on tensionless elastic subgrade

Waly, Hassan Aly Hassan, M.S.

King Fahd University of Petroleum and Minerals (Saudi Arabia), 1992

U·M·I
300 N. Zeeb Rd.
Ann Arbor, MI 48106

NONLINEAR BEHAVIOR OF CYLINDER-PLATE JUNCTION ON TENSIONLESS ELASTIC SUBGRADE

BY

HASSAN ALY HASSAN WALY

A Thesis Presented to the

FACULTY OF THE COLLEGE OF GRADUATE STUDIES

KING FAHD UNIVERSITY OF PETROLEUM & MINERALS

DHAHRAN, SAUDI ARABIA

In Partial Fulfillment of the
Requirements for the Degree of

MASTER OF SCIENCE

In

CIVIL ENGINEERING

JANUARY, 1992

KING FAHD UNIVERSITY OF PETROLEUM AND MINERALS
DHAHRAN, SAUDI ARABIA

COLLEGE OF GRADUATE STUDIES

This thesis, written by ***HASSAN ALY HASSAN WALY*** under the direction of his Thesis Advisor and approved by his Thesis Committee, has been presented to and accepted by the Dean of the College of Graduate Studies, in partial fulfillment of the requirements for the degree of

MASTER OF SCIENCE IN CIVIL ENGINEERING

THESIS COMMITEE

Dr. A. A. Khathlan (Chairman)

Dr. M. H. Baluch (Member)

Dr. A. A. Al-Musallam (Member)

Dr. G. J. Al-Sulaimani
Department Chairman

Dr. Ala A-Rabeh
Dean, College of Graduate Studies

22 - 2 - 1992.

Date

To My Beloved Parents, Brothers, Sister

and to Those Who Shared Their Care and Concern

ACKNOWLEDGEMENT

First of all, I thank " *ALLAH* " for giving me the health and patience to produce this work which I hope will be useful for mankind as *HE* and our Prophet *MOHAMMED, peace be upon him*, ordered us as muslims to work for the prosperity of mankind and to seek knowledge where ever it is.

Acknowledgement is due to *King Fahd University of Petroleum and Minerals* for giving me the opportunity to achieve this work through its tremendous facilities.

I would like to express my deep appreciation and sincere gratitude to my thesis advisor, *Dr. A. A. Al-Khathlan*, for his patience, guidance, his generous support and encouragement. I would also like to express my gratefulness to the other committee members, *Dr. M. H. Baluch*, and *Dr. A. A. Al-Musallam*, for their valuable suggestions, helpful remarks and their kind co-operation.

TABLE OF CONTENTS

Chapter 3

THE PLATE-SUBGRADE SYSTEM

Chapter 4

THE SOLUTION FOR A CIRCULAR CYLINDER

Chapter 5

SOLUTION FOR THE CYLINDER-PLATE JUNCTION

Chapter 6

NUMERICAL RESULTS

Chapter 7

SUMMARY AND CONCLUSIONS

APPENDICES

LIST OF FIGURES

ABSTRACT

Name : **Hassan Aly Hassan Waly**

Title : **NONLINEAR BEHAVIOR OF CYLINDER-PLATE JUNCTION ON TENSIONLESS ELASTIC SUBGRADE**

Major Field : **Civil Engineering**

Date : **January 1992**

The problem of a cylinder-plate junction resting on tensionless elastic subgrade and subjected to point load and point moment that act at the top edge of the cylinder is investigated. An energy minimization technique is utilized to analyze the plate-subgrade system. A displacement function for the plate is assumed in terms of generalized Bessel functions in the radial direction and Fourier series in the angular direction. The solution for a thin circular cylinder is obtained according to the equations derived by Flugge for this problem. The solution of the cylinder-plate junction is accomplished by achieving the continuity conditions at the cylinder-plate interface for the displacements and the edge forces. A computer program is developed to solve the problem iteratively, but efficiently, to predict the nonlinear behavior produced by the loss of contact between the plate and the unbonded subgrade. Numerical results will be presented to show the validity and accuracy of the utilized approach.

MASTER OF SCIENCE

KING FAHD UNIVERSITY OF PETROLEUM AND MINERALS
DHAHRAN, SAUDI ARABIA

January 1992

خلاصة الرسالة

اسم الطالب : حسن علي حسن والي .

عنوان الدراسة : السلوك غير الخطي لوصلة من بلاطة واسطوانة ، مرتكزة على تربة مرنه غير قابلة للشد .

التخصص : هندسة مدنية .

تاريخ الشهادة : يناير ١٩٩٢م .

في هذا البحث يتم دراسة مسألة الوصلة المكونة من بلاطة واسطوانة والمرتكزة على تربة مرنة غير قابلة للشد عند تعرضها لحمل رأسي وعزم حدي يعملان على الحد العلوي للاسطوانة .

يتم تحليل نظام البلاطة والتربة المرنة عن طريق استعمال الاسلوب التقني لتقليل الطاقة . تُفرض دالة الازاحة للبلاطة كطرف في دوال بزل في الاتجاه القطري ومتسلسلات فورير في الاتجاه الزاوي .

يُحضر حل الاسطوانة الدائرية الرفيعة طبقاً للمعادلات المشتقة بواسطة فلوجا والخاصة بهذه المسألة . أما الحل الكامل لمسألة الوصلة ، فيتم انجازه بتحقيق ظروف الاستمرارية عند سطح اتصال البلاطة مع الاسطوانةلكل من الازاحات والقوى الحديه.

ويتم عمل برنامج كمبيوتر لحل مسألة الوصلة تكرارياً ، وبأقل عدد ممكن من العمليات الحسابية ، لتقدير السلوك غير الخطي الناتج عن فقدان التماسك بين البلاطة والتربة في مناطق الشد .

سيتم عرض نتائج عددية لبيان مدى صحة ودقة التحليل المستخدم .

درجة الماجستير في العلوم الهندسية
جامعة الملك فهد للبترول والمعادن
الظهران ، المملكة العربية السعودية

يناير ١٩٩٢

Chapter 1

INTRODUCTION

1.1 General

The problem of plates resting on elastic subgrade is encountered in many civil engineering structures. They are frequently used as column footings, pile caps, footings of towers, circular tanks and many other types of structures. This problem is also encountered in the construction of concrete slabs for highways and airport runways.

To deal with the plate problem, an idealized model for the subgrade should be assumed. The subgrade may be modeled as a group of individual springs with a subgrade stiffness coefficient K, which is referred to as the Winkler model. Alternatively, it may be modeled as an elastic half space where the shear deformation of the subgrade is taken into consideration. Another model which utilizes a three-dimensional elastic space may also be assumed.

In general, plates on elastic subgrade may be divided into two categories, bonded and unbonded. The first implies that the plate and the subgrade always have the same upward and downward displacement. In the unbonded case, which is referred to as tensionless, the subgrade will deform with the plate when it moves downward but will separate from it when the plate moves upward. In other words, the subgrade does not

provide any tensile pressure to the plate. As a result, the plate will lose contact with the subgrade in certain parts. It is common knowledge that very weak subgrades usually produce full contact. However, as their stiffness increase, partial contact is likely to occur.

The behavior of a thin plate on tensionless or unbonded elastic subgrade is complicated by the fact that the shape and size of the contact region between the plate and the subgrade is not known in advance. The shape and size of the contact region depend on the plate size, the relative stiffness of the plate to that of the subgrade, and in certain cases on the load configuration that act on the plate.

It should be mentioned that when the plate is subjected to one type of loading, the shape and size of the contact zone will not depend on the level of the load. However, when it is subjected to a combination of loads, the shape and size of the contact zone will be affected greatly by the distribution and levels of the applied loads. In other words, the problem will become nonlinear, and the principle of superposition become inapplicable. As a result, a closed form solution for such a problem is very difficult, if not impossible, to obtain.

The problem of elastic stress analysis of shell intersections has recently become an active field of research. These intersections usually produce high stress concentration levels at the junction. These intersections could be between any two different types of shells. One of the most common types of the intersection problem is the cylinder- flat plate problem. It is known that a flat plate is a special case of a shell. In addition, the

governing differential equation of a plate on elastic subgrade is very similar to the equation for thin shells. Therefore, the problem of cylinder-shell intersection could be treated as a cylinder-plate intersection resting on elastic subgrade. This will significantly simplify the analysis of the shell intersection problem. However, when the subgrade is of the unbonded type, the stress distribution and the stress levels at the intersection will be greatly affected when the plate has partial contact with the subgrade.

1.2 Description of the problem

The proposed work is concerned with analyzing a structure that consists of a thin vertical circular cylinder attached to a thin annular circular plate resting on tensionless Winkler subgrade as shown in figure (1.1). The outer edge of the plate is assumed to be free. The cylinder may be subjected to a concentric vertical load P and a tipping moment M_o that act at the top edge of the cylinder, which is free to displace. Since the cylinder is rigidly connected to the plate, the applied loads are transmitted to the plate and then to the subgrade.

It is known that when the plate is bonded to the subgrade, the problem of the plate on elastic subgrade has a linear behavior. In the case of unbonded contact, the subgrade is unable to provide any tensile forces causing the plate to partially uplift (figure 1.2). This loss of contact between the plate and the subgrade redistributes the subgrade reaction under the plate. Consequently, a redistribution of the stress resultants at the junction will occur.

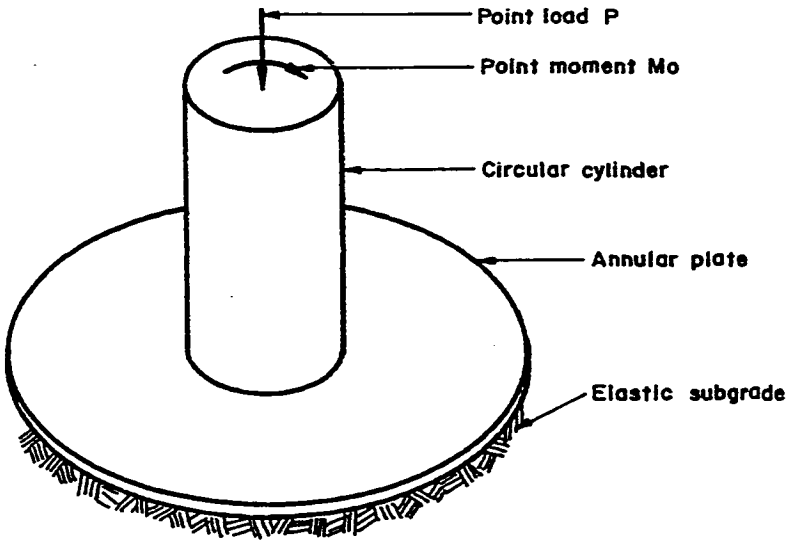

Figure 1.1: Cylinder-plate junction
resting on unbonded elastic subgrade

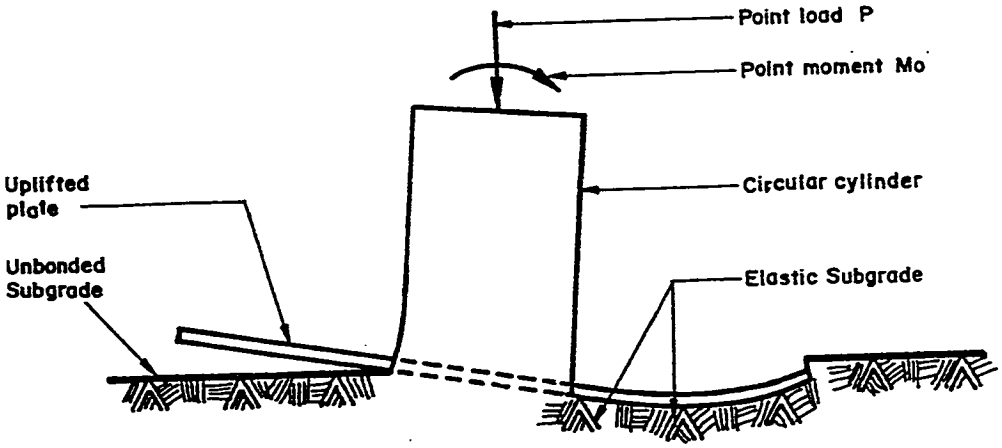

Figure 1.2.a: Partial uplift of the plate of a junction resting on unbonded elastic subgrade

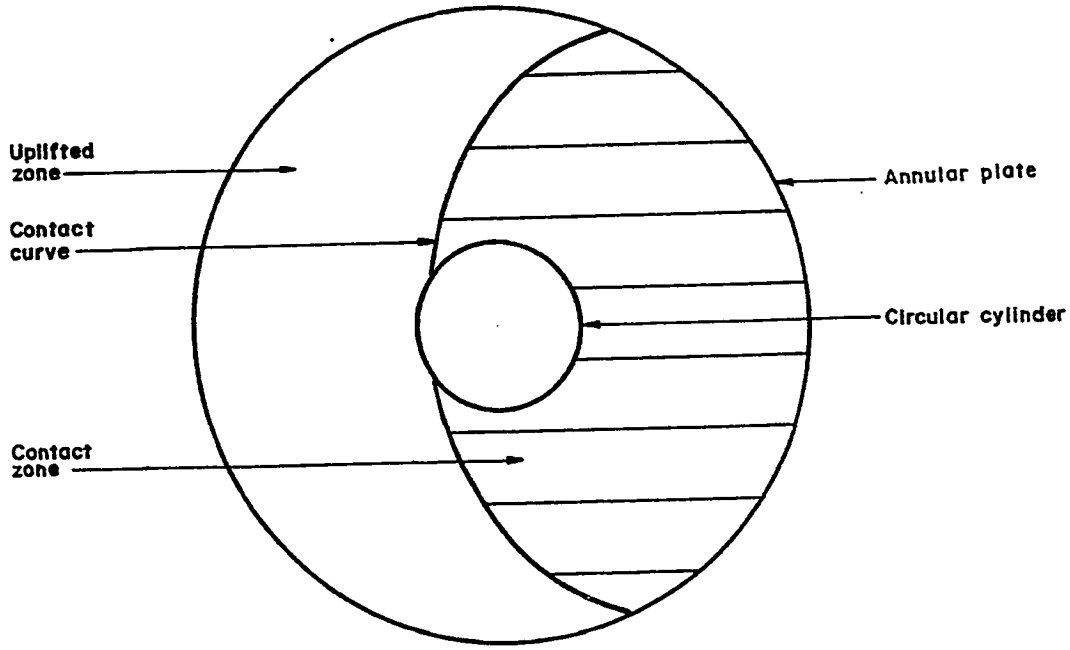

Figure 1.2.b: Top view of the contact zone of the plate with the elastic subgrade

1.3 Research objectives

The main objective of this research is to analyze a structure that consists of a thin circular cylinder attached to a thin circular annular flat plate resting on tensionless Winkler type of subgrade. The analysis will include the investigation of the contact region of the plate with the subgrade as well as the stress resultants at the plate- cylinder junction. A computer program will be developed to perform the analysis for the above mentioned structural system. The developed technique will make it possible to investigate the following problems:

1- The effect of the relative stiffness of the elastic subgrade reaction coefficient K to the bending stiffness, D, of the plate. Previous work has proved that the contact region is affected primarily by this relative stiffness.

2- The effect of the relative stiffness of the cylinder to the bending stiffness of the plate. It is expected that the radius to thickness ratio of the cylinder will play a significant role in the stress levels at the junction.

3- The effect of the ratio of the applied moment M_o to the applied force P. It is expected that due to the nonlinearity of the problem, this ratio will affect the behavior of the problem significantly.

The effect of these parameters will be investigated thoroughly in combination with each other. This investigation will undoubtedly result in better understanding of the behavior of the whole system.

1.4 Approach and methodology

To analyze the stated problem, an efficient and sufficiently accurate approach has to be derived. As mentioned earlier, a closed form solution for such a problem subjected to general loading conditions is very difficult to obtain. Therefore, a semi-analytical solution will be adopted. An energy minimization technique will be utilized to derive the mathematical solution of the plate-subgrade system. In addition, the solution of the cylinder will be based on Flugge's equations [20]. The nonlinear behavior of the problem will be dealt with through an iterative procedure. The complete solution for the problem will be performed as follows:

1- Derive a mathematical solution for an annular plate resting on tensionless elastic subgrade. A displacement function for the transverse deflection of the plate will be assumed in terms of generalized Bessel's functions [21,22] in the radial direction and harmonics in the angular direction. This assumed displacement function will be forced to satisfy the applied boundary conditions of the plate. The solution of the plate problem will be completed by minimizing the total potential energy of the plate-subgrade system.

2- Develop a solution for the circular cylinder. The analysis of the cylinder will be based on the set of equations derived by Flugge [20] for a semi-infinite circular cylinder subjected to edge loads only. A relationship analogous to the stiffness matrix equation will be derived for the lower edge of the cylinder for each harmonic. In addition, the membrane solution for the cylinder will be utilized to handle the external loads.

3- Through a general computer program combining the solution for the plate problem and the cylinder problem, the continuity between both structures will be achieved at the junction. Through continuity of the displacements at the junction, the edge forces could be prescribed in terms of the displacement function of the plate. This will modify the boundary conditions of the plate and as a result the energy equation. Since the contact region of the plate with the subgrade is not known apriori, an efficient iterative solution will be needed to treat this nonlinear behavior of the problem. This iterative solution will continue until convergence for the contact zone and the edge forces at the inner boundary are achieved. Throughout the analysis, force and moment equilibrium of the system will be checked out to monitor the accuracy of the solution.

1.5 Verification of the results

Upon the development of the previously mentioned approach, results will be checked and verified using available information about the behavior of similar problems. It should be pointed out that no solution is currently available for this specific problem. However, solutions have been obtained by others that cover segments of the problem or limiting cases of some of the main parameters. These available solutions will be used, whenever applicable, to confirm the validity and accuracy of the developed technique.

Chapter 2

LITERATURE REVIEW

2.1 Introduction

In the present chapter, the available literature on the subject of the plates on elastic subgrade will be reviewed. Studies investigating bonded and unbonded behavior will be presented separately. In addition, previous work on the stress analysis of plate-cylinder intersection problems will be reviewed.

2.2 Plates on bonded subgrade

In the earliest studies on the subject, only bonded subgrades were considered. Timoshenko and Woinowsky-Kreiger [1], developed a solution for an infinite circular solid plate subjected to a concentrated load at the center by assuming a Kelvin functions solution for the plate displacement. The solution was completed by considering vertical equilibrium of forces acting on a small circle at the origin.

Recently, Kastikadelis and Kallivokas [2], investigated the problem of clamped plates on Pasternak-type elastic subgrade using the boundary element method. The plate may have holes and may be subjected to concentrated loads, line loads and uniform loads. The analysis presented

deflections, stress resultants, subgrade reaction and support reactions at the boundary.

Bezine [3] investigated the problem of plates on elastic subgrade using the boundary element method. The bending of the plate was solved by using the original boundary integral equation method involving the fundamental solution for the plate flexure problem. The solution was assumed to be in the form of Kelvin function of the first order. By discretizing the integral equation, it was possible to eliminate the boundary unknowns.

Kastikadelis and Armenakas [4], investigated the problem of clamped plates on elastic Winkler subgrade by solving the boundary integral equation for plates of any shape. The plates may be subjected to general loading conditions.

2.3 Plates on unbonded subgrade

Recently, investigators started to pay more attention to the problem of the unbonded contact between plates and elastic subgrades. Most soil-structure contact problems actually fall in this category.

The earliest effort was by Weitsman [5] who investigated the contact problem between an infinite elastic plate and a semi-infinite elastic half-space. The plate was subjected to a concentric point load. Weitsman used the Fredholm integral equation to solve this contact problem and to obtain an approximate solution for the radius of contact. His results were verified by Keer et al. [6], who investigated the contact problem between a layer and an elastic half-space. The layer, which models the plate, was

subjected to an axisymmetric type of loading. The Fredholm integral equation has been used to treat this problem. The integral equation was proved to be a homogeneous equation which made it possible to write the contact radius as an eigenvalue problem. The integral equation was then solved numerically to the desired degree of accuracy.

Another paper by Weitsman [7], included an investigation of the contact problem between infinite plates on elastic subgrade modeled as either elastic half space or as Winkler type. The effect of a concentric point load with or without uniform pressure was investigated. An analytical solution for the differential equation that governs the problem was introduced. In addition, he investigated the same problem for an infinite beam subjected to the same loads and used the same technique for the solution.

Gladwell and Iyer [8] solved the unbonded contact problem between a circular plate and and an elastic half-space. The plate is pressed by means of rotationally symmetric distributed loads and its own weight. A Hankel transform solution was used for the half-space and the plate deflection was determined by inverting the plate equation. The coefficients expanded in a power series form were obtained by equating the deflection of the plate and the half-space at a number of points in the contact region.

Villagio [9], solved the boundary value problem for a rectangular plate on tensionless Winkler subgrade. The plate was free at the boundary and was subjected to a concentric point load. An explicit form for the contact region was assumed. The differential equation for the contact region was solved using Kelvin functions in the radial direction and Fourier series in the tangential direction. He expressed the outer boundary conditions in

Fourier series form and solved the differential equation of the uplifted part using the classical solution for bending of plates. By satisfying the boundary conditions and continuity between the two parts along the contact curve, the solution was obtained for that problem.

Another solution using a combination of Navier-type and Levy-type solutions was obtained by Li and Dempesy [9]. The plate was subjected to centrally symmetric vertical loading. The problem was transformed into the solution of two coupled integral series equations over an unknown contact region. Special attention was given to the singular behavior at the corners.

Ascione and grimaldi [10] investigated the unbonded contact between a solid plate and an elastic subgrade. They used a variational approach which was considered to be the most convenient approach to obtain an approximate solution. The plate was subjected to vertical pressure that act on part of the plate. A displacement function in the form of power series was assumed to represent the deflected shape of the plate.

Selvadorai [11] solved the contact problem of a Reissner plate and an isotropic elastic half-space. The plate may be subjected to axisymmetric uniform loads that act on a finite area at the center of the plate. He used a power series function to represent the deflected shape for the plate. He accomplished the solution by minimizing the total potential energy of the system.

Another solution using a combination of Navier-type and Levy-type solutions was obtained by Li and Dempesy [12]. The plate was subjected to centrally symmetric vertical loading. The problem was transformed into

the solution of two coupled integral series equations over an unknown contact region. Special attention was given to the singular behavior at the corners.

It should be pointed out that all the previously mentioned work considered axisymmetric loading conditions only. This made it possible to assume an explicit form for the contact region. However, the problem of solid plates resting on tensionless elastic subgrade and subjected to eccentric point loads was not investigated, although it is a very common problem.

One of the very few attempts to solve the nonaxisymetric problem was by Celep [13]. He used an energy approach to solve the nonaxisymmetric contact problem of a circular solid plate on tensionless Winkler subgrade, where the plate was subjected to an eccentric point load and a moment in addition to uniform pressure. The displacement function was assumed in terms of Bessel functions in radial direction and Fourier cosine series in the angular direction. These functions were selected since they represent the free vibration modes of a free plate. The study investigated the effect of the relative stiffness of the plate to the subgrade and also the load configuration on the shape and size of the contact region.

Using the Galerkin method, Celep [14] also solved the contact problem of a rectangular plate that rest on tensionless elastic subgrade. The plate was subjected to an eccentric point load and a moment in each of the cartesian coordinate directions. The displacement function for the plate was assumed in terms of the eigen-functions for the free vibration of a free

beam in each direction of the cartesian coordinates.

Also Celep et al [15] solved the problem of a circular plate that rest on tensionless unilateral support at the outer boundary. The plate was subjected to a uniform line load that acts on an arc of a circle. The solution of the problem was achieved by matching the classical solution of bending of plates for both the inner solid plate and the outer annular plate. In addition, Celep [16] solved the contact problem for the axisymmetric vibration of a circular plate on tensionless elastic subgrade. The plate was subjected to a concentric point load which was a function of time. The problem was solved using Galerkin's method by assuming a displacement function for the plate in terms of Bessel functions.

2.4 Cylinder-plate intersection problems

The problem of stress analysis of plate- cylinder intersections has been widely investigated. The evaluation of the stress concentration at the junction was the main goal of these studies.

For the problem of a nozzle attached to a flat plate, Hulbert, et al. [17] investigated the problem of plates with single or clustered nozzles using the boundary point least squares method where the nozzle was subjected to edge loads at the top. The stresses in the nozzle and transverse bending deformations in the plate were investigated.

Campen [18] investigated the stress distribution in an arbitrarily loaded nozzle-to-flat plate connection. A finite element method was developed to solve this problem including both mechanical and thermal effects. The

general solution for the displacement functions for the plate and the cylinder were assumed to be in series form. The proposed method was used for determining the peak stresses at the intersection for relatively small ratios of the inner radius to the outer radius of the plate.

In addition, Redekop [19] investigated the three- dimensional behavior of a hollow circular cylinder normally intersecting with a flat plate. The geometry of the intersection was divided into three segments, the cylinder, the plate and a circular ring connecting them. Boundary conditions between the ring and the plate and the cylinder were satisfied using the numerical boundary least squares method while all the other boundary conditions were satisfied exactly using the governing elasticity equations.

2.5 Current status of the research

The literature review indicates that the bonded behavior of plates on elastic subgrade has been investigated thoroughly for general loading and boundary conditions. However, almost all of the studies of the unbonded behavior have been confined to the axisymmetric behavior. In addition, the importance of the cylinder-plate problem was emphasized. Therefore, it is very clear that there is a need for an investigation of the nonaxisymmetric behavior of unbonded plate-cylinder structures. Such an investigation will fill an existing void in the knowledge in that field.

Chapter 3

THE PLATE-SUBGRADE SYSTEM

3.1 Introduction

In this chapter the theoretical formulation for the solution of an annular plate resting on tensionless elastic subgrade will be presented. The plate may be subjected to a general state of transverse loading at the inner edge. These forces include distributions of shear force and radial bending moment expanded in terms of Fourier cosine series. The outer edge is to remain free from loads. Since the subgrade can react in compression only, a possible lift-off region is expected in certain cases. To analyze the problem, a displacement function in terms of general Bessel functions in the radial direction, and Fourier cosine series in the angular direction will be assumed. The solution of the plate-subgrade system will be accomplished by minimizing the total potential energy stored in the system of the plate and the subgrade.

3.2 Theoretical assumptions

The following assumptions will be made during the analysis of the described plate-subgrade system.

1- All materials are linear, elastic, homogeneous and isotropic for the plate and the subgrade.

2- The Kirchhoff hypothesis for small bending deformations, for thin

plates, or so-called classical theory for thin plates [1,23], will be adopted to analyze the plate.

3- The ratio of the inner radius to the outer radius of the plate does not exceed 0.3.

4- Regarding the subgrade itself, the smooth tensionless Winkler model will be considered where the subgrade reaction at a certain point is proportional to the deflection at that point in the compression zone only.

3.3 Description of the plate-subgrade system

3.3.1 Geometry and externally applied loads

The plate system consists of an annular plate which has an inner radius r_i, and outer radius r_o, as shown in figure (3.1). The plate has a bending stiffness $D_p = \frac{E t_p^3}{12(1-\nu^2)}$, where E, t_p, ν are the plate's modulus of elasticity, thickness, and Poisson's ratio, respectively. The plate rests on elastic subgrade with modulus of subgrade reaction K. The subgrade is assumed to be of the unbonded type. It should be noted that the bonded type subgrade is a special case of the unbonded problem, and consequently could be treated easily with the approach developed in this thesis.

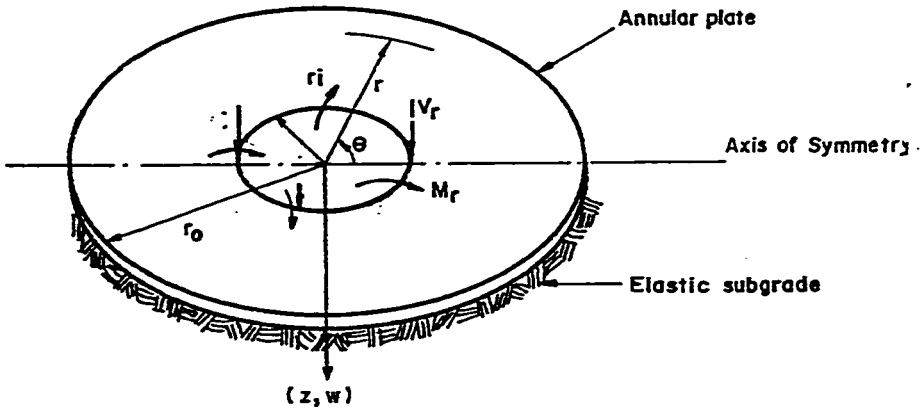

Figure 3.1: Coordinate system for an annular plate

The polar coordinates system of the plate r, 0, and z is shown in figure (3.1). The direction of the displacement function of the plate $W(r,\theta)$, is taken to be positive downward. The plate will be loaded transversely at its inner radius. These loads are general distributions of shearing forces V_r and radial bending moment M_r expressed in terms of Fourier cosine series.

3.3.2 Plate element

Using a differential plate bending element in polar coordinates, figure (3.2), the stress resultants acting on that element can be shown. These stress resultants can be expressed in terms of the displacement function of the plate $W(r,\theta)$. For example, two bending moments and one twisting moment act on the surfaces of the given element and have the following expressions

$$M_r = -D_p[\frac{\partial^2 W}{\partial r^2} + \nu(\frac{1}{r}\frac{\partial W}{\partial r} + \frac{1}{r^2}\frac{\partial^2 W}{\partial \theta^2})] \tag{3.1}$$

$$M_\theta = -D_p[\frac{1}{r}\frac{\partial W}{\partial r} + \frac{1}{r^2}\frac{\partial^2 W}{\partial \theta^2} + \nu\frac{\partial^2 W}{\partial r^2}] \tag{3.2}$$

$$M_{r\theta} = -(1-\nu)\, D_p(\frac{1}{r}\frac{\partial^2 W}{\partial r \partial \theta} - \frac{1}{r^2}\frac{\partial W}{\partial \theta}) \tag{3.3}$$

where M_r, M_θ, $M_{r\theta}$ are the radial, tangential and twisting moments. Similarly, two shear quantities act on the element which are

$$Q_r = -D_p\frac{\partial}{\partial r}(\Delta W) \tag{3.4}$$

$$Q_\theta = -D_p\frac{1}{r}\frac{\partial}{\partial \theta}(\Delta W) \tag{3.5}$$

where Q_r, Q_θ are the radial and the tangential shear. The Laplacian

operator Δ is defined as follows

$$\Delta = \frac{\partial^2}{\partial r^2} + \frac{1}{r}\frac{\partial}{\partial r} + \frac{1}{r^2}\frac{\partial^2}{\partial \theta^2} \tag{3.6}$$

To represent the boundary conditions of the plate, the Kirchhoff shear is needed and defined as

$$V_r = -D_p[\frac{\partial}{\partial r}(\Delta W) + \frac{1-\nu}{r}\frac{\partial}{\partial \theta}(\frac{1}{r}\frac{\partial^2 W}{\partial r \partial \theta} - \frac{1}{r^2}\frac{\partial W}{\partial \theta})] \tag{3.7}$$

3.4 Plate problem formulation

3.4.1 Governing differential equation

When the plate is in partial contact with the subgrade, its domain can be divided into two zones, the contact zone I and the uplifted zone II as shown in figure (3.3). The governing differential equation for zone I is

$$D_p \Delta \Delta W(r,\theta) + K W(r,\theta) = 0 \tag{3.8}$$

In addition, the differential equation for zone II will be

$$D_p \Delta \Delta W(r,\theta) = 0 \tag{3.9}$$

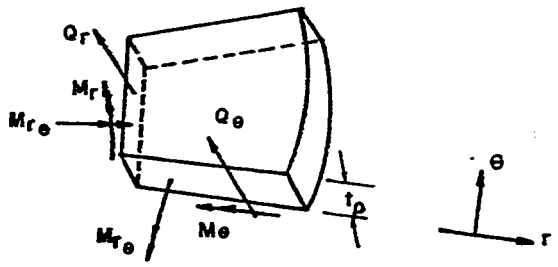

Figure 3.2: Plate bending element

Independently, equations (3.8) and (3.9) can be solved analytically in the form of Bessel functions solution and the classical solution for a plate bending problem, respectively. These solutions can be used to obtain an exact solution for an axisymmetric plate problem where the contact curve has an explicit form as a circle. However, for the general state of loadings, an explicit form for the contact zone can not be obtained, which means that it is not possible to obtain a closed-form solution. Therefore, for general loading conditions, the governing differential equation for the plate-subgrade system will be as follows

$$D_p \Delta \Delta W(r,\theta) + \Omega(W) K W(r,\theta) = 0 \tag{3.10}$$

where $\Omega(W)$ is the contact function and defined as

$$\Omega(W) = \begin{cases} 1 & \text{for } \textit{the contact zone } (W > 0) \\ 0 & \text{for } \textit{the uplifted zone } (W \leq 0) \end{cases} \tag{3.11}$$

Equation (3.10) is nonlinear, so it can not be solved in closed form. Thus an approximate technique is needed for the solution. The Ritz method is one of the most suitable alternatives and will be adopted to solve the plate-subgrade system by assuming a suitable displacement function for the plate.

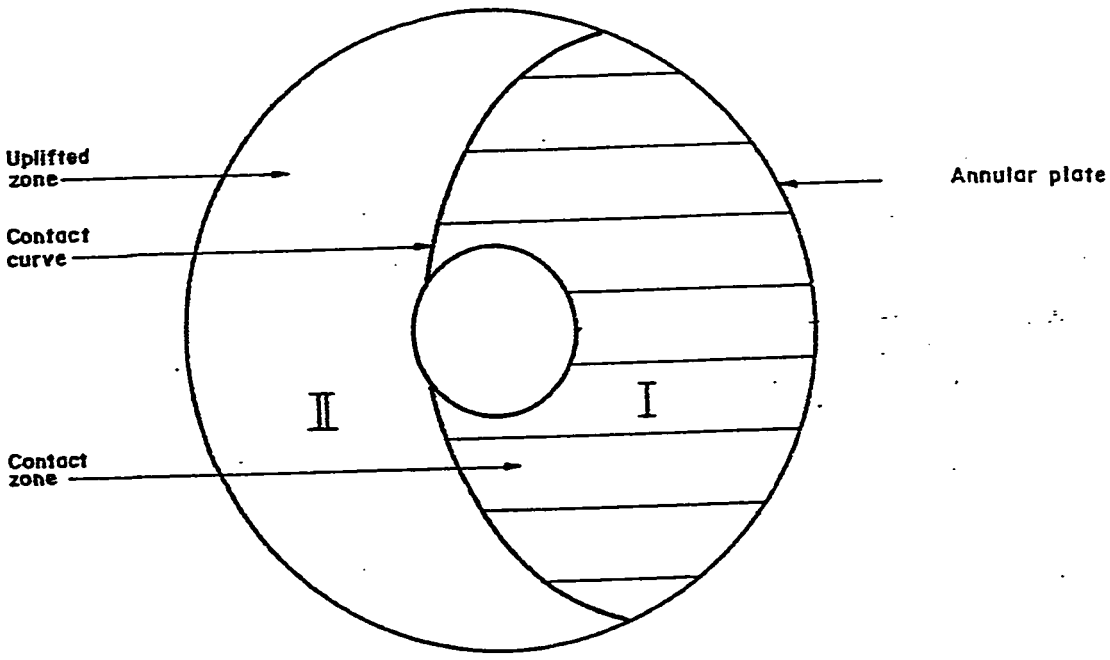

Figure 3.3: Contact and uplifted zones for an annular plate on unbonded subgrade

3.4.2 Displacement function

A displacement function that models the deflected shape of the plate under any general state of loading is assumed to be of the following form in the polar coordinates

$$W(r,\theta) = E^*_0 + E^*_1 r\cos\theta + \sum_{n=0}^{\infty} E_n w_n(r)\cos n\theta \qquad (3.12)$$

where E^*_0, E^*_1 are constants used to model the rigid translation and rigid rotation of the plate, respectively. In addition, E_n represent a group of constants corresponding to the different harmonics in the Fourier series. The radial displacement function $w_n(r)$ will be defined as

$$w_n(r) = A_n ber_n(\lambda_n r) + B_n bei_n(\lambda_n r) + C_n \ker_n(\lambda_n r) + kei_n(\lambda_n r) \quad (3.13)$$

where A_n, B_n, C_n, are constants, and λ_n is the eigen-value of the boundary value problem and the four quantities need to be evaluated according to the prescribed boundary conditions for each harmonic. The functions ber_n, bei_n, $\ker_n$, kei_n are the Kelvin functions of the first and second kinds, respectively, as defined in Appendix A.

3.4.3 Boundary conditions formulations

As indicated in the previous section, there are four unknowns that define the shape function for each harmonic, A_n, B_n, C_n, and λ_n. Therefore, four boundary conditions for the plate are needed.

At the inner edge, the plate will be subjected to general distributions of the radial shear and radial bending moment expressed in Fourier series as follows

$$M_r = \sum_{n=0}^{\infty} M_n \cos n\theta \tag{3.14}$$

$$V_r = \sum_{n=0}^{\infty} V_n \cos n\theta \tag{3.15}$$

At the outer edge, which is to remain stress-free, the two boundary conditions are

$$M_r = 0 \tag{3.16}$$

$$V_r = 0 \tag{3.17}$$

The four boundary conditions can be rewritten in terms of the displacement function $w_n(r)$ by substituting equations (3.1) and (3.7) into equations (3.14)-(3.17). This will result in

$$\frac{d}{dr}\left(\frac{d^2 w_n}{dr^2} + \frac{1}{r}\frac{dw_n}{dr} - n^2\frac{w_n}{r^2}\right) - \frac{(1-\nu)}{r_i} n^2 \left(\frac{dw_n}{dr} - \frac{w_n}{r_i}\right) = \frac{-V_n}{D_p E_n} \tag{3.18}$$

$$\frac{d^2 w_n}{dr^2} + \nu\left(\frac{1}{r_i}\frac{dw_n}{dr} - n^2\frac{w_n}{r_i^2}\right) = \frac{-M_n}{D_p E_n} \tag{3.19}$$

$$\frac{d}{dr}\left(\frac{d^2 w_n}{dr^2} + \frac{1}{r}\frac{dw_n}{dr} - n^2\frac{w_n}{r^2}\right) - \frac{(1-\nu)}{r_0} n^2 \left(\frac{dw_n}{dr} - \frac{w_n}{r_0}\right) = 0 \tag{3.20}$$

$$\frac{d^2 w_n}{dr^2} + \nu\left(\frac{1}{r_0}\frac{dw_n}{dr} - n^2\frac{w_n}{r_0^2}\right) = 0 \tag{3.21}$$

By introducing equation (3.13) into equations (3.18)-(3.21) and arranging the resulting equations in a matrix form, one can obtain

$$\begin{bmatrix} & B(\lambda_n) & \end{bmatrix} \begin{Bmatrix} A_n \\ B_n \\ C_n \\ 1 \end{Bmatrix} = \begin{Bmatrix} V^b_n \\ M^b_n \\ 0 \\ 0 \end{Bmatrix} \tag{3.22}$$

where

$$V^b_n = \frac{-V_n}{D_p E_n} \tag{3.23}$$

$$M^b_n = \frac{-M_n}{D_p E_n} \tag{3.24}$$

Equation (3.22) can be written in a compact form as follows

$$[B]\{T\} = \{l\} \tag{3.25}$$

where $[B]$ is a matrix that depends on λ_n, $\{T\}$ is a vector including the unknown constants A_n, B_n, C_n and $\{l\}$ is a vector containing the values of the externally applied loads at the boundaries. The elements of the matrix $[B]$ are defined in Appendix B. By examining equations (3.22) and (3.25), one may observe that the system of equations can be solved directly to determine the four unknowns λ_n, A_n, B_n, C_n. However, in the case that both V^b_n and M^b_n are equal to zero, i.e. when there are no applied edge loads for that specific harmonic, equation (3.25) becomes homogenous. As a result, matrix $[B]$ becomes singular, and the value of λ_n ought to be determined by setting the determinant of $[B]$ to zero.

By examining the assumed displacement function, equation (3.13), which includes Kelvin functions, it can be seen that it is impossible to determine a root λ_n which will make the determinant of $[B]$ equal to zero.

As a result, an alternative displacement function is needed to handle the special case of a homogenous set of equations. The new function is

$$w_n(r) = A_n J_n(\lambda_n r) + B_n I_n(\lambda_n r) + C_n K_n(\lambda_n r) + Y_n(\lambda_n r) \qquad (3.26)$$

This new function replaces the Kelvin functions by ordinary Bessel function of the first and second kinds and they are defined in Appendix A. The new function proved to be useful in the analysis and produced the needed values for the root and the constants. The reason behind that is the fact that the Bessel functions used in equation (3.26) represent the free vibration modes for an annular plate, which is not the case for Kelvin functions used in equation (3.13).

So to summarize, the deflected shape corresponding to each harmonic can be assumed in one of the two forms expressed in equations (3.13) or (3.26). Depending on whether there are externally applied loads for that harmonic or not, either one of the two equations will be utilized.

3.4.4 The Ritz method

The Ritz method is one of the most popular techniques for obtaining solutions of complicated problems. This method will be used to obtain an approximate solution for the plate-subgrade system. By minimizing the total potential energy stored in the system, it is possible to obtain a system of linear algebraic equations which could be solved iteratively to obtain the unknown constants of the displacement function, E_n.

The total potential energy of the system is

$$\Pi^{*} = U_p + U_s - W_p \tag{3.27}$$

where U_p, U_s, W_p are the strain energy of the plate, the strain energy of the subgrade, and the work done by the applied loads, respectively.

The strain energy equation of the plate in polar coordinates is [1, 23]

$$U_p = \frac{1}{2} D_p \int_0^{2\pi} \int_{r_i}^{r_o} \Big[(\Delta W)^2 - 2(1-\nu) \frac{\partial^2 W}{\partial r^2} \left(\frac{1}{r} \frac{\partial W}{\partial r} + \frac{1}{r^2} \frac{\partial^2 W}{\partial \theta^2} \right) + 2(1-\nu) \left(\frac{1}{r} \frac{\partial^2 W}{\partial r \partial \theta} - \frac{1}{r^2} \frac{\partial W}{\partial \theta} \right)^2 \Big] r \, dr \, d\theta \tag{3.28}$$

On the other hand, the strain energy stored in the elastic subgrade is

$$U_s = \frac{1}{2} \int_0^{2\pi} \int_{r_i}^{r_o} \Omega(W) \, K \, W^2 \, r \, dr \, d\theta \tag{3.29}$$

In addition, the work done by the external loads can be expressed as follows

$$W_p = -\int_0^{2\pi} \sum V_n \cos n\theta \, W \, r_i \, d\theta + \int_0^{2\pi} \sum M_n \cos n\theta \, \frac{\partial W}{\partial r} \, r_i \, d\theta \tag{3.30}$$

Using equation (3.12) into equations (3.28)-(3.30) and substituting the results into equation (3.27), the total potential energy of the system can be expressed as follows

$$\begin{aligned} \Pi^{*} = \frac{1}{2} D_p \int_{r_i}^{r_o} \sum \Big[& E^2{}_n a_n \left(w_n'' + \frac{1}{r} w_n - n^2 w_n \right)^2 \\ & - 2(1-\nu) E^2{}_n a_n \left\{ w_n'' \left(\frac{1}{r} w_n' - \frac{n^2}{r^2} w_n \right) \right\} \\ & + 2(1-\nu) E^2{}_n a_n^{*} \left(\frac{-n}{r} w_n' + \frac{n}{r^2} w_n \right)^2 \Big] r \, dr \\ & + K \int_0^{\pi} \int_{r_i}^{r_o} \Omega \left(E_0^{*} + E_1^{*} r \cos\theta + E_n w_n \cos n\theta \right) \times \end{aligned}$$

$$(E_o^* + E_1^* r\cos\theta + E_m w_m \cos m\theta)\, r\, dr\, d\theta$$

$$+ \{V_o(E_o^* + E_o w_o) + V_1 (E_1^* + E_1 r_i) + \sum_2^\infty V_n E_n w_n\}\, r_i a_n$$

$$- \{M_o E_o w_o' + M_1(E_1^* + E_1 w_1')$$

$$+ \sum_2^\infty M_n E_n w_n'\}\, r_i a_n \qquad (3.31)$$

where

$$\int_0^{2\pi} \cos n\theta \cos m\theta\, d\theta = \begin{cases} 2\pi, & n=m=0 \\ 0, & m\neq n \\ \pi, & m=n \end{cases}$$

$$\int_0^{2\pi} \sin n\theta \sin m\theta\, d\theta = \begin{cases} 0, & n=m=0 \\ 0, & m\neq n \\ \pi, & m=n \end{cases}$$

$$a_o = 2\pi,\ a_n = \pi,\ n\geq 1 \qquad (3.32)$$

$$a_o^* = 0,\ a_n^* = \pi,\ n\geq 1 \qquad (3.33)$$

According to Ritz method, in order to minimize the total potential energy Π^*, the derivatives of Π^* with respect to the unknown constants E^*_0, E^*_1, E_n have to be equal to zero as $\frac{\partial \Pi^*}{\partial E_0^*}=0$, $\frac{\partial \Pi^*}{\partial E_1^*}=0$, $\frac{\partial \Pi^*}{\partial E_n}=0$, for $n=0, 1, 2,\ldots,\infty$.

Differentiating equation (3.31) with respect to the rigid displacement terms yield

$$2K \int_0^\pi \int_{r_i}^{r_o} \Omega\, (E_o^* + E_1^* r\cos\theta + E_n w_n \cos n\theta)\ r\, dr\, d\theta$$

$$+ V_o (2\pi r_i) = 0 \qquad (3.34)$$

$$2K\int_0^{\pi}\int_{r_i}^{r_o}\Omega\,(E_o^{*}+E_1^{*}\,r\cos\theta+E_n\,w_n\cos n\theta)\,r^2\cos 0\,d0$$

$$+(V_1\,r_i^2-M_1\,r_i)\,\pi=0 \qquad (3.35)$$

Then setting the derivatives of equation (3.31) with respect to the remaining constants E_n ($n\geq 0$) to zero, one obtains

$$D_p\int_{r_i}^{r_o}\sum[E_n a_n(w_n''+\frac{1}{r}w_n-n^2w_n)^2$$

$$-2(1-\nu)\,E_n\,a_n\,\{w_n''(\frac{1}{r}w_n'-\frac{n^2}{r^2}w_n)\}$$

$$+2(1-\nu)\,E_n\,a_n^{*}(\frac{-n}{r}w_n'+\frac{n}{r^2}w_n)^2]\,r\,dr$$

$$+2K\int_0^{\pi}\int_{r_i}^{r_o}\Omega\,(E_o^{*}+E_1^{*}\,r\cos 0+E_m\,w_n\cos m0)\,w_n\cos n0\;\;r\,dr\,d0$$

$$+\{V_o\,w_o+V_1\,r_i+\sum V_n\,w_n\}\,r_i a_n$$

$$-\{M_o\,w_o'+M_1\,w_1'+\sum M_n\;w_n'\}\,r_i\,a_n=0 \qquad (3.36)$$

3.4.5 Matrix formulation of the energy equation

By writing equations (3.34), (3.35), and (3.36) for each harmonic and arranging them in matrix form, one obtains

$$[G]\{E\}=\{L\} \qquad (3.37)$$

where $[G]$, $\{E\}$, and $\{L\}$ represent the energy matrix, the vector of the unknown constants, and the load vector, respectively.

It should be pointed out that the energy matrix $[G]$ is a symmetric matrix . The elements inside the matrix $[G]$, can be evaluated by carrying out the necessary integrations over the domain of the plate. Since the rigid

displacement constants, (i.e. E^*_0 and E^*_1) are separated from the other constants, the first two rows and columns of $[G]$, will be defined separately. The elements in the first row are

$$G(1,1) = 2K\int_0^{\pi}\int_{r_i}^{r_o}\Omega\, r\, dr\, d\theta \tag{3.38}$$

$$G(1,2) = 2K\int_0^{\pi}\int_{r_i}^{r_o}\Omega\, r^2\cos\theta\, dr\, d\theta \tag{3.39}$$

$$G(1,m+3) = 2K\int_0^{\pi}\int_{r_i}^{r_o}\Omega\, w_m \cos m\theta\, r\, dr\, d\theta, \qquad m\geq 0 \tag{3.40}$$

Similarly, the elements in the second row can be determined as follows

$$G(2,2) = 2K\int_0^{\pi}\int_{r_i}^{r_o}\Omega\, r^3\cos^2\theta\, dr\, d\theta \tag{3.41}$$

$$G(2,m+3) = 2K\int_0^{\pi}\int_{r_i}^{r_o}\Omega\, w_m \cos m\theta\, r^2\cos\theta\, dr\, d\theta, \quad m\geq 0 \tag{3.42}$$

Other elements will be classified as diagonal and off- diagonal elements to simplify the presented equations.

The diagonal elements are determined using

$$\begin{aligned} G(n+3,n+3) = D_p\int_{r_i}^{r_o}[a_n(w_n'' + \frac{1}{r}w_n - n^2 w_n)^2 \\ - 2(1-\nu)\, a_n\{w_n''(\frac{1}{r}w_n' - \frac{n^2}{r^2}w_n)\} \\ + 2(1-\nu)\, a_n^*(\frac{-n}{r}w_n' + \frac{n}{r^2}w_n)^2\, r\, dr \\ + 2K\int_0^{\pi}\int_{r_i}^{r_0}\Omega\,(w_n\cos n\theta)^2\, r\, dr\, d\theta, \qquad n\geq 0 \end{aligned} \tag{3.43}$$

On the other hand, the off- diagonal elements could be evaluated as follows

$$G(n+3,m+3) = 2K\int_0^{\pi}\int_{r_i}^{r_0} \Omega\, w_n \cos n\theta\; w_m \cos m\theta\; r\, dr\, d\theta\,,$$

$$n \neq m,\ m \geq 0 \qquad (3.44)$$

It should be pointed out that the off-diagonal terms indicate the coupling between the different harmonics. By examining equation (3.44), it is clear that if the contact function Ω does not depend on θ, the off-diagonal terms will vanish, indicating no coupling between the harmonics. The vector { E } in equation (3.37) which includes the unknown constants, could be defined as follows

$$\{E\}^T = \{E^*_0, E^*_1, E_0, \ldots\ldots, E_n\} \qquad (3.45)$$

In addition, the elements of the force vector { L } could be determined as follows

$$L(1) = -2\pi r_i V_0 \qquad (3.46)$$

$$L(2) = -\pi r_i^2 V_1 + \pi r_i M_1 \qquad (3.47)$$

$$L(n+3) = a_n(-V_n w_n + M_n w_n'), \qquad n \geq 0 \qquad (3.48)$$

It should be noted that the iterative solution and the assumption of the contact function Ω will transform the nonlinear behavior of the problem into a set of linear algebraic equations (3.37). Every iteration will lead to an improvement in the contact zone and thus the solution will converge.

3.5 Solution procedure

The solution of the plate-subgrade system will be completed by developing a computer program based on the derived energy approach.

Through the numerical part of the solution, it will be needed to calculate the values of the Kelvin and ordinary Bessel functions as well as their derivatives. These functions will be assumed in power series forms. In addition, derivatives will be evaluated according to the governing recurrence formulas for each function [21], (Appendix A). Also, as indicated in section 3.4.4, the computation of the $[G]$ matrix requires a significant amount of integration. All these integrations will be performed numerically using the Gauss-Legendre repeated quadrature in the polar coordinates [21,24].

The following steps illustrate the solution procedure of the system as follows

1- Specify control data such as the plate dimensions, the bending stiffness of the plate, the stiffness of the subgrade and the prescribed boundary conditions at the inner edge of the plate.
2- The solution starts by assuming full contact between the plate and the subgrade or in other words, the contact function Ω will be equal to 1 in all of the plate domain. By satisfying the boundary conditions of the plate, the constants A_n, B_n, C_n and the root λ_n will be determined for each harmonic.
3- Calculating the elements inside the matrix $[G]$ in addition to the load vector $\{L\}$. Hence, solving equation (3.37) yields the unknown constant

vector {E}.

4- Calculate the displacements at Gauss points and hence determine the revised values of the contact function Ω at these points.

5- By revising the solution, new constants A_n, B_n, C_n are obtained in addition to the root λ_n, for each harmonic of the applied loads.

6- Re-solving the energy equation (3.37) produces new unknown constants vector {E}, which produces a refined solution.

7- The solution will be revised and will continue until the fulfillment of the convergence criterion. The solution will be checked in each iteration for the stabilization of the contact zone in addition to monitoring the equilibrium of the total vertical forces and the moments that act on the plate.

8- When the convergence criterion is satisfied, the deflection and the contact curve for the plate will be obtained. In addition, the stress resultants and stresses anywhere in the plate may then be determined.

The solution procedure is summarize in a flow chart in figure (3.4).

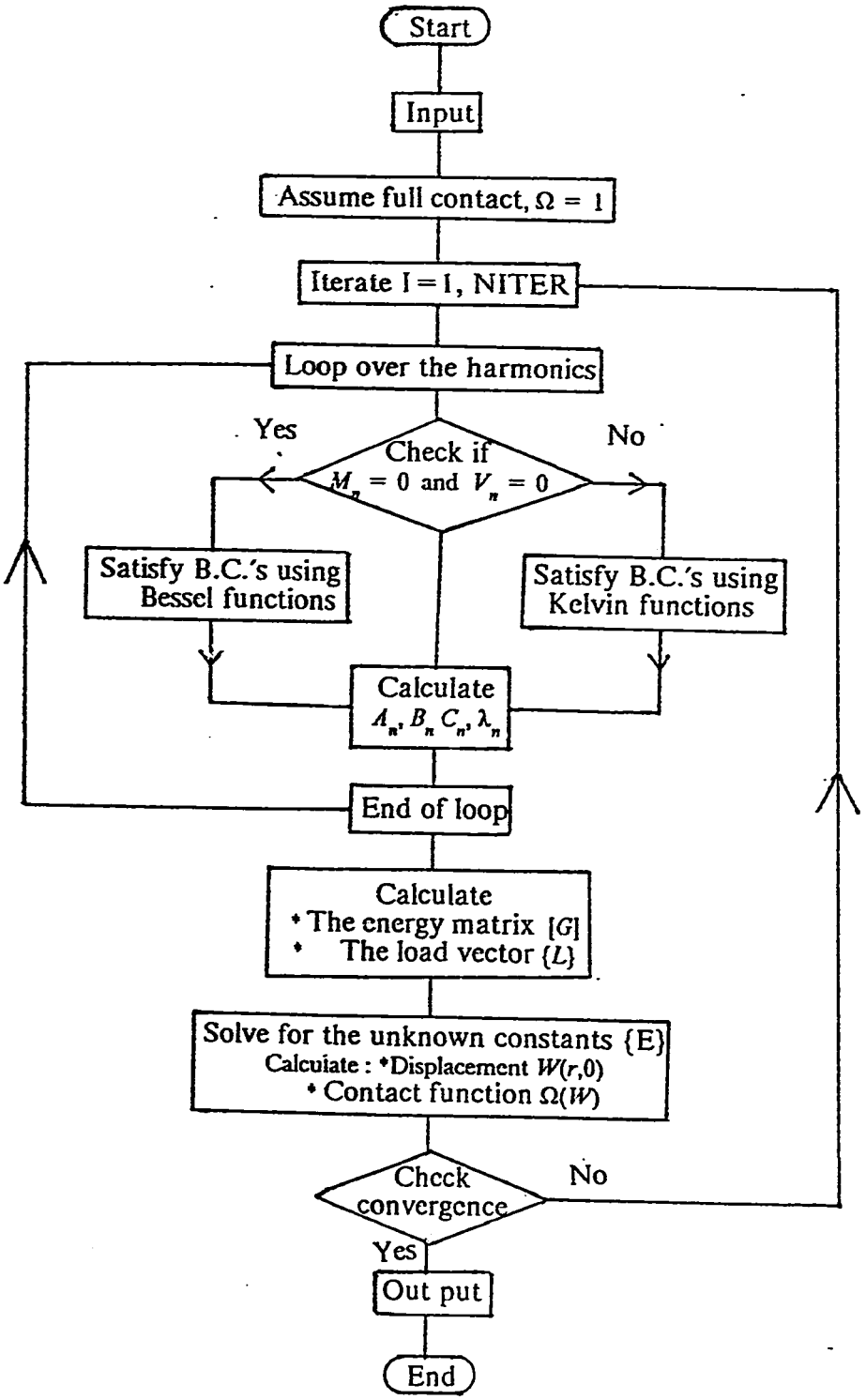

Figure (3.4) Scheme of the solution for the plate problem

3.6 Plate equilibrium

To monitor the convergence of the solution and to verify the final answer, force and moment equilibrium need to be checked at every iteration. It should be noted that the harmonics corresponding to n=0 and n=1 will be used to represent the applied concentrated load P and the tipping moment M_0, respectively.

By taking the summation of the externally applied shear on the plate and the subgrade reaction, the following equation needs to be satisfied

$$P = -2\pi r_i V_0 = \int_0^{2\pi}\int_{r_i}^{r_0} K\Omega\, W(r,0)\, r\, dr\, d\theta \qquad (3.49)$$

Similarly, by summing the moments about the center of the plate for the externally applied shear and moment on the plate and the subgrade reaction yields

$$M_0 = -\pi r_i^2 V_1 + \pi r_i M_1 = \int_0^{2\pi}\int_{r_i}^{r_0} K\Omega\, W(r,0)\, r^2\cos\theta\, dr\, d\theta \qquad (3.50)$$

It should be pointed out that the integral equations (3.49) and (3.50) will be evaluated numerically according to the Gauss-Legendre quadrature procedure.

Chapter 4

THE SOLUTION FOR A CIRCULAR CYLINDER

4.1 Introduction

In this chapter, the solution for a thin circular cylinder will be presented. The analysis of the cylinder will be based on one of the most accurate solutions, which was developed by Flugge [20]. Actually, several different solutions for the cylinder equation exist, each with its own advantages and disadvantages. In general, simplified equations tend to produce inaccurate results and vice versa. Flugge's equations [20] represent the best choice since they are relatively simple but also accurate.

The cylinder may be subjected to edge loads only. therefore, the problem could be treated as an edge load problem. The cylinder is assumed to be long enough so that each of the cylinder edges could be analyzed independent of the other edge. The displacement functions for the cylinder will be assumed to be exponential in the axial direction and sinusoidal in the angular direction.

Based on Flugge's equations [20], one can derive a relationship, analogous to the stiffness matrix relationship, for the lower edge of the cylinder for each harmonic. This relationship will be instrumental in satisfying the continuity conditions between the plate and the cylinder.

4.2 Theoretical assumptions

The following assumptions will be made for the analysis of the cylinder problem.

1- The material of the cylinder is linear, elastic, and homogeneous.

2- The cylinder is assumed to be thin with a minimum radius to thickness ratio of 10.

3- Flugge's equations for small deformations in a thin circular cylinder will be used.

4- The cylinder is subjected to edge loads only.

5- The cylinder is long enough to justify its treatment as semi-infinite.

4.3 Description of the cylinder problem

The cylinder has a radius r_i and a thickness t_c. The bending stiffness of the cylinder $D_c = \frac{Et_c^3}{12(1-\nu^2)}$, where E and ν are the modulus of elasticity and Possion's ratio for the cylinder, respectively. The length of the cylinder is assumed to be slightly larger than its critical length to justify its treatment as semi-infinite. However, the cylinder should not be too long otherwise the P- Δ effect might affect the overall behavior. The cylinder is subjected to an axial load P and a tipping moment M_0 that act at the center of the top edge (figure 4.1).

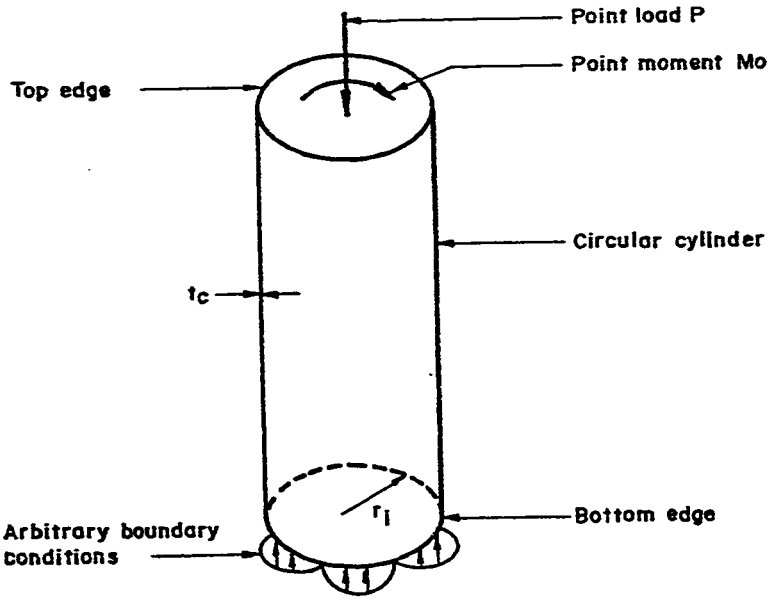

Figure 4.1: Cylinder system coordinate

The top edge of the cylinder will be free to displace while the lower edge may be subjected to any arbitrary boundary conditions as shown in figure (4.1).

4.4 Behavior of the problem

It should be pointed out that the analysis of the cylinder for the harmonics n=0 and n=1, will be treated separately from the other harmonics, $n \geq 2$. In the first case, the membrane analysis will be performed separately from the bending analysis. The bending analysis for those harmonics will be obtained from Flugge's equations [20]. However, the membrane analysis will be derived independently since it could not be obtained from Flugge's equations [20]. One should note that the bending solution will decay along the cylinder length while the membrane solution will remain constant.

In the second case, $n \geq 2$, the membrane solution will be interconnected with the bending solution. The utilized approach (Flugge's model) has the capability to give a combined membrane-bending solution for the general harmonics $n \geq 2$. It has to be pointed out that in this case, the combined solution will decay along the cylinder length at different rates.

To get the complete solution for the cylinder, algebraic summation for the individual solutions of each harmonic should be done. This indicates that the behavior of the cylinder is linear. So, the nonlinear behavior which governs the plate problem will not be introduced in the solution of the cylinder.

4.5 Formulation of the solution

As mentioned before, the formulation of the cylinder solution will be based on the solution given by Flugge [20]. Both the bending solution and the membrane solution will be considered.

4.5.1 Displacement functions

The displacement functions for the circular cylinder will be periodic in the θ direction. They could be expressed using cosine and sine Fourier series depending on their periodicity.

The axial, tangential, and radial displacements will have the following forms, respectively

$$u^c = \sum_{n=0}^{\infty} u^c_n \cos n\theta \ , \tag{4.1.a}$$

$$v^c = \sum_{n=0}^{\infty} v^c_n \sin n\theta \ , \tag{4.1.b}$$

$$w^c = \sum_{n=0}^{\infty} w^c_n \cos n\theta \tag{4.1.c}$$

where the coefficients u^c_n, v^c_n, w^c_n are functions of z. The cylinder coordinate axes z, θ are shown in figure (4.2). The positive directions of these displacements are shown in figure (4.2).

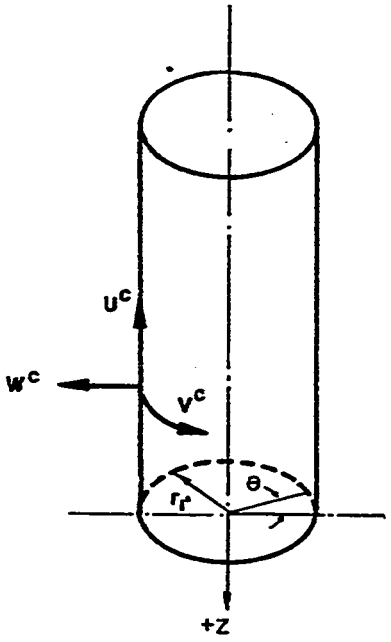

Figure 4.2: Sign convention for the displacements of the cylinder

4.5.2 Governing differential equations

Equations (4.2) through (4.9) have all been derived by Flugge [20] and are presented here for the sake of completion.

Since the treated problem is an edge load problem, i.e., the cylinder is free from internal pressures, the governing differential equations are homogeneous. In this way, for each harmonic n, a set of three simultaneous differential equations with only one independent variable z could be arrived at:

$$u^c_n'' - \frac{1-\nu}{2} n^2 u^c_n + \frac{1+\nu}{2} n v^c_n' + \nu w^c_n' - k^c \left(\frac{1-\nu}{2} n^2 v^c_n + w^{c'''}_n + \frac{1-\nu}{2} n^2 w^c_n'\right) = 0 \qquad (4.2.a)$$

$$-\frac{1-\nu}{2} n v^c_n' - n^2 v^c_n + \frac{1-\nu}{2} v^c_n'' - n w^c_n + k^c \left(\frac{(3-\nu)}{2} v^c_n'' + \frac{3(1-\nu)}{2} n w^c_n''\right) = 0 \qquad (4.2.b)$$

$$\nu u^c_n' + n v^c_n + w^c_n + k^c\left(-\frac{1-\nu}{2} n^2 u^c_n' - u^{c'''}_n - \frac{3-\nu}{2} n v^c_n'' + w^{''''c}_n - 2n^2 w^c_n'' + n^4 w^c_n - 2n^2 w^c_n + w^c_n\right) = 0 \qquad (4.2.c)$$

where in general $(\ )' = \frac{\partial}{\partial z}$, and $k^c = \frac{t^2_c}{12 r_i^2}$, which is a very small term compared to unity.

4.5.3 Solution of the differential equations

The governing differential equations (4.2) have constant coefficients

and may be solved by assuming exponential functions in the z direction for the three displacements,

$$u^c_n = A^c e^{\zeta z/r_i}, \tag{4.3.a}$$

$$v^c_n = B^c e^{\zeta z/r_i}, \tag{4.3.b}$$

$$w^c_n = C^c e^{\zeta z/r_i} \tag{4.3.c}$$

where A^c, B^c, C^c are complex constants and ζ is a complex root.

By substituting (4.3) into (4.2), the following three ordinary linear equations in terms of the constants A^c,B^c,C^c are obtained:

$$\{\zeta^2 - \frac{1-\nu}{2} n^2 (1+k^c)\} A^c + \{\frac{1-\nu}{2} \zeta n\} B^c + \{\nu \zeta - k^c (\zeta^3 + \frac{1-\nu}{2} \zeta n^2)\} C^c = 0 \tag{4.4.a}$$

$$\{\frac{1+\nu}{2} \zeta n\} A^c + \{-\frac{1-\nu}{2} \zeta^2 + n^2 - \frac{3}{2} (1-\nu) k^c \zeta^2\} B^c + \{n - \frac{3-\nu}{2} k^c \zeta^2 n\} C^c = 0 \tag{4.4.b}$$

$$\{\nu \zeta - k^c (\zeta^3 + \frac{1+\nu}{2} \zeta n^2)\} A^c + \{n - \frac{3-\nu}{2} k^c \zeta^2 n\} B^c + \{1 + k^c(\zeta^4 - 2\zeta^2 n^2 + n^4 - 2n^2 + 1\} C^c = 0 \tag{4.4.c}$$

Since these equations are homogeneous, The solution for constants A^c, B^c, C^c may be obtained by setting the determinant of the coefficient matrix to zero. By expanding the determinant, one can obtain the following formula

$$\zeta^8 - 2(2n^2 - \nu)\zeta^6 + \{\frac{1-\nu^2}{k^c} + 6n^2(n^2-1)\}\zeta^4 - 2n^2\{2n^4 - (4-\nu)n^2 + (2-\nu)\}\zeta^2 + n^4(n^2-1)^2 = 0 \tag{4.5}$$

By solving equation (4.5), the following four roots are obtained

$$\zeta_1 = \kappa_1 + i\,\eta_1, \qquad \zeta_2 = \kappa_1 - i\,\eta_1 \tag{4.6.a}$$

$$\zeta_3 = \kappa_2 + i\,\eta_2, \qquad \zeta_4 = \kappa_2 - i\,\eta_2 \tag{4.6.b}$$

It should be mentioned that since the treated problem is a semi-infinite cylinder, the other four roots are discarded since they represent exponentially increasing displacements with decreasing z.

By substituting the roots from (4.6) into the displacement equations (4.2), the following relations for the displacements are found:

$$u^c_n = e^{\kappa_1 z/r_i}\{(A^c_1 + A^c_2)\cos(\eta_1 z/r_i) + i\{(A^c_1 - A^c_2)\sin(\eta_1 z/r_i)$$
$$+ e^{\kappa_2 z/r_i}\{(A^c_3 + A^c_4)\cos(\eta_2 z/r_i) + i\{(A^c_3 - A^c_4)\sin(\eta_2 z/r_i) \tag{4.7.a}$$

$$v^c_n = e^{\kappa_1 z/r_i}\{(B^c_1 + B^c_2)\cos(\eta_1 z/r_i) + i\{(B^c_1 - B^c_2)\sin(\eta_1 z/r_i)$$
$$+ e^{\kappa_2 z/r_i}\{(B^c_3 + B^c_4)\cos(\eta_2 z/r_i) + i\{(B^c_3 - B^c_4)\sin(\eta_2 z/r_i) \tag{4.7.b}$$

$$w^c_n = e^{\kappa_1 z/r_i}\{(C^c_1 + C^c_2)\cos(\eta_1 z/r_i) + i\{(C^c_1 - C^c_2)\sin(\eta_1 z/r_i)$$
$$+ e^{\kappa_2 z/r_i}\{(C^c_3 + C^c_4)\cos(\eta_2 z/r_i) + i\{(C^c_3 - C^c_4)\sin(\eta_2 z/r_i) \tag{4.7.c}$$

By solving (4.4.a), (4.4.b) for each root of equation (4.6), two of the constants, A^c_j, B^c_j, can be expressed in terms of the third one, C^c_j, as follows:

$$A^c_j = \alpha_j C^c_j \qquad j = 1,\ldots, 4 \tag{4.8.a}$$

$$B^c_j = \beta_j C^c_j \qquad j = 1,\ldots, 4 \tag{4.8.b}$$

where α_j, β_j are known complex coefficients. By substituting for the constants from (4.8) into (4.7) one can obtain a general formula that represents any of the displacements or stress quantities in the following form:

$$f_n = q\{e^{\kappa_1 z/r_i}[(a_1 C_1 + a_2 C_2)\cos(\eta_1 z/r_i) + (a_1 C_2 - a_2 C_1)\sin(\eta_1 z/r_i)]$$

$$+ e^{\kappa_2 z/r}[(a_3C_3 + a_4C_4)\cos(\eta_2 z/r_i) + (a_3C_4 - a_4C_3)\sin(\eta_2 z/r_i)]\} \quad (4.9)$$

where f_n is a general function of the coordinate z that represents any displacement or stress resultant in the cylinder. The quantities q, a_1, a_2, a_3, and a_4 are known coefficients derived by Flugge (Table 5.1, page 228, in reference [20]) which vary according to the specific quantity to be represented by f_n. The remaining constants C_1, C_2, C_3, and C_4 will be determined according to the four prescribed boundary conditions at the analyzed edge.

4.5.4 Stress resultants

In general, a cylinder edge is acted upon by four stress resultants, axial bending moment, direct shear, axial force and twisting shear M^c_z, S^c_z, N^c_z, T^c_z, as shown in figure (4.3). The effective shear quantity S^c_z is equivalent to Kirchhoff shear in the analysis of plates. Each of these quantities can be expressed as a function of the three displacement quantities (see equation (5.9) in reference [20]). By examining the contribution of each of these stress resultants to the equilibrium of the cylinder one will notice that only the axisymmetric component of N^c_z, which corresponds to n=0, contributes to vertical equilibrium. Similarly, the anti-symmetric components of N^c_z and M^c_z, which correspond to n=1, contribute to the moment equilibrium of the cylinder, while S^c_z and T^c_z contribute to the lateral force equilibrium. The high harmonics ($n \geq 2$) of all the stress quantities are known to be self-equilibrating. All of the stress resultant quantities could be obtained from equation (4.9).

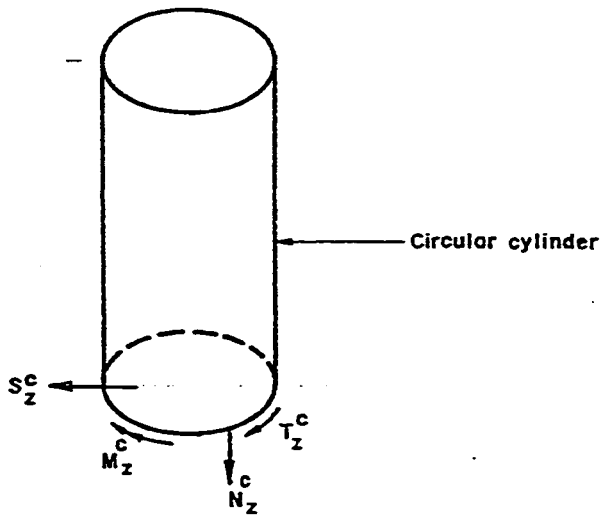

Figure 4.3: Sign convention for the stress resultants of the cylinder

4.6 Analysis of the cylinder

4.6.1 general

The analysis of the cylinder will focus on analyzing the lower edge of the cylinder. At this edge, four arbitrary boundary conditions may be prescribed for each harmonic and a stiffness matrix will be derived for each of these harmonics.

4.6.2 Boundary conditions

For each harmonic at the lower edge, the four constants C_1, C_2, C_3, and C_4 should be determined. This will be achieved by prescribing four quantities out of the stress resultants $M^c_z, S^c_z, T^{c^*}_z, N^c_z$ and the displacements $w^{c^*}, w^c, v^{c^*}, u^c$. It should be mentioned that the derivative with respect to 0 for the terms T^c_z, v^c_z will be used. This will make it possible to define all the quantities in terms of Fourier cosine series.

4.6.3 Stiffness matrix derivations

The matrix equations will be derived independently for n=0, n=1, and n ≥2. This will be done for the lower edge of the cylinder (z=0). The analysis will include both the membrane and the bending solutions. It should also be pointed out that in the following section for the harmonics n=0 and n=1, the constants C_1, and C_2 correspond to the membrane

solution. Therefore, they will be discarded from the analysis since the membrane solution will be performed separately from the bending solution. It should be noted that the subscript "m" will refer to the membrane analysis.

4.6.3.1 Analysis for n = 0

By solving equation (4.5), two different roots will be obtained $\zeta_1 = 0$, which contributes to the membrane solution, while $\zeta_3 \neq 0$, which contributes to the bending solution.

Membrane solution:

Using vertical equilibrium of the cylinder, one obtains

$$(N^c_{0z})_m = -\frac{P}{2\pi r_i} \tag{4.10}$$

From stress-strain relations

$$(w^c_0)_m = \frac{-\nu(N^c_{0z})_m}{Et_c} \tag{4.11}$$

In addition, the cylinder may also experience a rigid translation u_{0r}. Therefore, one obtains

$$(u^c_0)_m = u_{0r} \tag{4.12}$$

Bending solution:

Using equation (4.9), the following relations for the edge forces and displacements may be derived,

$$M^c_{0z} = f_{11}C_3 + f_{12}C_4 \tag{4.13}$$

$$S^c_{0z} = f_{21}C_3 + f_{22}C_4 \tag{4.14}$$

$$w^{c}{}_{0}' = d_{11}C_3 + d_{12}C_4 \tag{4.15}$$

$$w^{c}{}_{0} = d_{21}C_3 + d_{22}C_4 \tag{4.16}$$

In addition, equilibrium and continuity will show that

$$T^{c}{}_{0z}' = 0, N^{c}{}_{0z} = 0, v^{c}{}_{0}' = 0, u^{c}{}_{0} = 0 \tag{4.17}$$

Rearranging equations (4.13) and (4.14) in a matrix form yields,

$$\begin{Bmatrix} M^{c}{}_{0z} \\ S^{c}{}_{0z} \end{Bmatrix} = \begin{bmatrix} f_{11} f_{12} \\ f_{21} f_{22} \end{bmatrix} \begin{Bmatrix} C_3 \\ C_4 \end{Bmatrix} = [f]\{c\} \tag{4.18}$$

Introducing the membrane solution from equation (4.11) and rearranging equations (4.15) and (4.16) in a matrix form yields,

$$\begin{Bmatrix} w^{c}{}_{0}' \\ w^{c}{}_{0} - (w^{c}{}_{0})_m \end{Bmatrix} = \begin{bmatrix} d_{11} d_{12} \\ d_{21} d_{22} \end{bmatrix} \begin{Bmatrix} C_3 \\ C_4 \end{Bmatrix} = [d]\{c\} \tag{4.19}$$

By inverting equation (4.19) and substituting it into equation (4.18), the symmetric stiffness matrix will be obtained in the following form

$$\begin{Bmatrix} M^{c}{}_{0z} \\ S^{c}{}_{0z} \end{Bmatrix} = \begin{bmatrix} k_{11} k_{12} \\ k_{21} k_{22} \end{bmatrix} \begin{Bmatrix} w^{c}{}_{0}' \\ w^{c}{}_{0} - (w^{c}{}_{0})_m \end{Bmatrix} \tag{4.20}$$

where the stiffness matrix for this harmonic $[k_0]$ is equal to:

$$[k_0] = [f]\ [d]^{-1} \tag{4.21}$$

4.6.3.2 Analysis for n = 1

Solving equation (4.5) will produce two roots, $\zeta_1 = 0$, which contributes to the membrane solution and $\zeta_3 \neq 0$, which contributes to the bending solution. The same procedure used for n = 0 will be followed for the harmonic n = 1

Membrane solution:

Using moment equilibrium of the cylinder, one obtains

$$(N^c_{1z})_m = -\frac{M_0}{\pi r_i^2} \tag{4.22}$$

From stress-strain relations

$$(w^c_1)_m = \frac{-\nu(N^c_{1z})_m}{Et_c} \tag{4.23}$$

In addition, the cylinder may also experience a rigid rotation γ_r which produces a rigid translation and a rigid rotation as follows

$$(u^c_1)_m = r_i \gamma_r \tag{4.24}$$

$$(w^{c'}_1)_m = \gamma_r \tag{4.25}$$

Bending solution:

Using equation (4.9), the following relations for the edge forces may be derived:

$$M^c_{1z} = f_{11}C_3 + f_{12}C_4 \tag{4.26}$$

$$S^c_{1z} = f_{21}C_3 + f_{22}C_4 \tag{4.27}$$

$$N^c_{1z} = \frac{f_{11}}{r_i}C_3 + \frac{f_{12}}{r_i}C_4 \tag{4.28}$$

$$T^{c\bullet}_{1z} = f_{21}C_3 + f_{22}C_4 \tag{4.29}$$

Equations (4.26) and (4.28) show that the two stress resultants M^c_{1z} and N^c_{1z} are linearly dependent. Of course, this is because the two quantities together should satisfy the moment equilibrium of the cylinder. Therefore, only one of these two quantities , M^c_{1z}, will be used in the remaining analysis for n = 1. Similarly, the two stress resultants S^c_{1z}, $T^{c\bullet}_{1z}$ are related

and only the direct shear stress S^c_{1z} will be utilized.

Rearranging equations (4.26) and (4.27) in a matrix form yields,

$$\begin{Bmatrix} M^c_{z1} \\ S^c_{z1} \end{Bmatrix} = \begin{bmatrix} f_{11} f_{12} \\ f_{21} f_{22} \end{bmatrix} \begin{Bmatrix} C_3 \\ C_4 \end{Bmatrix} = [f]\{c\} \tag{4.30}$$

Obtaining the membrane solution, a similar matrix for the displacements could be obtained in the form

$$\begin{Bmatrix} w^c_1 - (w^c_1)_m \\ w^c_1 - (w^c_1)_m \end{Bmatrix} = \begin{bmatrix} d_{11} d_{12} \\ d_{21} d_{22} \end{bmatrix} \begin{Bmatrix} C_3 \\ C_4 \end{Bmatrix} = [d]\{c\} \tag{4.31}$$

By inverting equation (4.31) and substituting it into equation (4.30), the symmetric stiffness matrix will be obtained in the following form:

$$\begin{Bmatrix} M^c_{z1} \\ S^c_{z1} \end{Bmatrix} = \begin{bmatrix} k_{11} k_{12} \\ k_{21} k_{22} \end{bmatrix} \begin{Bmatrix} w^c_1 - (w^c_1)_m \\ w^c_0 - (w^c_0)_m \end{Bmatrix} \tag{4.32}$$

where the stiffness matrix for this harmonic $[k_1]$ is equal to

$$[k_1] = [f][d]^{-1} \tag{4.33}$$

4.6.3.3 Analysis for n≥2

In the same manner as done before for n = 0 and n = 1, a stiffness matrix for the general harmonic $n \geq 2$ can be derived. It is worth mentioning that all these harmonics $n \geq 2$ are always self-equilibrating. In other words, the value of the resultant for any of the force quantities is always zero. For example, the resultant of the axial moment corresponding to the n-th harmonic, M^c_{zn}, is

$$\text{Moment Resultant} = \int_0^{2\pi} M^c_{zn} \cos n\theta \cos\theta \, r_i \, d\theta = 0, \qquad n \geq 2 \tag{4.34}$$

This means that the forces or the displacements for these harmonics could be prescribed without the need for any external supports.

By solving equation (4.5), two nonzero roots ζ_1 and ζ_3 will be obtained. This implies that the membrane solution and the bending solution are combined.

From equation (4.9) one can obtain,

$$M^c_{zn} = f_{11}C_1 + f_{12}C_2 + f_{13}C_3 + f_{14}C_4 \tag{4.35}$$

Similar expressions for S^c_{zn}, N^c_{zn}, $T^{c^*}_{zn}$ could be obtained.

Expressing M^c_{zn}, S^c_{zn}, N^c_{zn}, $T^{c^*}_{zn}$ in a matrix form, yields

$$\{R_n\} = [f_n]\{C_n\} \tag{4.36}$$

where $\{R_n\}^T = \{M^c_{zn}\ S^c_{zn}\ N^c_{zn}\ T^{c^*}_{zn}\}$ and $\{C_n\}^T = \{C_1\ C_2\ C_3\ C_4\}$

A similar derivation for the displacements results in

$$\{R^*_n\} = [d_n]\{C_n\} \tag{4.37}$$

where $\{R^*_n\}^T = \{w^{c'}_n\ w^c_n\ u^c_n\ v^{c^*}_n\}$

Substituting for $\{C_n\}$ from equation (4.37) into equation (4.36) gives

$$\begin{Bmatrix} M^c_{zn} \\ S^c_{zn} \\ N^c_{zn} \\ T^{c^*}_{zn} \end{Bmatrix} = \begin{bmatrix} k_{11} & k_{12} & k_{13} & k_{14} \\ & k_{22} & k_{23} & k_{24} \\ & & k_{33} & k_{34} \\ & & & k_{44} \end{bmatrix} \begin{Bmatrix} w^{c'}_n \\ w^c_n \\ u^c_n \\ v^{c^*}_n \end{Bmatrix} \tag{4.38}$$

where the symmetric stiffness matrix $[K_n]$ is equal to

$$[K_n] = [f_n][d_n]^{-1} \tag{4.39}$$

Finally, the previous derivations will produce a 2×2 stiffness matrix for the each of the harmonics n = 0 and n = 1, and a 4×4 stiffness matrix for each of the remaining harmonics $n \geq 2$. These matrices will be

introduced in the plate solution presented in chapter 3 to achieve continuity between the two structural components.

Chapter 5

SOLUTION FOR THE CYLINDER-PLATE JUNCTION

5.1 Introduction

To complete the analysis of a cylinder-plate junction resting on tensionless elastic subgrade, one has to combine the sub-problems of plate on unbonded subgrade, circular cylinder, and plane-stress in such away to achieve continuity at the junction.

In the present chapter, and including the derivations in chapters 3 and 4, the continuity formulation for the displacement and the edge forces at the junction will be obtained. By utilizing the appropriate continuity conditions, the edge forces at the junction may be expressed in terms of the displacement function of the plate. Hence, modified operations in the boundary equations formulation for the plate will be needed. Consequently, the energy equation of the system will have a different synthesis, typically in the term of the work done by the external loads acting on the plate.

5.2 Plane stress problem

5.2.1 Introduction

During the analysis of the plane stress problem, the plate will be considered as an infinite plate. This may be justified by the assumption that the ratio $\frac{r_i}{r_o}$ will be less than 0.30. Hence, the in-plane stresses will decay along the radius of the plate, and thus satisfying the boundary conditions that in-plane forces at the outer boundary should vanish.

5.2.2 Plane stress element

Using a plate element in the polar coordinates (figure 5.1), the positive direction of the stress resultants, the radial, the tangential and the shear stress resultants, N^p_r, N^p_θ, $N^p_{r\theta}$ are indicated. In addition, the displacements u^p and v^p in the radial and the tangential directions, respectively, are shown.

5.2.3 Solution for the problem

The governing differential equation for the plane stress problem in the polar coordinates is the well-known biharmonic equation (see reference [25])

$$\Delta\Delta\Psi(r,\theta) = 0 \qquad (5.1)$$

where $\Psi(r,\theta)$ is the Airy stress function. The solution for this equation, considering that the plate will be subjected to even distribution of loading, is

$$\Psi(r,\theta) = b_0 \ln r + \frac{c_1}{r}\cos\theta + \sum_{n=2}^{\infty}(c_n r^{-n} + d_n r^{-n+2})\cos n\theta \qquad (5.2)$$

where the constants b_0, c_1, c_n, d_n have to be determined according to the prescribed boundary conditions at the inner boundary for each harmonic.

5.2.4 Boundary conditions

The plate may be subjected to the following boundary conditions at its inner boundary

$$N_r^p = \sum_{n=0}^{\infty}(N_r)_n \cos n\theta \qquad (5.3)$$

$$N_{r\theta}^p = \sum_{n=0}^{\infty}(N_{r\theta})_n \sin n\theta \qquad (5.4)$$

These prescribed boundary conditions should be satisfied for each harmonic.

5.2.5 Stress resultants

The stress resultants for the plate are evaluated using the following relationships

$$N_r^p = \frac{1}{r}\frac{\partial\Psi}{\partial r} + \frac{1}{r^2}\frac{\partial^2\Psi}{\partial\theta^2} \qquad (5.5)$$

$$N_\theta^p = \frac{\partial^2\Psi}{\partial r^2} \qquad (5.6)$$

$$N_{r\theta}^p = -\frac{\partial}{\partial r}\left(\frac{1}{r}\frac{\partial\Psi}{\partial\theta}\right) \qquad (5.7)$$

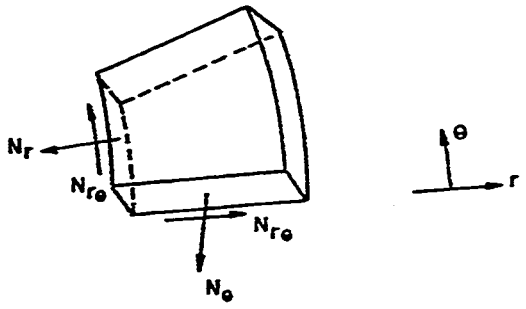

Figure 5.1.a: Sign convention of in-plane forces

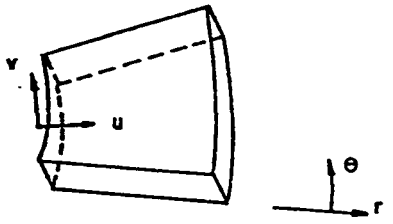

Figure 5.1.b: Sign convention of in-plane displacements

By substituting equation (5.2) into equations (5.5), (5.6) and (5.7), the following expressions for the stress resultants are obtained

$$N_r^p = \frac{b_o}{r^2} - \frac{2c_1}{r^3}\cos\theta$$

$$- \sum_{n=2}^{\infty} (c_n n(n+1)r^{-(n+2)} + d_n(n-1)(n+2)r^{-n})\cos n\theta \qquad (5.8)$$

$$N_\theta^p = -\frac{b_o}{r^2} + \frac{2c_1}{r^3}\cos\theta$$

$$+ \sum_{n=2}^{\infty} (c_n n(n+1)r^{-(n+2)} + d_n(n-1)(n-2)r^{-n})\cos n\theta \qquad (5.9)$$

$$N_{r\theta}^p = \frac{2c_1}{r^3}\sin\theta + \sum_{n=2}^{\infty} (c_n n(n+1)r^{-(n+2)} + d_n n(n-1)r^{-n})\sin n\theta \qquad (5.10)$$

It should be mentioned here that the stiffness of the plate in its plane is much larger than the bending stiffness of the cylinder for any harmonic. As a result, one may assume that the plate is infinitely rigid in its plane. Therefore, the values of the in-plane displacements of the plate at the inner edge will be zero. This assumption was tested for the axisymmetric case and was found to produce very minor errors.

5.3 General continuity equations at the junction

In this section the continuity equations for the displacements and the edge forces at the junction will be derived.

5.3.1 Displacement continuity

Through the continuity of the displacements at the cylinder-plate intersection, the four displacement quantities for the plate should be equal to those for the cylinder (figure 5.2). A set of four equations will represent the continuity conditions at the junction as follows:

$$W^{p'} = w^{c'} \tag{5.11}$$

$$W^{p} = -u^{c} \tag{5.12}$$

$$u^{p} = w^{c} \tag{5.13}$$

$$v^{p} = v^{c} \tag{5.14}$$

where the super-scripts p and c refer to the plate and the cylinder respectively.

However, since the plate was considered to be infinitely rigid in the in-plane direction, equations (5.13) and (5.14) will be replaced by:

$$u^{p} = w^{c} = 0 \tag{5.15}$$

$$v^{p} = v^{c} = 0 \tag{5.16}$$

This set of equations should be satisfied for each harmonic independently.

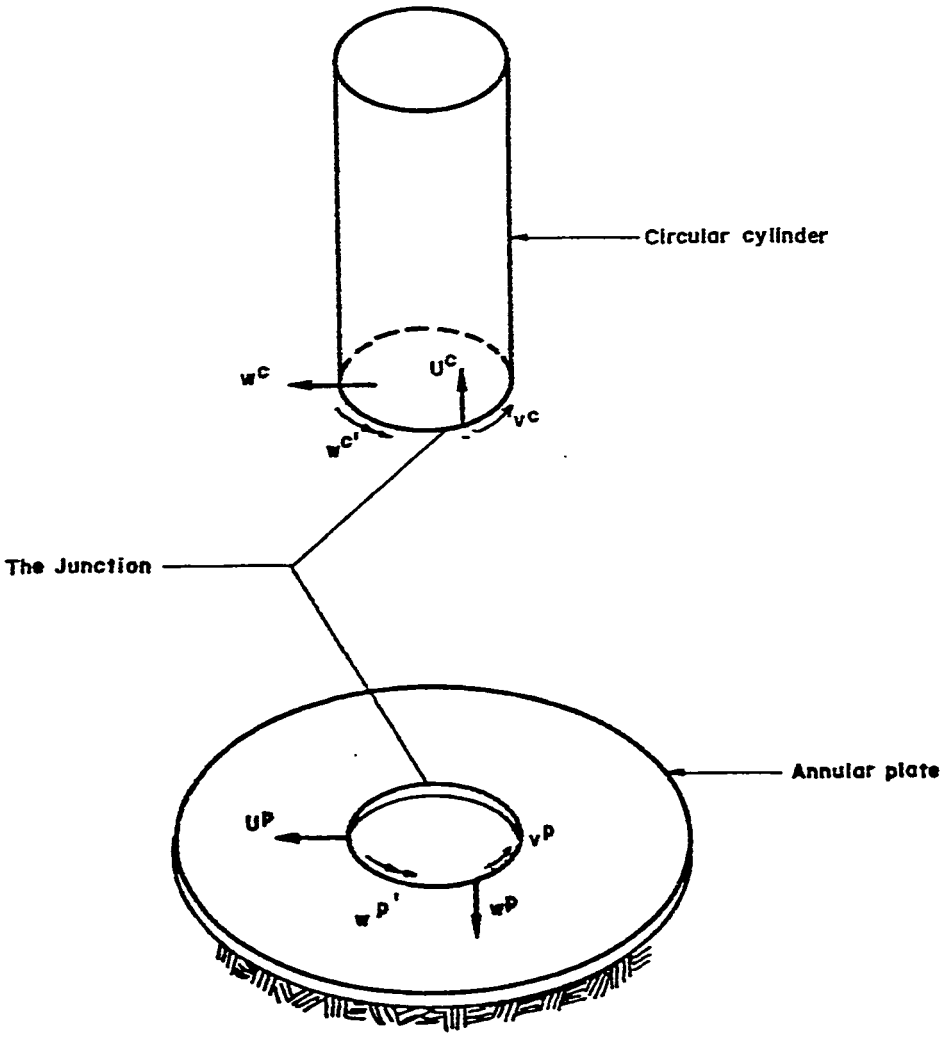

Figure 5.2: Edge displacement continuity

5.3.2 Edge forces continuity

In the same manner as has been done for the displacement continuity, four equations are introduced to represent the edge forces continuity at the junction, figure (5.3), as follows:

$$M_r^p = M^c_z \tag{5.17}$$

$$V_r^p = N^c_z \tag{5.18}$$

$$N_r^p = S^c_z \tag{5.19}$$

$$N_{r\theta}^p = T^c_z \tag{5.20}$$

This set of equations should also be satisfied for each harmonic.

5.4 Edge forces & plate displacement relationship

In chapter 3, the edge forces of the plate were prescribed as numerical values. However, in the cylinder-plate problem due to the continuity conditions at the junction, these values are not known at the outset. Therefore, the edge forces need to be expressed as functions of the plate displacement in addition to the prescribed external loads. In this section, the edge forces, the radial moment, and transverse shear will be formulated in terms of the transverse displacement function of the plate. This will facilitate the inclusion of the effect of the cylinder in the energy equation of the plate.

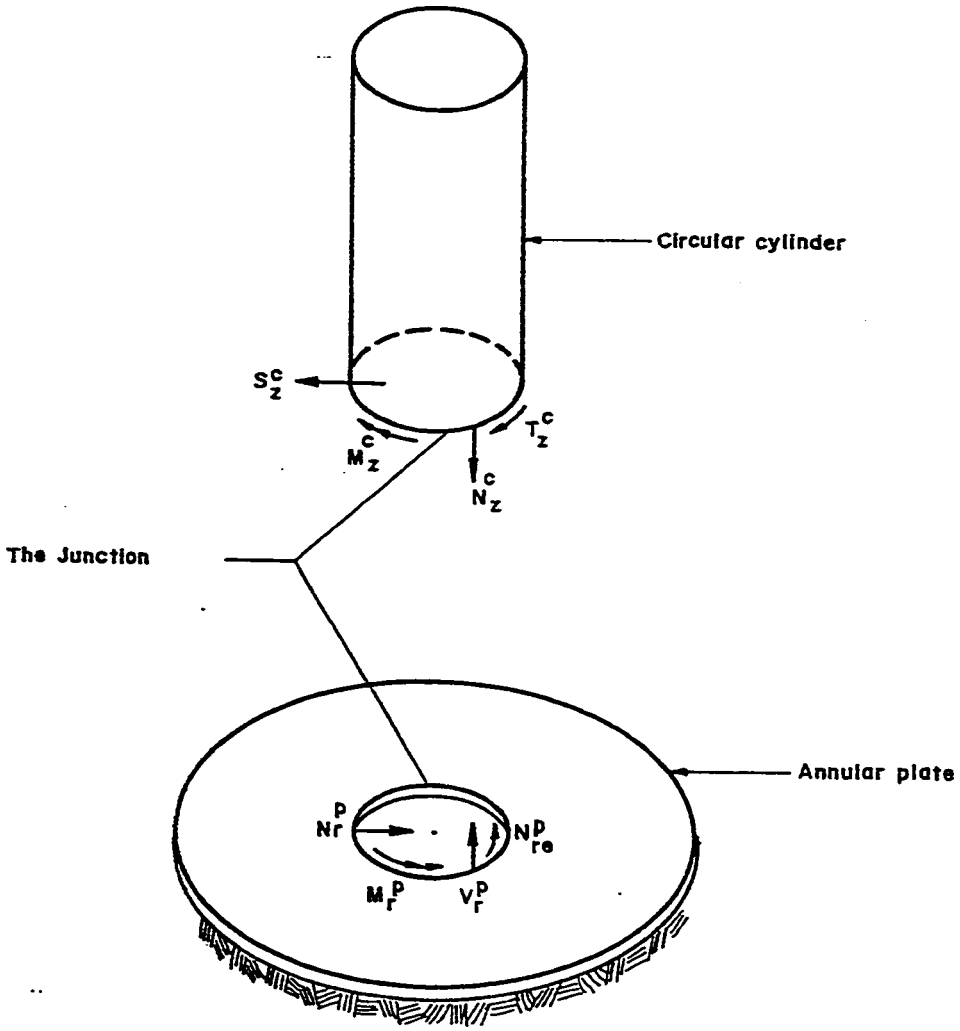

Figure 5.3: Edge forces continuity

5.4.1 Representation for n=0

Using the stiffness matrix for the cylinder from equation (4.20) and utilizing the continuity equations (5.11)-(5.20), it can be shown that

$$M^{p}_{r0} = M^{*}_{0} + E_0 (k^{0}_{12} w^{p'}_{0}) \tag{5.21}$$

$$V^{p}_{r0} = V^{*}_{0} \tag{5.22}$$

where

$$M^{*}_{0} = k^{0}_{11} (-w^{c}_{0})_m \tag{5.23}$$

$$V^{*}_{0} = (N^{c}_{z0})_m \tag{5.24}$$

5.4.2 Representation for n=1

By obtaining the stiffness matrix for the cylinder from equation (4.32) and using equations (5.11)-(5.20), one can obtain

$$M^{p}_{r1} = M^{*}_{1} + E_1 k^{1}_{12} (w^{p'}_{1} - \frac{w^{p}_{1}}{r_i}) \tag{5.25}$$

$$V^{p}_{r1} = V^{*}_{1} + E_1 \frac{k^{1}_{12}}{r_i} (w^{p'}_{1} - \frac{w^{p}_{1}}{r_i}) \tag{5.26}$$

where

$$M^{*}_{1} = -k^{1}_{11} (w^{c}_{1})_m \tag{5.27}$$

$$V^{*}_{1} = \frac{k^{1}_{11}}{r_i} (-w^{c}_{1})_m + (N^{c}_{z1})_m \tag{5.28}$$

5.4.2 Representation for n≥2

Utilizing the general stiffness matrix for the cylinder from equation (4.38) and using equations (5.11)-(5.20), one can obtain

$$M^p_m = E_n (k^n_{11} w^{p'}_n - k^n_{12} w^p_n) \tag{5.29}$$

$$V^p_m = E_n (k^n_{12} w^{p'}_n - k^n_{22} w^p_n) \tag{5.30}$$

It should be pointed out that the edge shear and moment have been formulated as functions of the displacement function of the plate for all the harmonics, in addition to numerical values of these forces for the harmonics n=0, n=1 only. Therefore, a modification of the boundary conditions formulation at the inner edge of the plate is necessary. Consequently, the energy equation will also be modified due to this modification.

5.5 Modified boundary conditions

In this section, the boundary conditions at the junction will be formulated independently for n=0, n=1, and n ≥2.

5.5.1 Boundary conditions for n=0

The boundary conditions should be satisfied at the inner and outer edges of the plate. At the inner edge, the original boundary conditions equations were given in equations (3.18), (3.19). By introducing equations (5.21) and (5.22), the new boundary conditions at the inner edge will be

$$\frac{d^2w_0}{dr^2} + \frac{\nu}{r_i}\left(\frac{dw_0}{dr}\right) - \frac{k^0_{12}}{D_p}\frac{dw_0}{dr} = \frac{-M^*_0}{D_pE_0} \tag{5.31}$$

$$\frac{d}{dr}\left(\frac{d^2w_0}{dr^2} + \frac{1}{r}\frac{dw_0}{dr}\right) = \frac{-V^*_0}{D_pE_0} \tag{5.32}$$

Similar expressions could be obtained at the outer edge where the radial moment and shear are zero as follows:

$$\frac{d^2w_0}{dr^2} + \frac{\nu}{r_0}\frac{dw_0}{dr} = 0 \tag{5.33}$$

$$\frac{d}{dr}\left(\frac{d^2w_0}{dr^2} + \frac{1}{r}\frac{dw_0}{dr}\right) = 0 \tag{5.34}$$

5.5.2 Boundary conditions for n=1

The derivation of this section will follow the same procedure used for n=0. At the inner edge, we substitute equations (5.25) and (5.26) into equations (3.18) and (3.19) to obtain the following equations:

$$\frac{d^2w_1}{dr^2} + \nu\left(\frac{1}{r_i}\frac{dw_1}{dr} - \frac{w_1}{r_i^2}\right) + \frac{k^1_{11}}{D_p}\left(\frac{dw_1}{dr} - \frac{w_1}{r_i}\right) = \frac{-M^*_1}{D_pE_1} \tag{5.35}$$

$$\frac{d}{dr}\left(\frac{d^2w_1}{dr^2} + \frac{1}{r}\frac{dw_1}{dr} - \frac{w_1}{r^2}\right) - \frac{(1-\nu)}{r_i}\left(\frac{dw_1}{dr} - \frac{w_1}{r_i}\right) + \frac{k^1_{11}}{r_iD_p}\left(\frac{dw_1}{dr} - \frac{w_1}{r_i}\right) = \frac{-V^*_1}{D_pE_1} \tag{5.36}$$

However at the outer edge, the moment and shear are zeros

$$\frac{d^2w_1}{dr^2} + \nu\left(\frac{1}{r_0}\frac{dw_1}{dr} - \frac{w_1}{r_0^2}\right) = 0 \tag{5.37}$$

$$\frac{d}{dr}\left(\frac{d^2w_1}{dr^2} + \frac{1}{r}\frac{dw_1}{dr} - \frac{w_1}{r^2}\right) - \frac{(1-\nu)}{r_0}\left(\frac{dw_1}{dr} - \frac{w_1}{r_0}\right) = 0 \qquad (5.38)$$

5.5.3 Boundary conditions for n≥2

At the inner edge, by substituting equations (5.29) and (5.30) into equations (3.18) and (3.19), one can obtain the following formulations for the moment and the shear corresponding to the n-th harmonic

$$\frac{d^2w_n}{dr^2} + \nu\left(\frac{1}{r_i}\frac{dw_n}{dr} - n^2\frac{w_n}{r_i}\right) - \frac{1}{D_p}\left(k^n_{12}\,w_n + k^n_{11}\,\frac{dw_n}{dr}\right) = 0 \qquad (5.39)$$

$$\frac{d}{dr}\left(\frac{d^2w_n}{dr^2} + \frac{1}{r}\frac{dw_n}{dr} - n^2\frac{w_n}{r^2}\right) - \frac{(1-\nu)n^2}{r_i}\left(\frac{dw_n}{dr} - \frac{w_n}{r_i}\right)$$

$$+ \frac{1}{D_p}\left(k^n_{12}\frac{dw}{dr} - k^n_{22}w_n\right) = 0 \qquad (5.40)$$

At the outer boundary, the moment and the shear are zero which yields the following equations:

$$\frac{d^2w_n}{dr^2} + \nu\left(\frac{1}{r_0}\frac{dw_n}{dr} - n^2\frac{w_n}{r_0^2}\right) = 0 \qquad (5.41)$$

$$\frac{d}{dr}\left(\frac{d^2w_n}{dr^2} + \frac{1}{r}\frac{dw_n}{dr} - n^2\frac{w_n}{r^2}\right) - \frac{(1-\nu)n^2}{r_0}\left(\frac{dw_n}{dr} - \frac{w_n}{r_0}\right) = 0 \qquad (5.42)$$

5.6 Modified energy minimization equation

In chapter 3, the total potential energy of the plate-subgrade system was expressed as follows

$$\Pi^* = U_p + U_s - W_p \qquad (5.43)$$

where now the strain energy of the plate and the strain energy of the

subgrade U_p and U_s will remain unchanged as derived in chapter 3. The term W_p represents the work done by the edge forces at the junction and obviously will be modified according to the previous derivations for these forces.

This term will be expressed in the following manner

$$W_p = \sum_{n=0}^{1} W_{l_n} + \sum_{n=0}^{\infty} W_{s_n} \tag{5.44}$$

where W_{l_n} is the work done by the numerical values of the radial shear and radial moment which appear for n = 0 and n = 1 only. The term W_{s_n} is the strain energy of those components expressed in terms of the cylinder stiffness coefficients and the plate displacement function. The derivation of the terms W_l and W_s will be done separately for the harmonics n = 0, n = 1 and n ≥2.

5.6.1 Work done for n = 0

The work done by the numerical values W_{l_0} and the strain energy of the term W_{s_0} can be obtained as follows

$$W_{l_0} = \int_0^{2\pi} \{M^*_0 E_0 w^{p'}_0 - V^*_0 (E^*_0 + E_0 w^p_0)\} r_i \, d\theta \tag{5.45}$$

By integrating the above equation, one obtains

$$W_{l_0} = \{M^*_0 E_0 w^{p'}_0 - V^*_0 (E^*_0 + E_0 w^p_0)\} 2\pi r_i \tag{5.46}$$

Similarly the strain energy stored in the cylinder is

$$W_{s_0} = \int_0^{2\pi} \{\frac{1}{2} k^0_{12} (E_0 w_0^{p'})^2\} r_i d\theta \tag{5.47}$$

Using the integration operation yields

$$W_{s_0} = \{\frac{1}{2} k^0_{12} (E_0 w_0^{p'})^2\} 2\pi r_i \tag{5.48}$$

5.6.2 Work done for n=1

The work done by the prescribed values is

$$W_{l_1} = \int_0^{2\pi} \{M^*_1 (E^*_1 + E_1 w^{p'}_1) - V^*_1 (E^*_1 r_i + E_1 w^p_1)\} r_i (\cos\theta)^2 d\theta \tag{5.49}$$

Integrating the above equation yields

$$W_{l_1} = \{M^*_1 (E^*_1 + E_1 w^{p'}_1) - V^*_1 (E^*_1 r_i + E_1 w^p_1)\} \pi r_i \tag{5.50}$$

In addition, the strain energy term for this harmonic is

$$W_{s_1} = \frac{1}{2} \int_0^{2\pi} \{k^1_{12} (w^{p'}_1 - \frac{w^p_1}{r_i}) (E^*_1 + E_1 w^{p'}_1) - \frac{k^1_{12}}{r_i} (w^{p'}_1 - \frac{w^p_1}{r_i}) (E^*_1 r_i + E_1 w^p_1)\} r_i (\cos\theta)^2 d\theta \tag{5.51}$$

Integrating the above equation gives

$$W_{s_1} = \frac{1}{2} k^1_{12} E_1^2 \{(w^{p'}_1)^2 - \frac{2}{r_i} w^{p'}_1 w^p_1 + \frac{1}{r_i^2} (w^p_1)^2\} \pi r_i \tag{5.52}$$

5.6.3 Work done for n≥2

Since there are no prescribed values of the radial shear and moment

corresponding to these harmonics, therefore

$$W_{t_n} = 0, \qquad n \geq 2 \tag{5.53}$$

In addition, the strain energy of the cylinder after integration will be as follows:

$$W_{s_n} = \frac{1}{2} E_n^2 \{k^n_{11} (w^p{}'_n)^2 - 2 k^n_{12} w^p{}_n w^p{}'_n + k^n_{22} (w^p{}_n)^2\} \pi r_i \tag{5.54}$$

5.7 Minimization of the total potential energy

As indicated in the previous section, the addition of the cylinder caused certain changes in the work terms of the energy equation. Therefore, the energy minimization equation presented in section 3.4.4 will require some modifications to incorporate the new changes in the work terms. However, these modifications will not affect at all the strain energy terms for the plate and the subgrade U_p, U_s. As a result, the derivatives with respect to the rigid body constants given earlier in equations (3.34) and (3.35) now become

$$\frac{\partial W_p}{\partial E^*_0} = -(2 \pi r_i) V^*_0 \tag{5.55}$$

$$\frac{\partial W_p}{\partial E^*_1} = (M^*_1 - V^*_1 r_i) \pi r_i \tag{5.56}$$

In addition, the derivatives with respect to E_0, E_1 are obtained as follows

$$\frac{\partial W_p}{\partial E_0} = \{E_0 k^0_{12} (w^p{}'_0)^2 + (M^*_0 w^p{}'_0 - V^*_0 w^p{}_0)\} 2 \pi r_i \tag{5.57}$$

$$\frac{\partial W_p}{\partial E_1} = \{E_1 k^1_{12}[(w^{p'}_1)^2 - \frac{2}{r_i} w^{p'}_1 w^p_1 + (\frac{w^p_1}{r_i})^2]$$

$$+ M^*_1 w^{p'}_1 - V^*_1 w^p_1\} \pi r_i \qquad (5.58)$$

Similarly, the derivatives with respect to each of the remaining unknown constants E_n, $n \geq 2$, were obtained as follows

$$\frac{\partial W_p}{\partial E_n} = E_n\{k^n_{11}(w^{p'}_n)^2 - 2 w^p_n w^{p'}_n + k^2_{22}(w^p_n)^2\} \pi r_i \qquad (5.59)$$

By replacing the equations from (5.55) to (5.59) into the energy matrices equations (3.34), (3.35), and (3.36) and arranging the resulting equations as a matrix relationship, one obtains the modified energy equation

$$[G]\{E\} = \{L\} \qquad (5.60)$$

It should be pointed out that the changes in the elements of the matrix $[G]$ will only be in the diagonal terms for $n=0$, $n=1$ and $n \geq 2$. As a result, all the off-diagonal terms in $[G]$ presented earlier in chapter 3 will remain unchanged. The revised diagonal terms will be

$$G(3,3) = 2K \int_0^{\pi} \int_{r_i}^{r_o} \Omega (w^p_0)^2 r \, dr \, d\theta + D_p \int_{r_i}^{r_o} Y r \, dr$$

$$- k^0_{12}(w^{p'}_0)^2 2\pi r_i \qquad (5.61)$$

$$G(4,4) = 2K \int_0^{\pi} \int_{r_i}^{r_o} \Omega (w^p_1 \cos\theta)^2 r \, dr \, d\theta + D_p \int_{r_i}^{r_o} Y r \, dr$$

$$- k^1_{12}[(w^{p'}_1)^2 - \frac{2}{r_i} w^{p'}_1 w^p_1 + (\frac{w^p_1}{r_i})^2] \pi r_i \qquad (5.62)$$

$$G(n+3,n+3) = 2K \int_0^{\pi} \int_{r_i}^{r_o} \Omega (w^p_n \cos n\theta)^2 r \, dr \, d\theta + D_p \int_{r_i}^{r_o} Y r \, dr$$

$$- \{k^n_{11} (w^{p'}_n)^2 - 2 k^n_{12} w^p_n w^{p'}_n$$

$$+ k^n_{22} (w^p_n)^2\} \pi r_i, \qquad n \geq 2 \tag{5.63}$$

where

$$Y = a_n(w^{p''}_n + \frac{1}{r} w^{p'}_n - n^2 w^p_n)^2$$

$$- 2(1-\nu) n a_n \{w^{p''}_n (\frac{1}{r} w^{p'}_n - \frac{n^2}{r^2} w^p_n)\}$$

$$+ 2(1-\nu) a^*_n (\frac{-n}{r} w^{p'}_n + \frac{n}{r^2} w^p_n)^2 \tag{5.64}$$

where

$$a_0 = 2\pi, \quad a_n = \pi, \quad n \geq 1 \tag{5.65}$$

$$a^*_0 = 0, \quad a^*_n = \pi, \quad n \geq 1 \tag{5.66}$$

To define the remaining terms of the energy equation (5.56), the elements in the modified force vector {L} could be obtained as follows

$$L(1) = -2\pi r_i V^*_o \tag{5.67}$$

$$L(2) = \pi r_i (M^*_1 - V^*_1 r_i) \tag{5.68}$$

$$L(3) = 2\pi r_i (M^*_0 w^{p'}_0 - V^*_0 w^p_0) \tag{5.69}$$

$$L(4) = \pi r_i \{M^*_1 w^{p'}_1 - V^*_1 w^p_1\} \tag{5.70}$$

$$L(n+3) = 0 , \quad n \geq 2 \tag{5.71}$$

This completes the necessary formulation to solve equation (5.60) for the unknown constants E_n.

5.8 Solution procedure

To analyze the complete plate-cylinder junction problem, a computer program was developed and coded in Fortran 77 language. The program was compiled and executed using the IBM-3090 main-frame in the Data Processing Center at King Fahd University of Petroleum and Minerals.

The solution procedure for the junction problem is no longer the same as the one for the plate problem shown in section 3.6. The main changes include incorporating the solution for the cylinder and the modifications of the boundary conditions and the energy matrices. The scheme of the junction solution procedure is shown in figure (5.4).

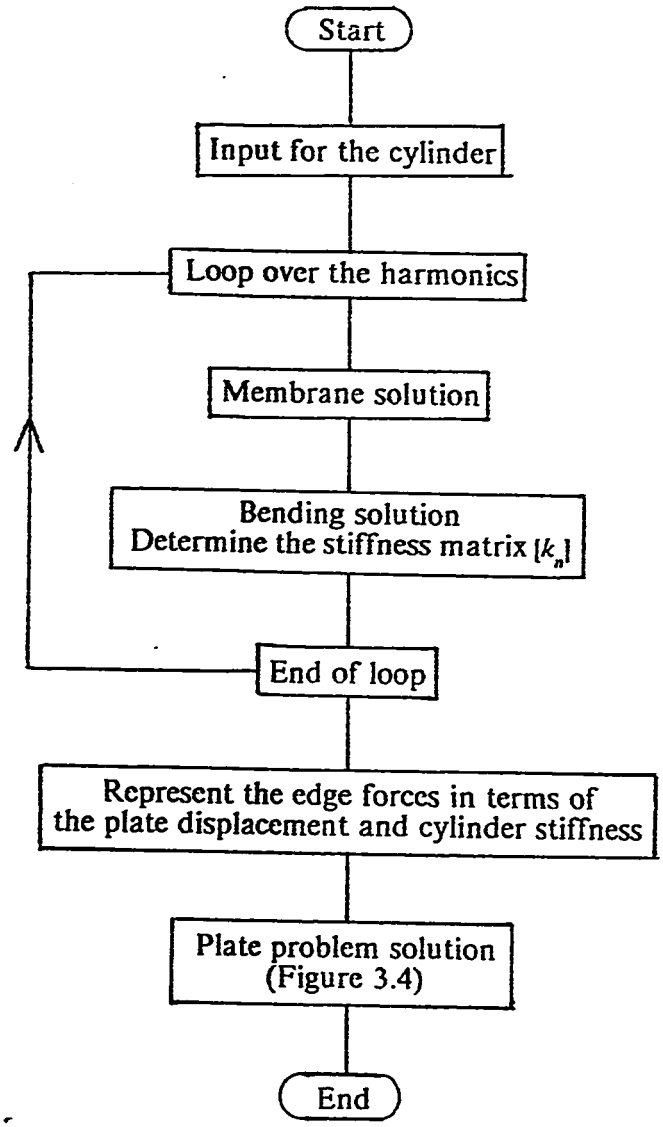

Figure (5.4) Scheme of the solution for the junction problem

Chapter 6

APPLICATIONS AND RESULTS

6.1 General

In this chapter, applications to the following problems will be presented

a- Axisymmetric and non-axisymmetric behavior of plates on unbonded elastic subgrade

b- Axisymmetric and non-axisymmetric behavior of cylinder-plate junction on unbonded elastic subgrade.

Through the analysis of these problems, the following objectives will be in sight:

1- To verify the validity of the approach and the solution procedure presented in the preceding chapters.

2- To investigate the convergence and stability of the suggested approach and determine the limitation on its validity.

3- To compare results with the available solutions, whenever possible.

4- To investigate the effect of the system parameters on the contact zone and the displacement of the plate, in addition to the stress distribution at the junction.

Throughout this chapter, it will be considered that the plate has an

outer radius $r_0 = 1.0$. The stiffness of the subgrade relative to the plate will be measured using the dimensionless subgrade stiffness $k = Kr_0^4/D_p$. In general subgrades with k <20 are considered soft, while subgrades with k >200 are considered stiff.

To perform the numerical integration of the terms in the energy matrix, several tests have been done and it was found that a 5×5 Gauss points, repeated two times scheme, gave very accurate results. As a result, this integration scheme was adopted.

6.2 Applications to the plate problem

Two different problems of plates resting on unbonded elastic subgrade were studied. These include the axisymmetric problem of a solid plate subjected to a concentric load and the non-axisymmetric problem of an annular plate subjected to a uniform arc load that acts at its inner boundary.

6.2.1 Solid plate problem

This problem considers a plate with a small inclusion at the center resting on tensionless elastic subgrade. The plate was subjected to a concentric point load (P = 1) distributed on the small inclusion as shown in figure (6.1). The plate was modeled as a solid plate by considering the rotation $\frac{\partial W}{\partial r} = 0$ at the inner boundary. It should be pointed out that

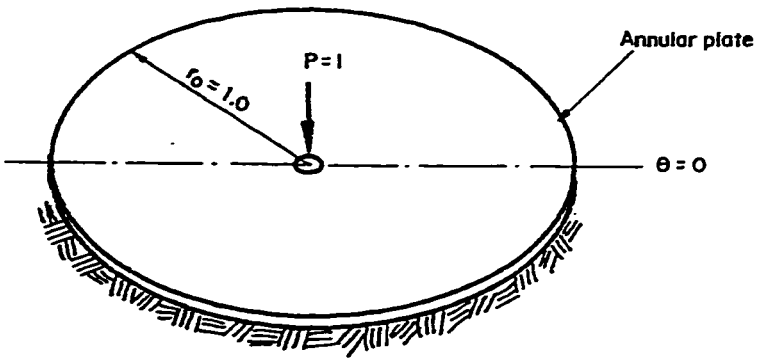

Figure 6.1: Axisymmetric solid plate

considering the radius of the inclusion to have a small value which is not zero helps in avoiding the singular behavior of the concentrated load, without affecting the accuracy of the solution. Due to the axisymmetric nature of the problem, only the harmonic n = 0 was considered to represent the displacement function in addition to the rigid translation term. The value of Poisson's ratio is v=0.33.

To asses the validity of the derived formulation, comparisons with the exact solution and another energy approach developed by Celep [13] have been performed.

Figure (6.2) shows the effect of the subgrade stiffness k on the radius of contact r_c, as obtained by the three different approaches. It shows that the plate experiences loss of contact when k exceeds 48. It also indicates that the present solution is in excellent agreement with the exact solution up to moderate values of the subgrade stiffness k and differs slightly when the subgrade becomes very stiff. On the other hand, Celep solution differs from the exact solution even for moderate subgrade stiffness. The disparity between the present approach and the exact solution for very stiff subgrades comes as no surprise. This is because the assumed displacement functions as adopted in this work, represent the exact solution when the plate is in full contact with the subgrade. As a result, when the contact zone becomes very small (for $k > 400$), the approach becomes less accurate.

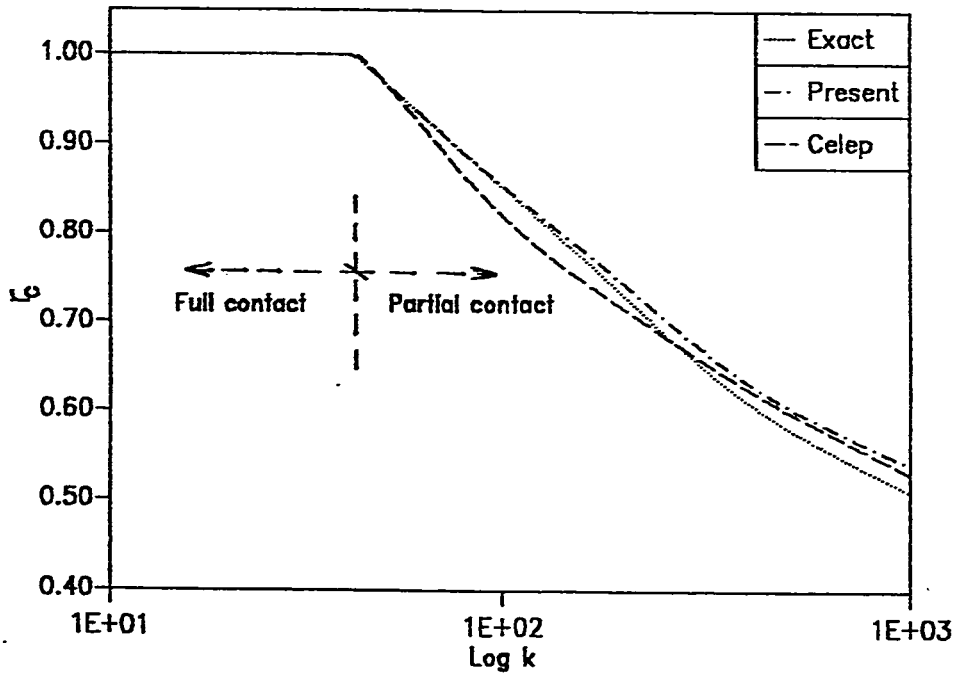

Figure 6.2: Radius of contact circle for a plate resting on tensionless Winkler subgrade subjected to point load P for various subgrade stiffness, ($r_0 = 1$)

Figure (6.3) shows the edge and central displacements, kW_e/P and kW_i/P, of the plate. It shows that the present solution is in excellent agreement with the exact solution for the central displacement for any k, and for the edge displacement up to moderate values of k. However, Celep solution shows considerable difference from the exact solution for both kW_e/P and kW_i/P.

Figure (6.4) shows plots for the displacement along a typical radius of the plate for the specific case of k=200. In this figure and the following ones, the positive values of the displacement are plotted down instead of up in order to model the actual deflected shape. It is clear that the deflected shape of the present solution coincides with the exact solution except for a small difference at the edge. On the other hand, the solution of Celep [13] produce a very different deflected shape. This could be explained by the fact that the effect of the subgrade stiffness is considered within the displacement function for the present and the exact solution through the root λ_n of the Kelvin function. On the other hand, Celep assumed a shape function for the displacement that does not depend on the subgrade stiffness. As a result, his solution will always show the same curvature regardless of the subgrade stiffness.

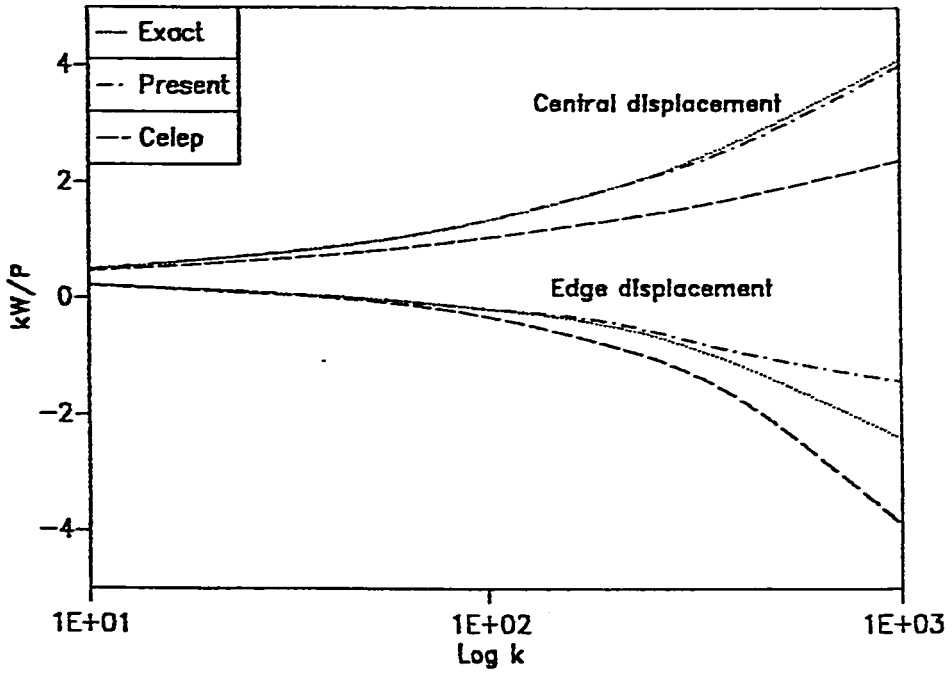

Figure 6.3: Edge and central displacements kW_e/P and kW_i/P for a plate resting on tensionless Winkler subgrade subjected to point load P for various subgrade stiffness, ($P = 1$, $r_0 = 1$)

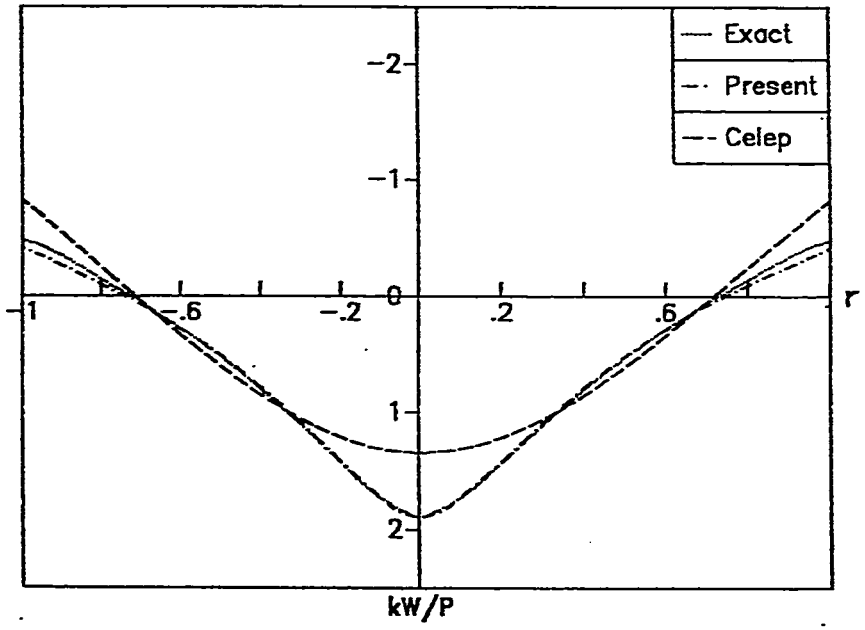

Figure 6.4: Displacement along symmetry axis of a plate resting on tensionless Winkler subgrade subjected to point load P, (P = 1, r_0 = 1, k = 200)

6.2.2 Annular plate problem

The problem considered in this section is an annular plate with an inner radius $r_i = 0.3$, resting on tensionless elastic subgrade as shown in figure (6.5). The plate is subjected to a uniform arc load of intensity q with an angle $= 2\theta_0$, that acts at the inner edge of the plate. The total applied load $P = (2\pi r_i)\, q \frac{\theta_0}{180}$ and is always equal to 1. Therefore, the intensity q will adjust with changing the angle θ_0 to keep the total applied load = 1.0.

To analyze the problem, the arc load distribution was expanded in terms of Fourier cosine series. It was found that 8 terms, i.e. n = 7, were sufficient to represent the distribution for values down to $\theta_0 = 15°$. However, ten terms of the displacement function, i.e. n = 9, in addition to the two rigid body terms were used in the solution to converge with good accuracy. The analysis has been done assuming that $\nu = 0.3$.

Figure (6.6.a) shows the contact curves of the plate for different values of the angle θ_0. Due to the symmetry of the problem about the axis $\theta = 0$, only half of the plate domain is shown. The figure indicates that the contact curve shifts to the right as θ_0 decreases, which actually means that the resultant applied moment on the plate is being increased. In addition, figure (6.6.b) shows that with decreasing the angle θ_0, the displacements increase along the radius $\theta = 0$.

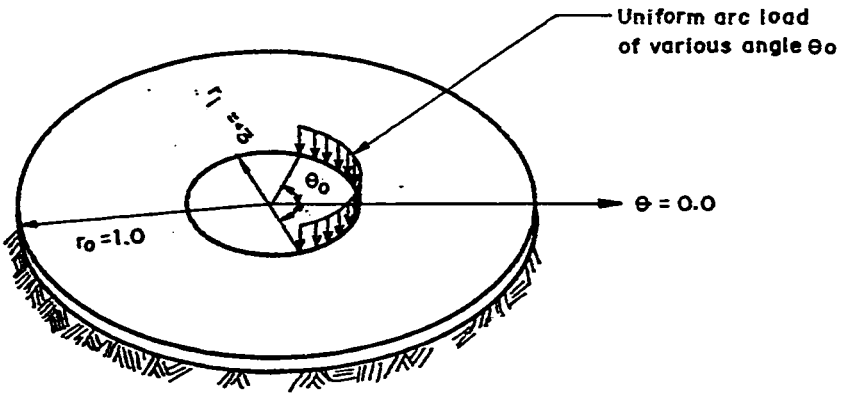

Figure 6.5: Annular plate subjected to an arc load

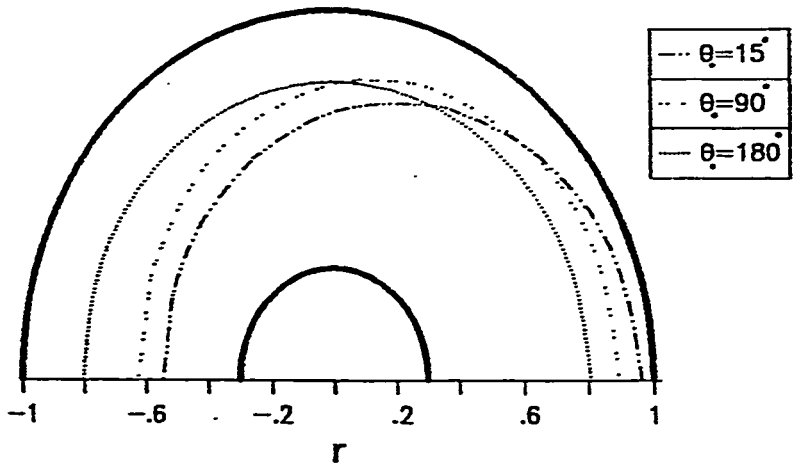

Figure 6.6.a: Contact curves of an annular plate resting on tensionless Winkler subgrade subjected to an arc load at the inner edge for various angles of the applied load, ($P = 1$, $r_i = .3$, $r_0 = 1$, $k = 100$)

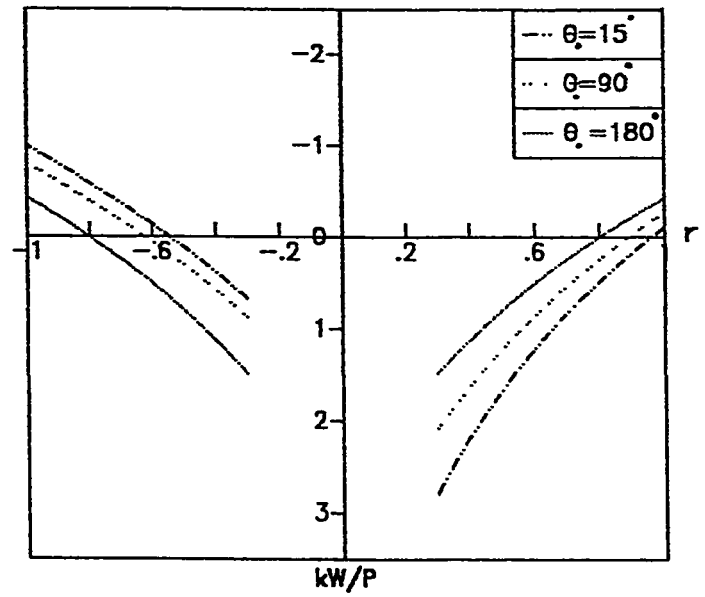

Figure 6.6.b: Displacement curves along symmetry axis of an annular plate resting on tensionless Winkler subgrade subjected to an arc load at the inner edge for various angles of the applied load, ($P = 1$, $r_i = .3$, $r_0 = 1$, $k = 100$)

Figure (6.7) shows the displacements around the inner and outer edges of the plate for various angles θ_0. The figure illustrates the effect of the higher harmonics on the deflections as the value of θ_0 becomes smaller. When $\theta_0 = 180$, the solution is represented by the lowest harmonic ($n = 0$) only. As the value of θ_0 decrease to 90°and15°, the harmonics $n = 1$ and $n \geq 2$ start to appear in the solution.

In addition, figure (6.8) indicates the changes in the magnitude and distribution of the radial moment in the plate along the axis $\theta = 0$ due to changing the value of θ_0.

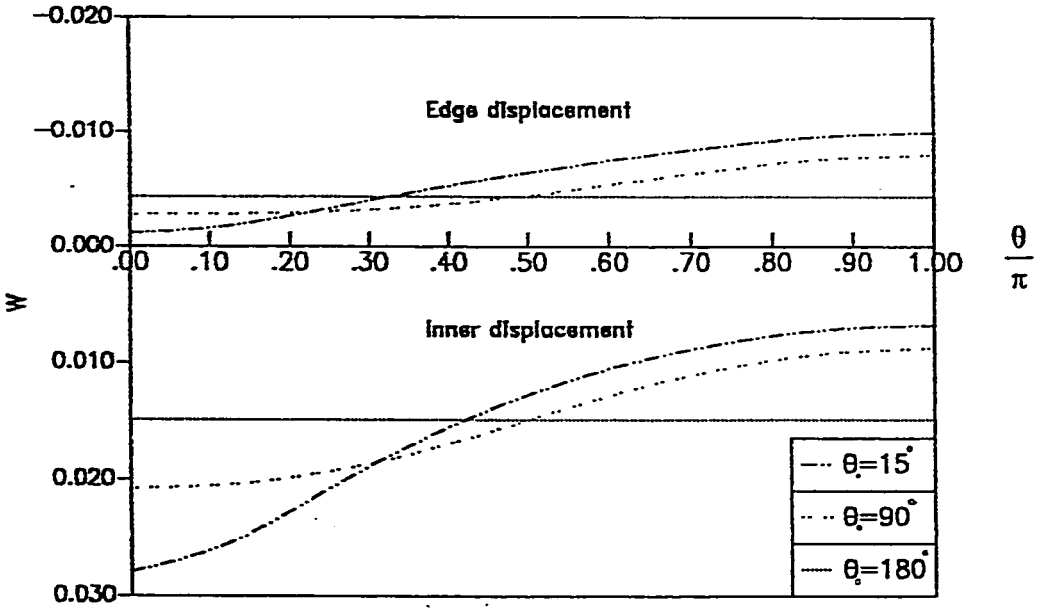

Figure 6.7: Distribution of the displacement along the inner and outer edges of an annular plate resting on tensionless Winkler subgrade subjected to an arc load at the inner edge for various angles of the applied load, ($P = 1$, $r_i = .3$, $r_o = 1$, $k = 100$)

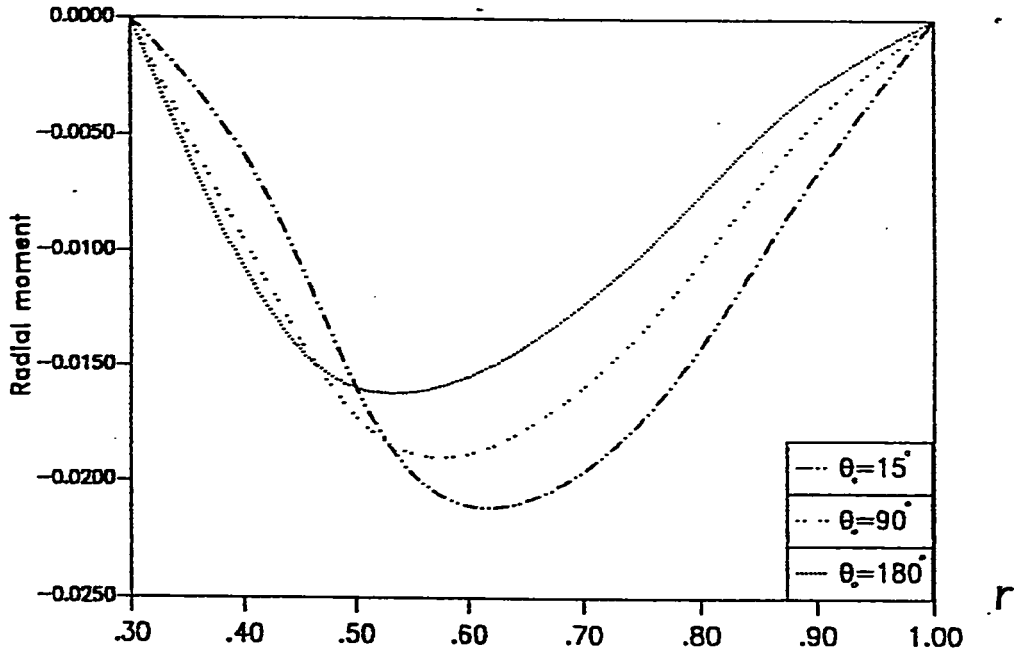

Figure 6.8: Distribution of the radial moment M_r along the radius at $\theta = 0$ of an annular plate resting on tensionless Winkler subgrade subjected to an arc load at the inner edge for various angles of the applied load, ($P = 1$, $r_i = .3$, $r_o = 1$, $k = 100$).

6.3 Applications to the junction problem

Two types of problems will be dealt with through this section, the axisymmetric and non-axisymmetric cylinder-plate junction resting on tensionless elastic subgrade.

To decide the number of terms of the displacement function of the plate to be considered in this solution, several test problems were attempted and it indicated that 7 terms of the displacement function including the rigid body terms, (i.e., n = 5), produced accurate results.

In this section, the presentation of the stress results includes plots for the radial moment and shear of the plate M^p_r, V^p_r, in addition to the transverse and twisting shears of the cylinder S^c_z, T^c_z. These four quantities are sufficient to describe the state of stress in the plate and the cylinder since they are related to the other stress resultants M^c_z, N^c_z, N^p_r, N^p_{r0} through the continuity conditions (equations 5.13-5.17)

6.3.1 Axisymmetric junction problem

The problem considered includes a circular cylinder with a radius r_i=0.2, attached to an annular plate resting on tensionless elastic subgrade as shown in figure (6.9). The junction is subjected to a concentric point load (P = 1) that acts at the top of the cylinder. The effect of the system parameters listed in the research objectives will be studied.

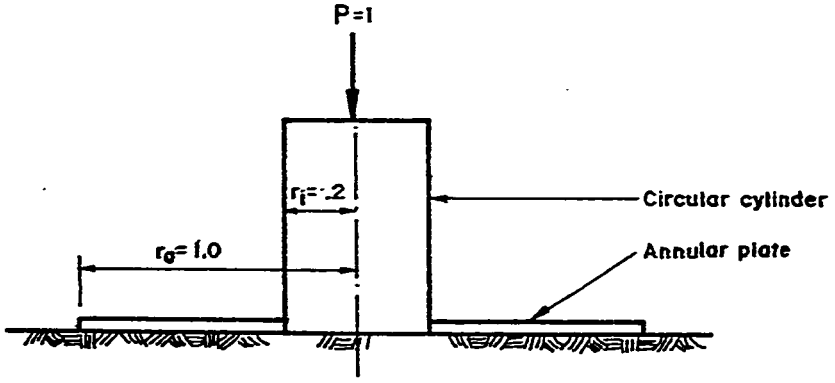

Figure 6.9: Axisymmetric junction problem

Figure (6.10) shows the contact radius r_c against the relative bending stiffness of the cylinder to that of the plate, $D^* = D_c/D_p$, for various dimensionless subgrade stiffness k. It indicates that as expected the contact radius decreases with increasing k. In addition, increasing D^* increases the contact radius which indicates that the cylinder is resisting the partial uplift of the plate from the subgrade.

Figure (6.11) shows the normalized plate displacement kW^p/P along the symmetry axis for various values of k. It shows the significant effect of the subgrade stiffness on the deflected shape. By examining the figure closely, one may observe that as k increases, the radius of contact becomes smaller, which implies that the displacement has to increase to maintain vertical equilibrium.

Figure (6.12) shows the displacement of the plate along the symmetry axis for various thickness ratios $T^* = t_c/t_p$. It shows that the maximum displacement which occurs at the inner edge, decreases when T^* is increased. In addition, the slope of the deflected curve at the inner radius approaches zero. This behavior is not surprising keeping in mind that as T^* becomes larger, the cylinder becomes very rigid in comparison to the plate and thus preventing it from rotation.

Figure (6.13) is a plot of the radial moment in the plate M^p_r versus k, for different values of T^*. It shows that the moment M^p_r is maximum and remain almost constant when the subgrade stiffness k is low.

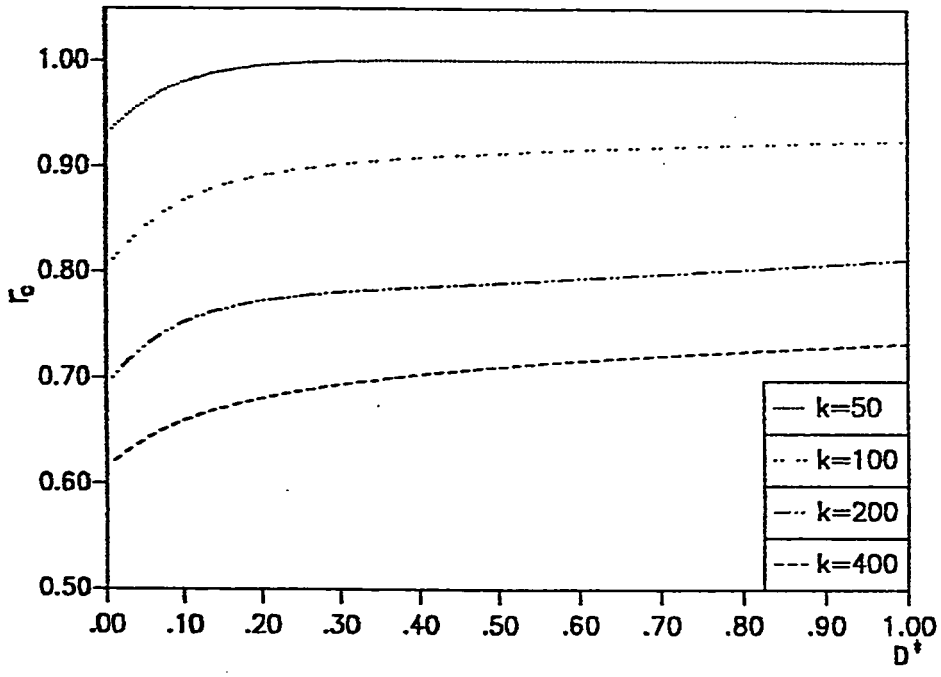

Figure 6.10: Contact radius curves of a cylinder-plate junction resting on tensionless Winkler subgrade subjected to point load P for various subgrade stiffness and and various ratios of D^*, ($r_i = .2$, $r_0 = 1$)

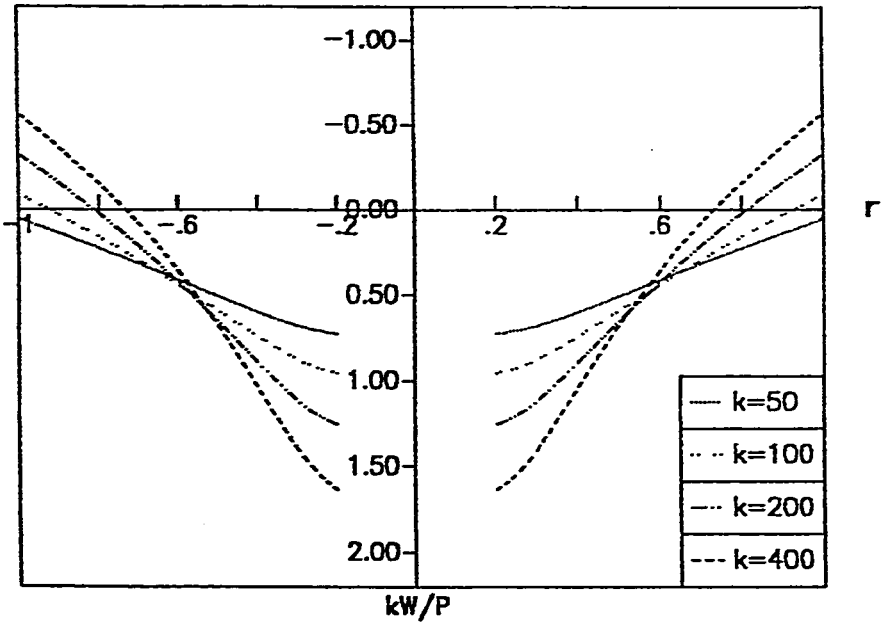

Figure 6.11: Displacement curves along symmetry axis of a cylinder-plate junction resting on tensionless Winkler subgrade subjected to point load P for various subgrade stiffness, ($P = 1$, $r_i = .2$, $r_0 = 1$)

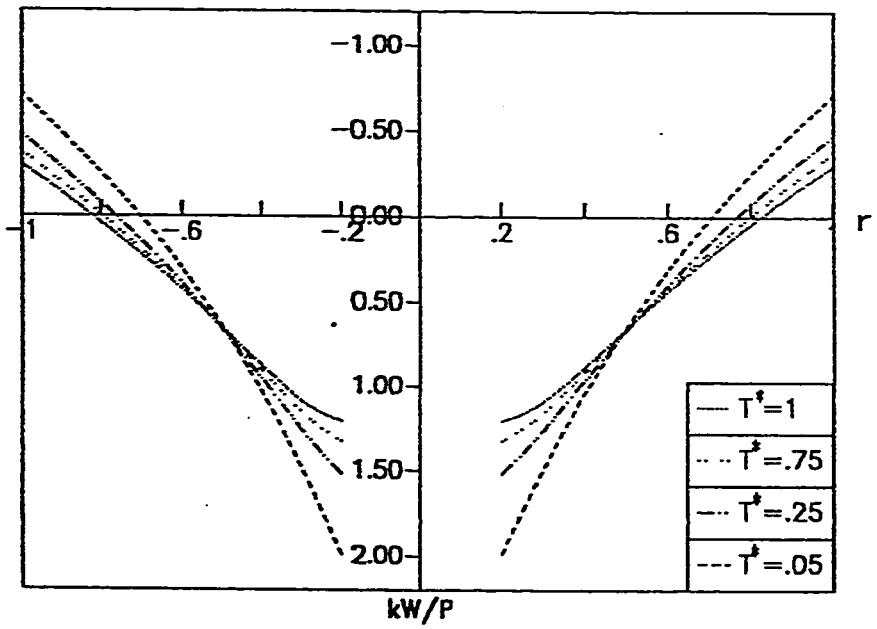

Figure 6.12: Displacement curves along symmetry axis of a cylinder-plate junction resting on tensionless Winkler subgrade subjected to point load P for various thickness ratio T^*, ($P=1$, $r_i=.2$, $r_o=1$, $k=200$)

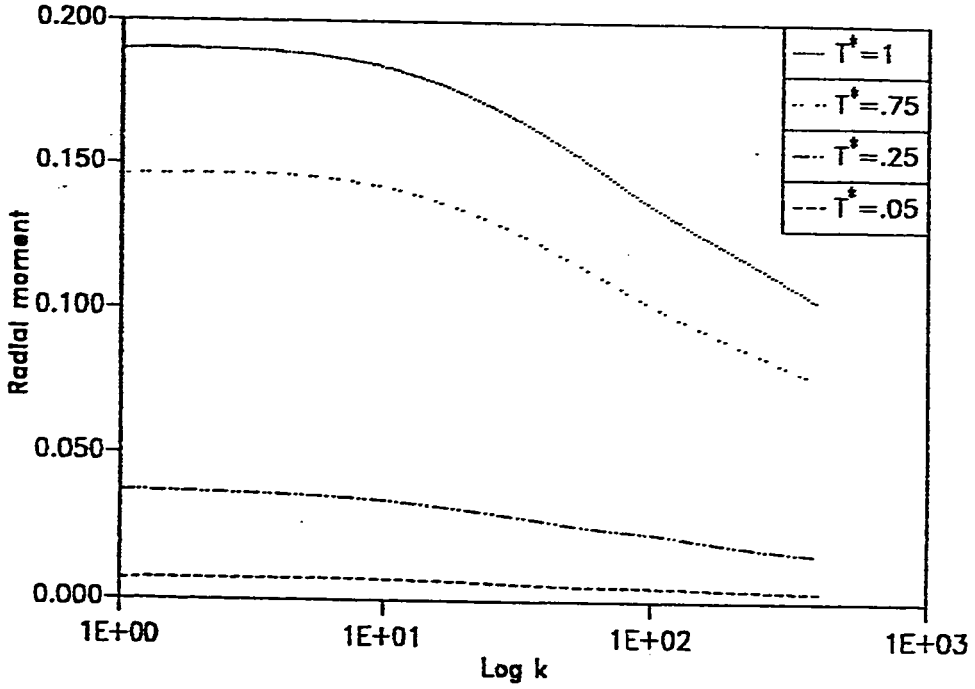

Figure 6.13: Radial moment M_r^P at a cylinder-plate junction resting on tensionless Winkler subgrade subjected to point load P for various subgrade stiffness and various thickness ratio T^*, ($P = 1$, $r_i = .2$, $r_0 = 1$)

In addition, the moment approaches zero as k increases. This behavior could be explained by observing that as the subgrade becomes stiffer the contact zone decreases and it is expected that for infinitely large k, the subgrade acts as an edge support at the inner boundary which makes the moment almost zero.

Figure (6.14) shows the distribution of the transverse shear S^c_z for the same case. It shows that the shear S^c_z exhibits a behavior similar to M^p_r.

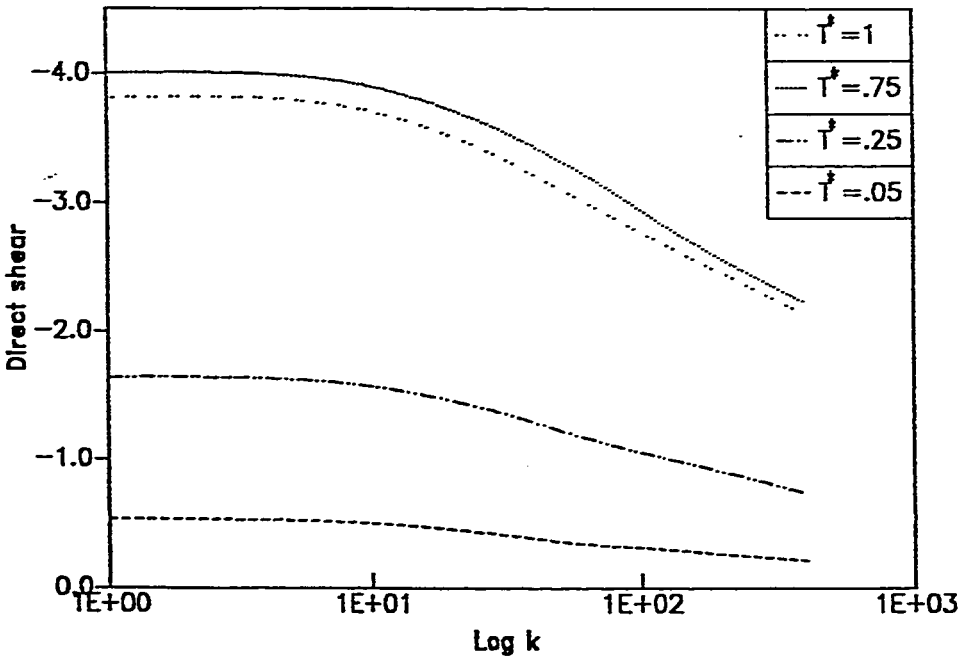

Figure 6.14: Direct shear S_z^c at a cylinder-plate junction resting on tensionless Winkler subgrade subjected to point load P for various subgrade stiffness and and various thickness ratio T^*, ($P=1$, $r_i=.2$, $r_o=1$)

6.3.2 Non-axisymmetric junction problem

In this section, the same plate-junction problem described in section 6.3.1 is subjected to a concentric point load (P = 1) and a point Moment M_0 of different levels as shown in figure (6.15). Through the analysis of this problem, the effect of the system parameters as listed in the objectives are thoroughly investigated.

6.3.2.1 The effect of the eccentricity

The ratio of the applied moment M_0 to the applied load P will be defined as the eccentricity e. In this section, the effect of different values of the eccentricity e on the size and shape of the contact zone as well as on the distribution of the stress resultants will be studied. In addition, the nonlinear behavior of the problem will be discussed.

Figure (6.16.a) shows the contact curves of the plate for different values of e. It indicates that the eccentricity has a very significant effect on the shape and size of the contact zone. Figure (6.16.b) shows the normalized displacement of the plate along the symmetry axis for the same eccentricities. It indicates that the displacement in the contact zone increases moderately with increasing e. However, the displacements increase significantly in the uplifted zone with increasing e. The above described behavior reveals the dominant effect of the applied moment on the overall behavior of the problem. A comparison between the curves in figure (6.16) illustrates very clearly the nonlinearity in the problem. By

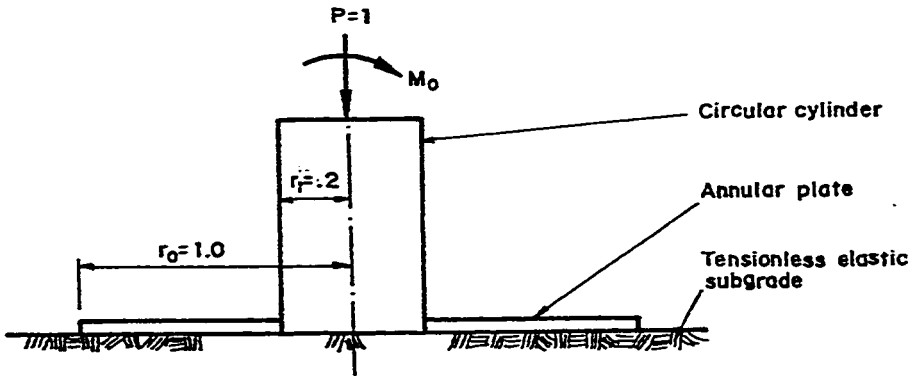

Figure 6.15: Non-axisymmetric junction problem

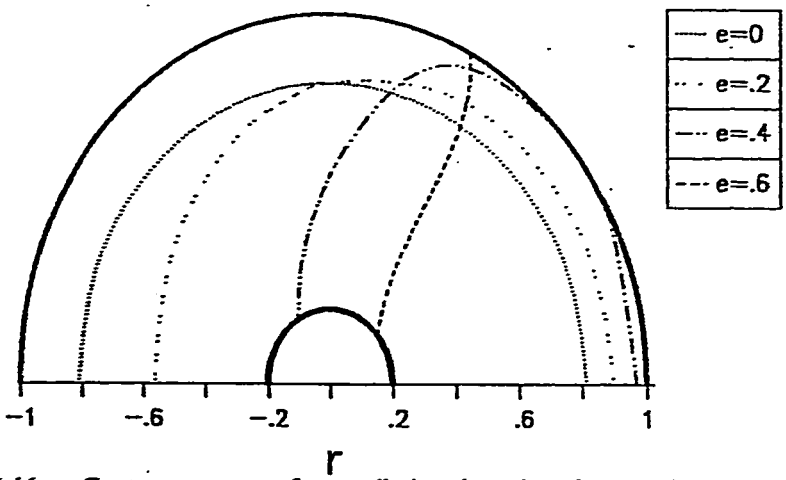

Figure 6.16.a: Contact curves of a cylinder-plate junction resting on tensionless Winkler subgrade subjected to a point load P and a point moment M_0 for various values of eccentricity e, ($P=1$, $r_i=.2$, $r_0=1$, $k=200$)

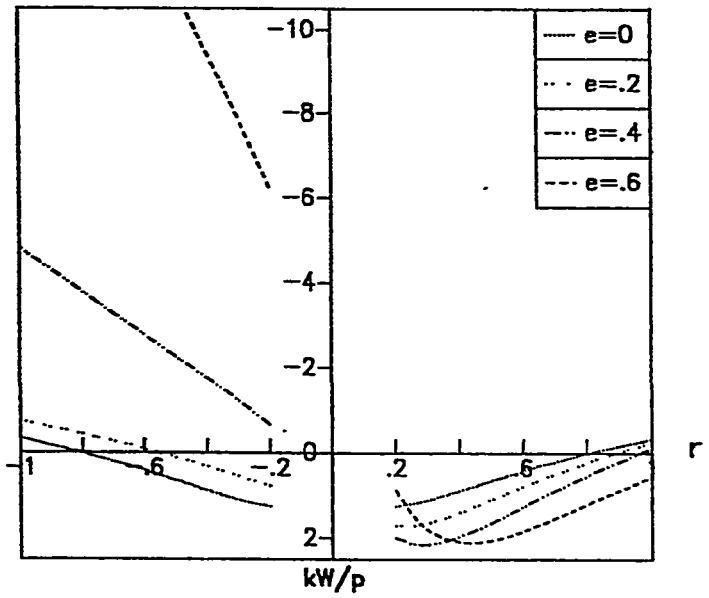

Figure 6.16.b: Displacement curves along symmetry axis of a junction resting on tensionless Winkler subgrade subjected to a point load P and a point moment M_0 for various values of eccentricity e, ($P=1$, $r_i=.2$, $r_0=1$, $k=200$)

doubling the applied moment, the contact zone has been totally changed, and the maximum displacement increased many folds.

It should be pointed out that the maximum eccentricity e which could be handled using this procedure was found to be e=.70, because of numerical difficulties. This maximum value may be considered a reasonable upper limit since it is expected that for higher values, the size of the contact zone become very small, which is not common.

Regarding the distribution of the stress resultants at the junction, figure (6.17) shows the effect of the level of the applied moment M_0 on the distribution of the radial bending moment M^p_r. The figure shows that the maximum value of the radial moment increases significantly with increasing the eccentricity e. Also, the moment starts to become negative at $\theta=\pi$ for moderate and high eccentricities. In addition, the effect of the harmonics $n\geq 2$ on the distribution of the moment is very clear for moderate and high eccentricities while for lower eccentricities, it almost consists of the harmonics n=0 and n=1.

Figure (6.18) shows the different distributions of the radial shear in the plate V^p_r at the junction for different values of e. Similarly, figure (6.19) shows the distribution of the transverse shear in the cylinder S^c_z at the junction. It exhibits the same behavior as the radial moment M^p_r.

Figure (6.20) shows the distribution of the twisting shear in the cylinder

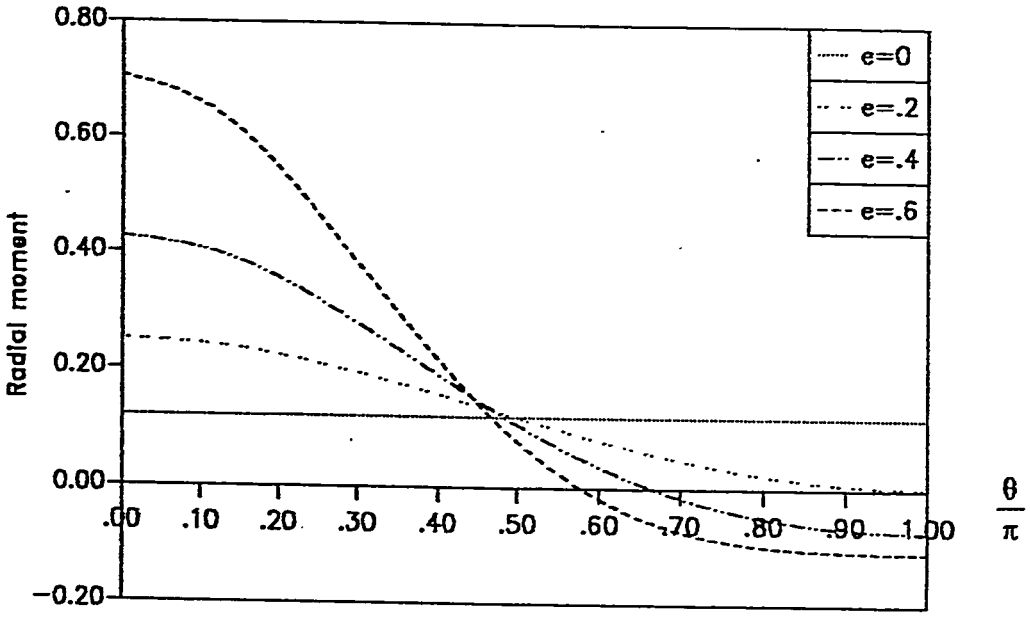

Figure 6.17: Distribution of the radial moment M_r^P of a cylinder-plate junction resting on tensionless Winkler subgrade subjected to point load P and a point moment M_0 for various values of eccentricity e, ($P=1$, $r_i=.2$, $r_e=1$, $k=200$).

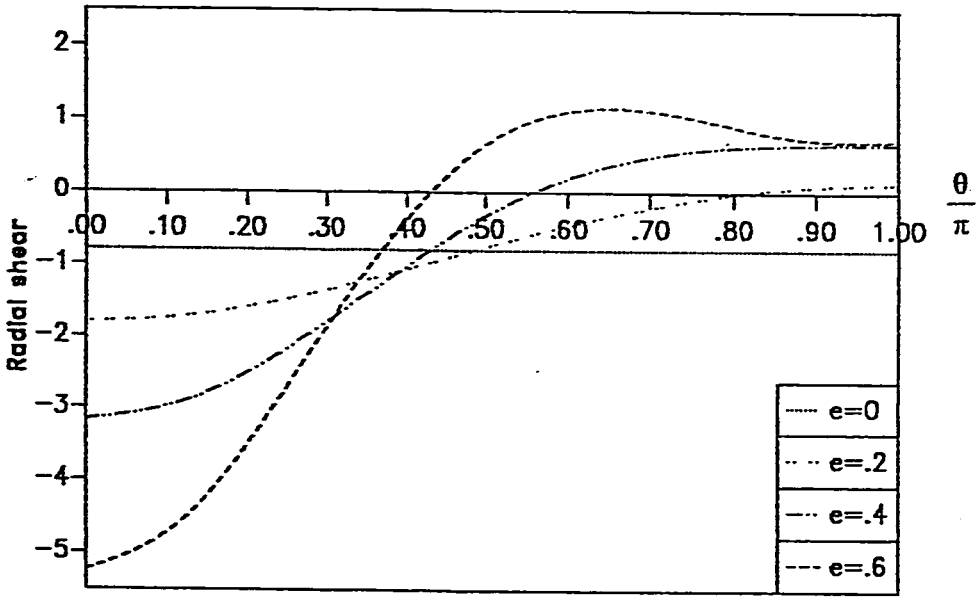

Figure 6.18: Distribution of the radial shear V_r^p of a cylinder-plate junction resting on tensionless Winkler subgrade subjected to point load P and a point moment M_0 for various values of eccentricity e, ($P=1$, $r_i=.2$, $r_0=1$, $k=200$).

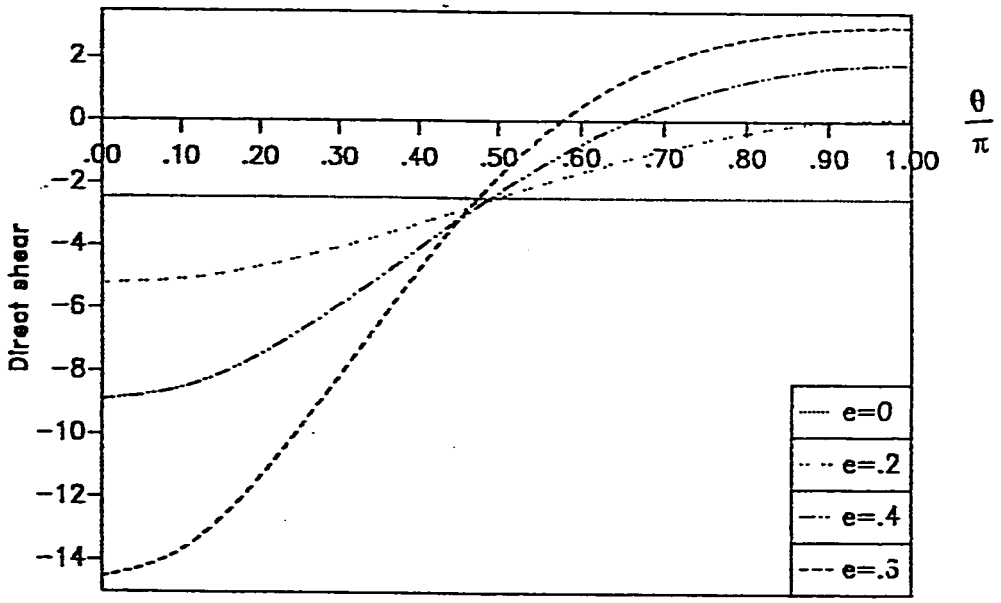

Figure 6.19: Distribution of the direct shear S_z^P of a cylinder-plate junction resting on tensionless Winkler subgrade subjected to point load P and point moment M_0 for various values of eccentricity e, ($P=1, r_i=.2, r_e=1, k=200$).

T^c_z around the cylinder-plate junction. It indicates that the value of the maximum shear increases with increasing e. In addition, this maximum value shifts from the center of the interface for moderate and higher eccentricities which indicates the effect of the higher harmonics $n \geq 2$ and the nonlinear behavior of the problem.

Figure (6.21) shows the distribution of the radial moment M^p_r along the radius of the plate at $\theta = 0$. Similarly, figure (6.22) shows the distribution of the in-plane stress resultant N^p_r along the radius of the plate at $\theta = 0$. It shows that N^p_r is decaying along the radius to be almost zero at the outer boundary, which is in agreement with the assumption made earlier in section 5.3 indicating that the plate is considered infinite.

To understand the convergence of the plate-cylinder junction problem, figure (6.23) shows the convergence of the resultant vertical force of the subgrade reaction. It shows that the resultant force of the subgrade reaction converges to the value of the applied load ($P = 1$) within 5 iterations. In addition, figure (6.24) shows the convergence for the resultant moment of the subgrade reaction about the center of the plate. It indicates also that this resultant moment approaches the same value of the applied moment ($M_0 = .4$) also within 5 iterations.

Figures (6.25) and (6.26) show the convergence of the contact zone and the displacement curve along the axis of symmetry, respectively. All the previous figures indicate that the approach is numerically stable and converges rapidly without any serious problems.

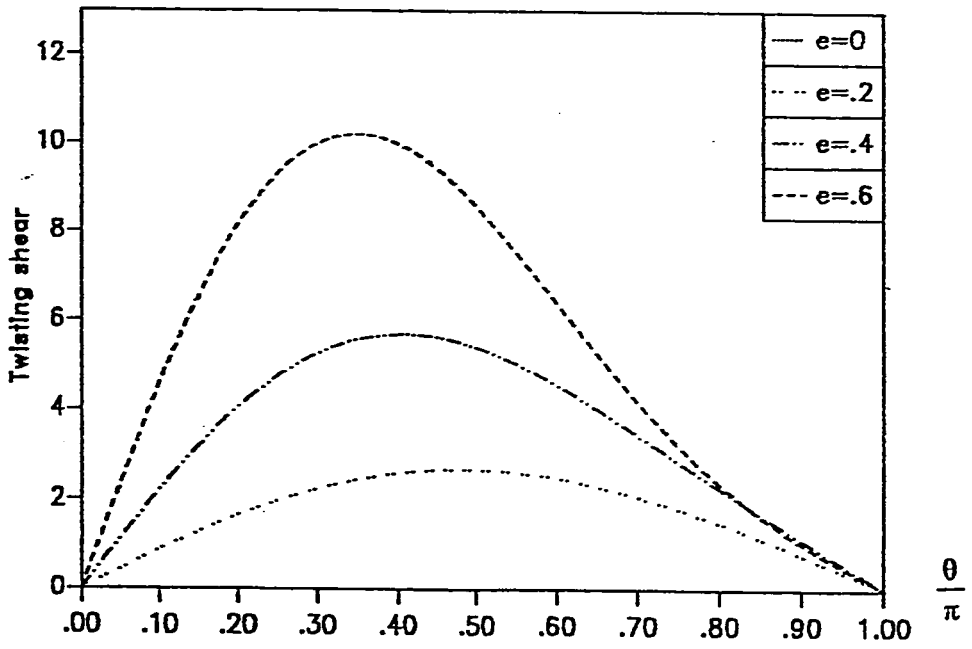

Figure 6.20: Distribution of the twisting shear T_z^c of a cylinder-plate junction resting on tensionless Winkler subgrade subjected to point load P and point moment M_0 for various values of eccentricity e, ($P=1, r_i=.2, r_e=1, k=200$).

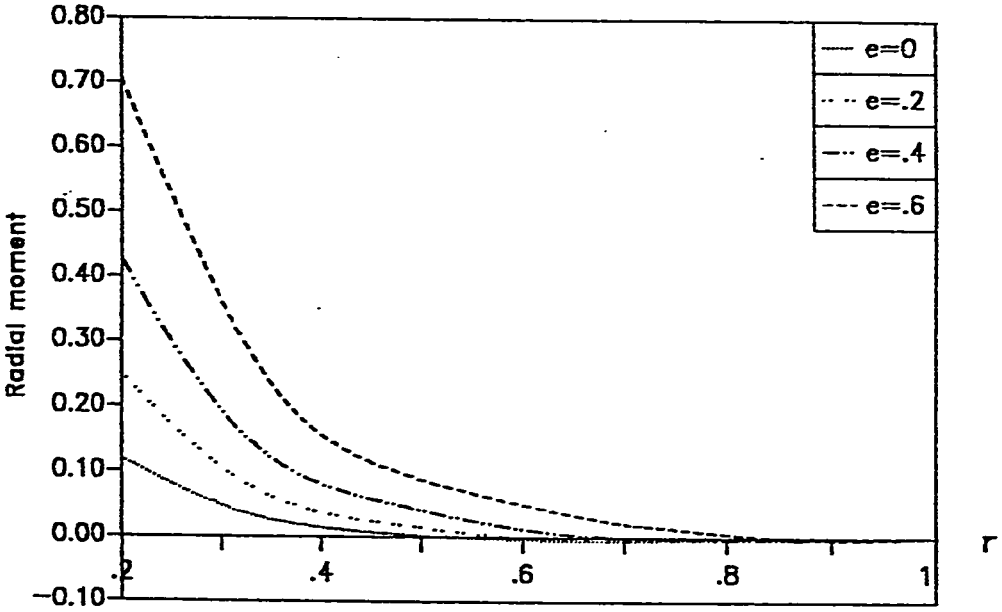

Figure 6.21: Radial moment M_r^P along the radius at $\theta = 0$ of a cylinder-plate junction resting on tensionless Winkler subgrade subjected to point load P and a point moment M_0 for various values of eccentricity e, ($P = 1$, $r_i = .2$, $r_0 = 1$, $k = 200$).

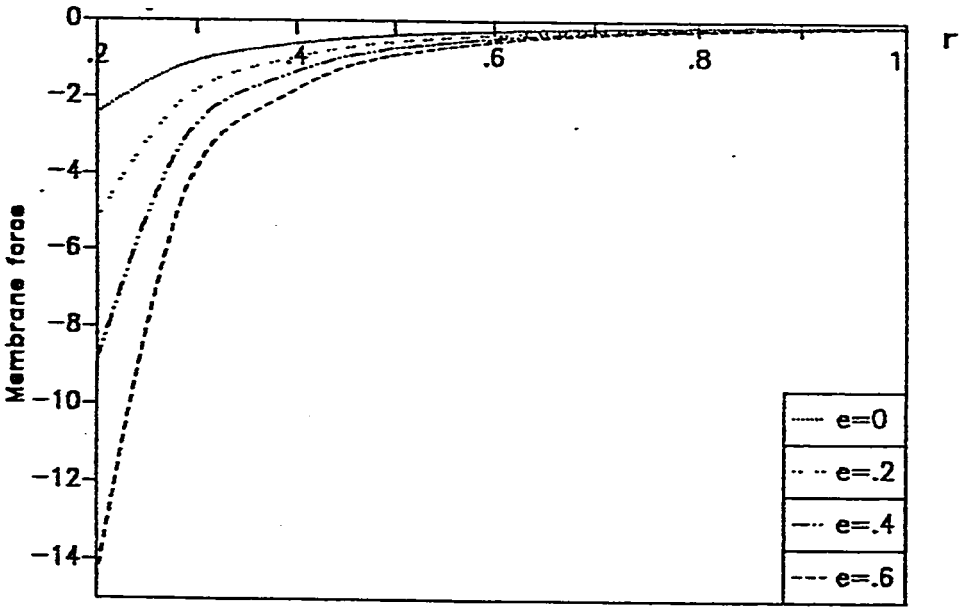

Figure 6.22: Stress resultant N_r^P along a radius at $\theta = 0$ of a cylinder-plate junction resting on tensionless Winkler subgrade subjected to point load P and a point moment M_0 for various values of eccentricity e, ($P = 1$, $r_i = .2$, $r_0 = 1$, $k = 200$).

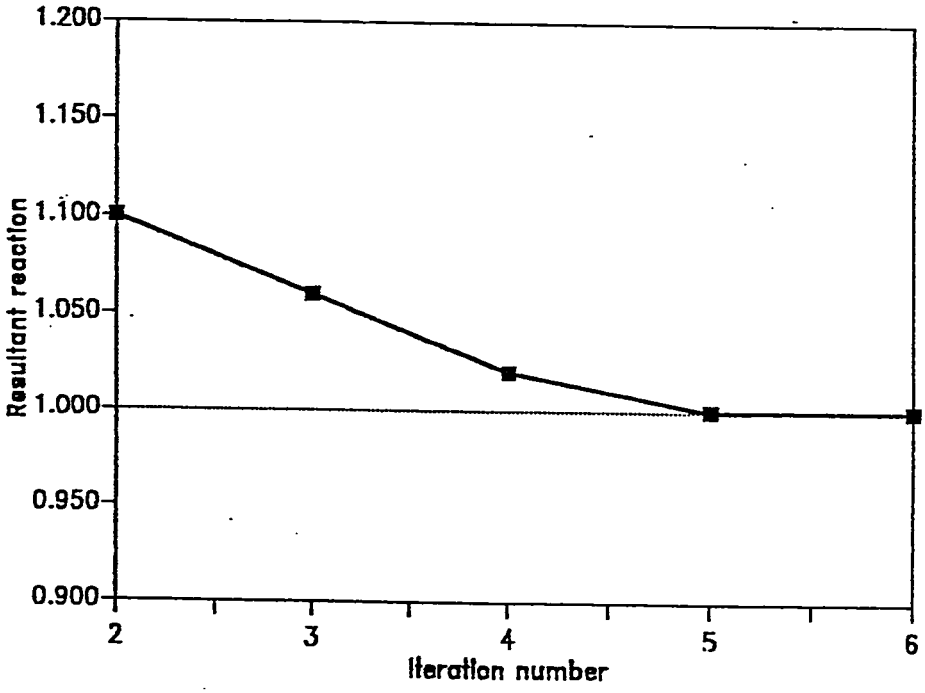

Figure 6.23: Convergence of the resultant of the subgrade reaction for a cylinder-plate junction resting on tensionless Winkler subgrade subjected to point load P and point moment M_0 for various iteration number, ($P = 1$, $M_0 = .4$, $r_i = .2$, $r_0 = 1$, $k = 200$).

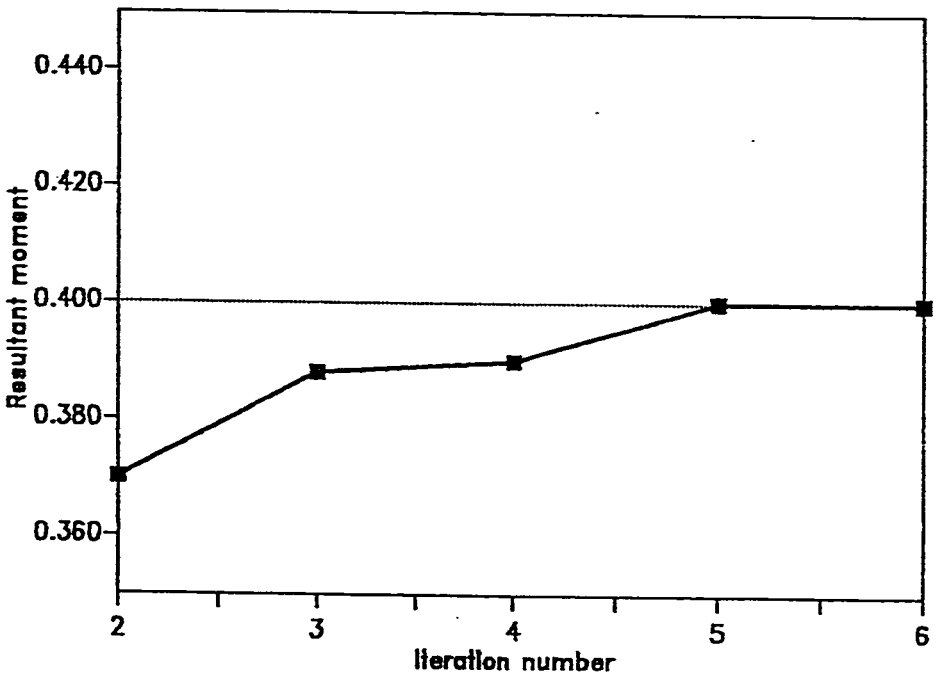

Figure 6.24: Convergence of the moment resultant of the subgrade reaction about the center of a cylinder-plate junction resting on tensionless Winkler subgrade subjected to point load P and point moment M_0 for various iteration number, ($P=1$, $M_0=.4$, $r_i=.2$, $r_0=1$, $k=200$).

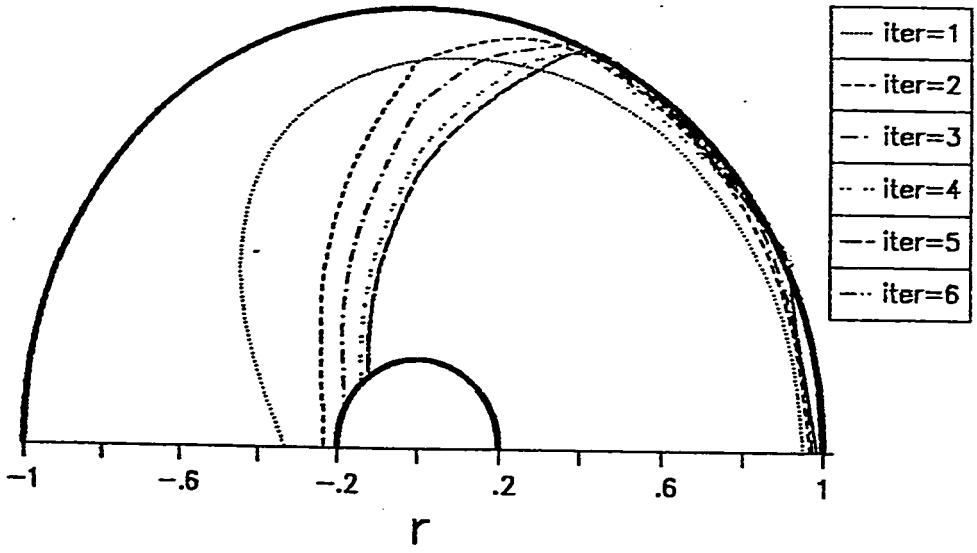

Figure 6.25: Convergence of the contact curve for a cylinder-plate junction resting on tensionless Winkler subgrade subjected to point load P and point moment M_0 for various iteration number, ($P = 1$, $M_0 = .4$, $r_i = .2$, $r_0 = 1$, $k = 200$).

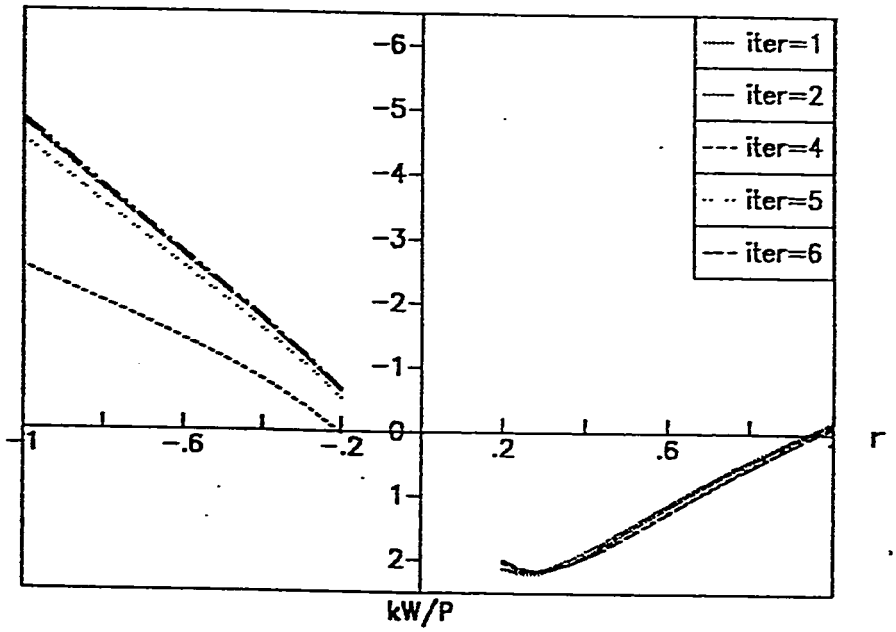

Figure 6.26: Convergence of the displacement for a cylinder-plate junction resting on tensionless Winkler subgrade subjected to point load P and point moment M_0 for various iteration number, ($P = 1$, $M_0 = .4$, $r_i = .2$, $r_0 = 1$, $k = 200$).

To investigate the distribution of the stresses at the junction, the following equations represent the radial and hoop stresses in the plate and the cylinder $\sigma^p_r, \sigma^p_\theta, \sigma^c_z, \sigma^c_\theta$, evaluated at the top and bottom surfaces of the plate in addition to the inner and outer surfaces of the cylinder; as follows:

$$(\sigma^p_r)^{bot}_{top} = \frac{N^p_r}{t_p} \pm \frac{6\,M^p_r}{t_p^2} \tag{6.1}$$

$$(\sigma^p_\theta)^{bot}_{top} = \frac{N^p_\theta}{t_p} \pm \frac{6\,M^p_\theta}{t_p^2} \tag{6.2}$$

$$(\sigma^c_z)^{in}_{out} = \frac{N^c_z}{t_c} \pm \frac{6\,M^c_z}{t_c^2} \tag{6.3}$$

$$(\sigma^c_\theta)^{in}_{out} = \frac{N^c_\theta}{t_c} \pm \frac{6\,M^c_\theta}{t_c^2} \tag{6.4}$$

Figures (6.27) and (6.28) show the distribution of the radial and hoop stresses at the top edge of the plate for the membrane force and the bending moment separately. The figures indicate that the membrane stresses are small compared to the bending stresses. Figures (6.29) and (6.30) show the equivalent distributions for the cylinder considering that $T^* = 1$. By comparing figures (6.27)-(6.30), one may notice that the bending component of the radial stress in the plate is the same as the bending component of the axial stress in the cylinder. On the other hand, the hoop stress in the plate is different from the hoop stress in the cylinder. This can be explained by recalling that the continuity equations at the junction apply in the radial direction only, and not in the hoop direction.

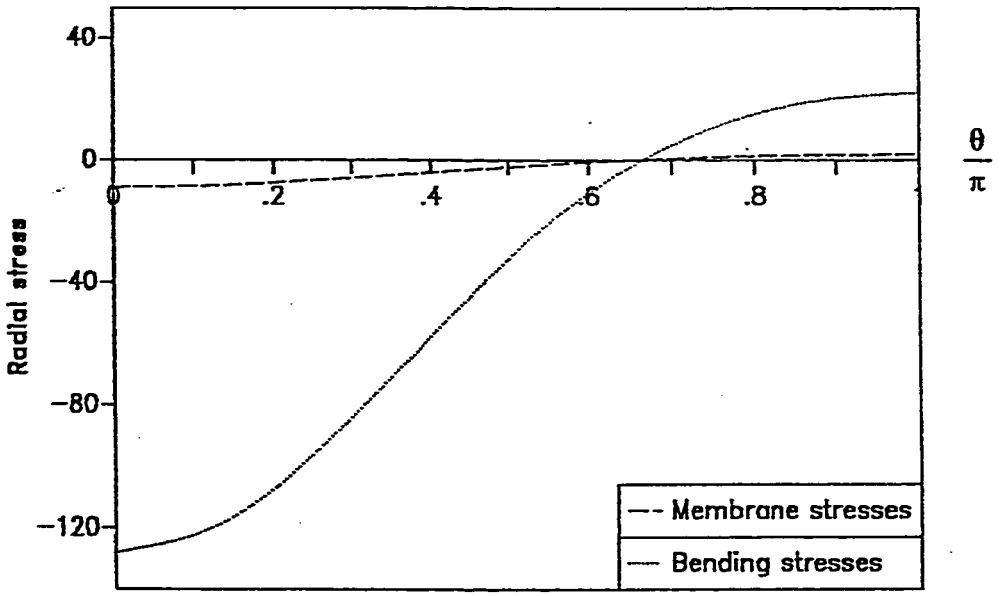

Figure 6.27: Distribution of the bending and membrane radial stresses at the top fibre of a plate of cylinder-plate junction resting on tensionless Winkler subgrade subjected to point load P and a point moment M_0 ($P=1$, $M_0=.4$, $r_i=.2$, $r_e=1$, $k=200$).

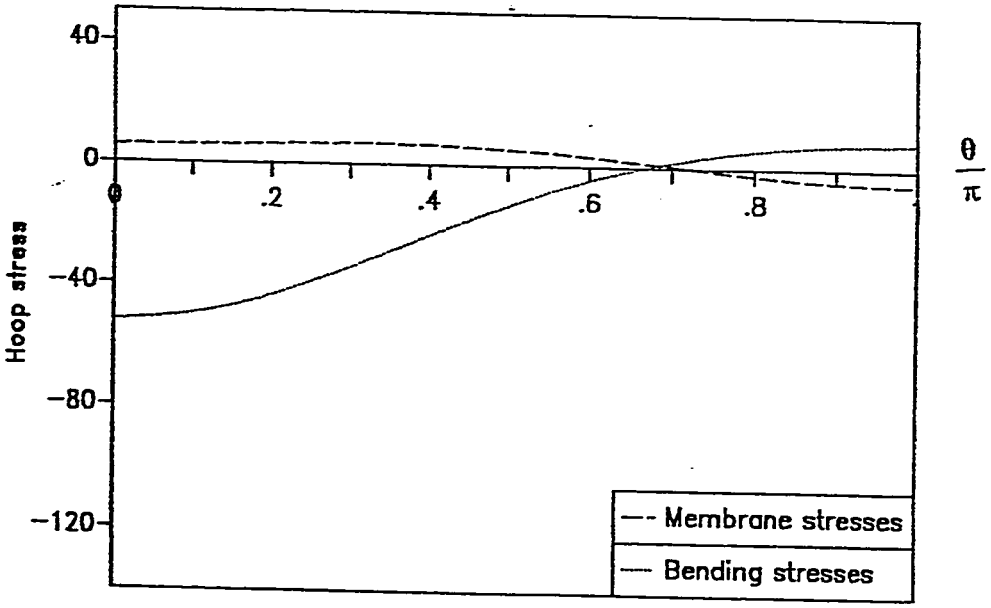

Figure 6.28: Distribution of the bending and membrane hoop stresses at the top fibre of a plate of a cylinder-plate junction resting on tensionless Winkler subgrade subjected to point load P and a point moment M_0, ($P = 1$, $M_0 = .4$, $r_i = .2$, $r_0 = 1$, $k = 200$).

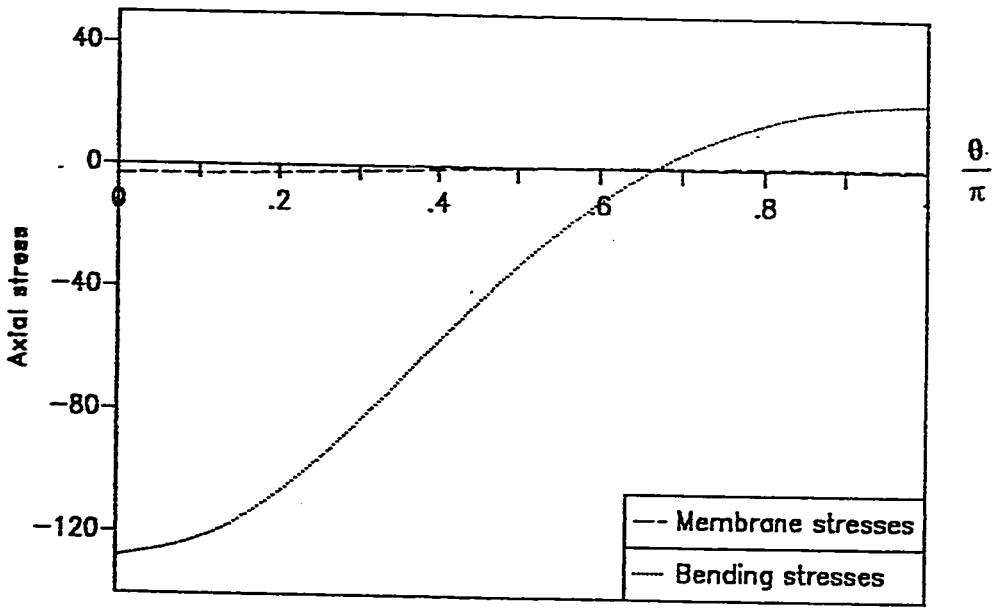

Figure 6.29: Distribution of the axial bending and membrane stresses at the outer fibre of a cylinder of a cylinder-plate junction resting on tensionless Winkler subgrade subjected to point load P and a point moment M_0, ($P=1$, $M_0=.4$, $r_i=.2$, $r_0=1$, $k=200$).

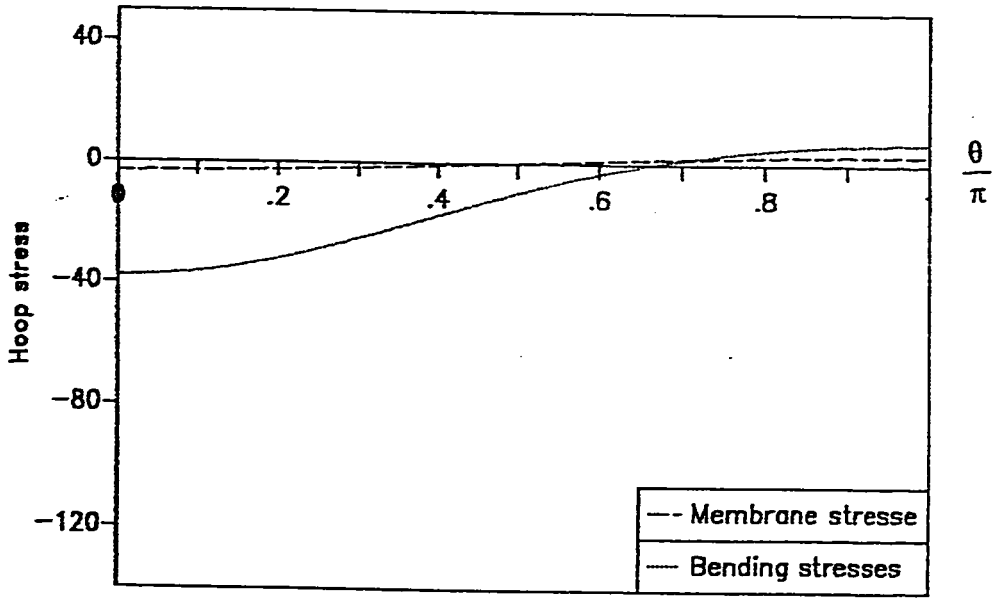

Figure 6.30: Distribution of the hoop bending and membrane stresses at the outer fibre of a cylinder of a cylinder-plate junction resting on tensionless Winkler subgrade subjected to point load P and a point moment M_0, ($P=1$, $M_0=.4$, $r_i=.2$, $r_0=1$, $k=200$).

6.3.2.2 The effect of the subgrade stiffness

Figure (6.31.a) shows the contact curves when the eccentricity e=0.2. It shows that the contact zone is almost a circle for different values of k. Figure (6.31.b) shows the displacement along the symmetry axis which indicates that the variation of the displacement in the contact zone is higher in comparison with the displacement of the uplifted zone.

Figure (6.32.a) shows the contact curves of the plate for various subgrade stiffness when the eccentricity e is increased to 0.4. It shows that the size of the contact zone is reduced for stiffer subgrade, which is in agreement with the results obtained earlier for the axisymmetric problem. Figure (6.32.b) shows plots for the displacement of the plate along the axis of symmetry. It indicates small variations in the displacement within the contact zone for different values of k, while the displacement in the uplifted zone increases steeply for stiffer subgrades. This behavior shows the sensitivity of the contact zone and the displacements to the subgrade stiffness parameter k. An inspection of figures (6.31) and (6.32) illustrates clearly the nonlinear effect of the subgrade on the problem. It shows the different behavior for the contact zone and the displacement due to doubling the applied moment.

In this section the analysis of the stresses will concentrate on the distribution of the radial moment M_r^p which is the most significant component of the junction stresses. Figures (6.33) and (6.34) shows the distribution of the radial moment M_r^p when e=0.2 and e=0.4 respectively.

It may be noticed that the effect of the subgrade stiffness on the distribution of the moment is much more pronounced for the lower eccentricity because the contact zone is more sensitive to changes in k.

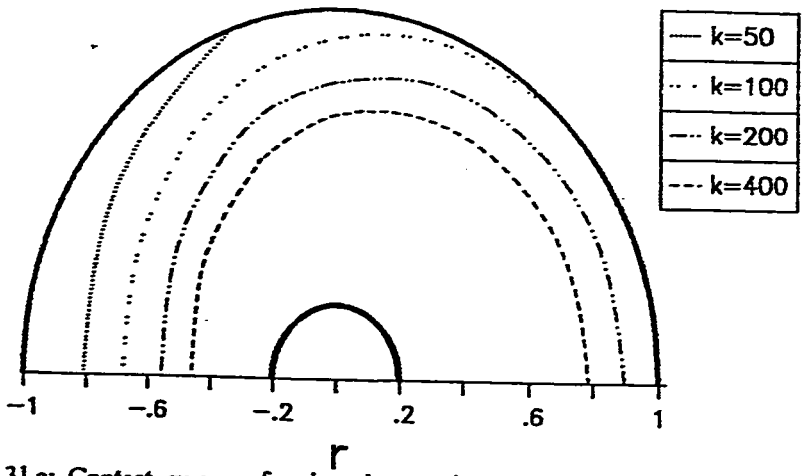

Figure 6.31.a: Contact curves of a junction resting on tensionless Winkler subgrade subjected to point load P and point moment M_0 for various subgrade stiffness, ($P = 1$, $M_0 = .2$, $r_i = .2$, $r_0 = 1$)

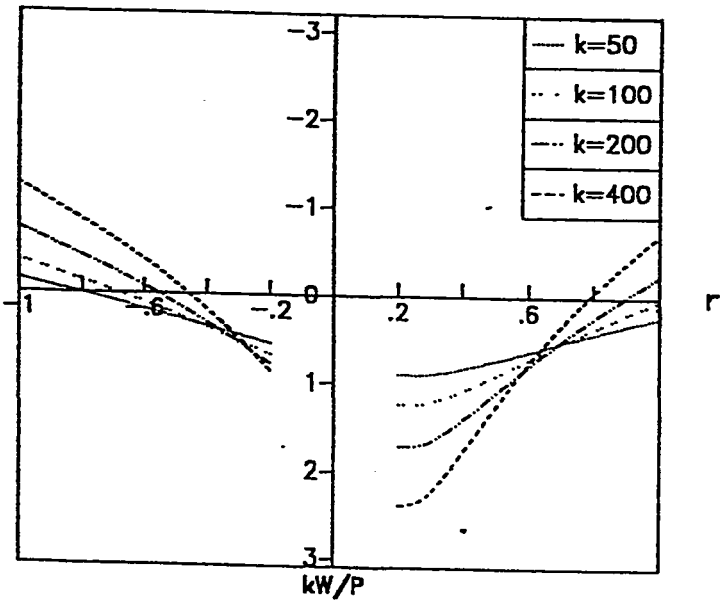

Figure 6.31.b: Displacement curves along symmetry axis of a junction resting on tensionless Winkler subgrade subjected to a point load P and a point moment M_0 for various subgrade stiffness, ($P = 1$, $M_0 = .2$, $r_i = .2$, $r_0 = 1$)

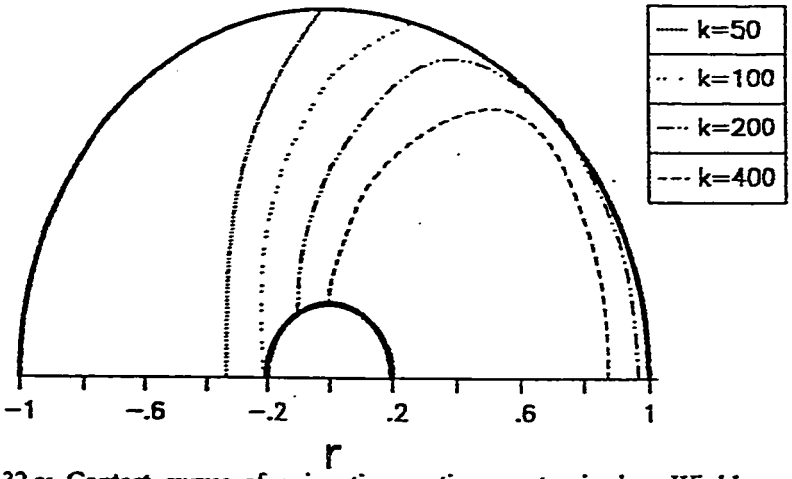

Figure 6.32.a: Contact curves of a junction resting on tensionless Winkler subgrade subjected to point load P and point moment M_0 for various subgrade stiffness, ($P = 1$, $M_0 = .4$, $r_i = .2$, $r_0 = 1$)

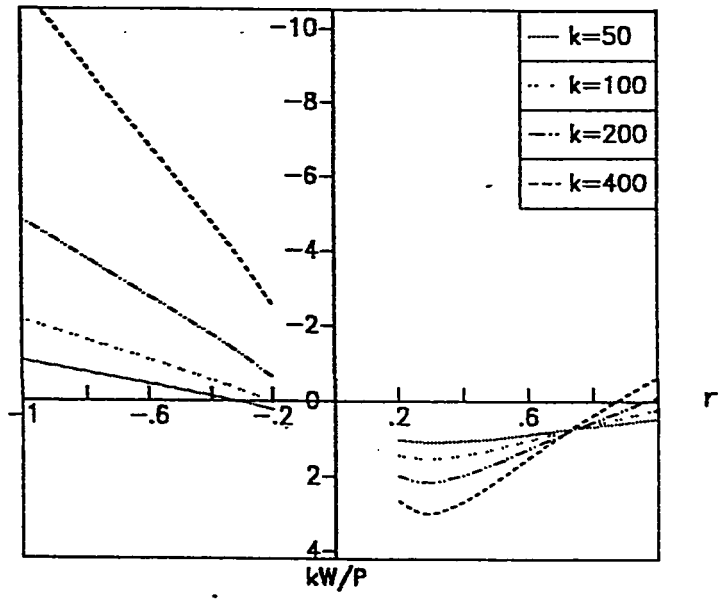

Figure 6.32.b: Displacement curves along symmetry axis of a junction resting on tensionless Winkler subgrade subjected to point load P and point moment M_0 for various subgrade stiffness, ($P = 1$, $M_0 = .4$, $r_i = .2$, $r_0 = 1$)

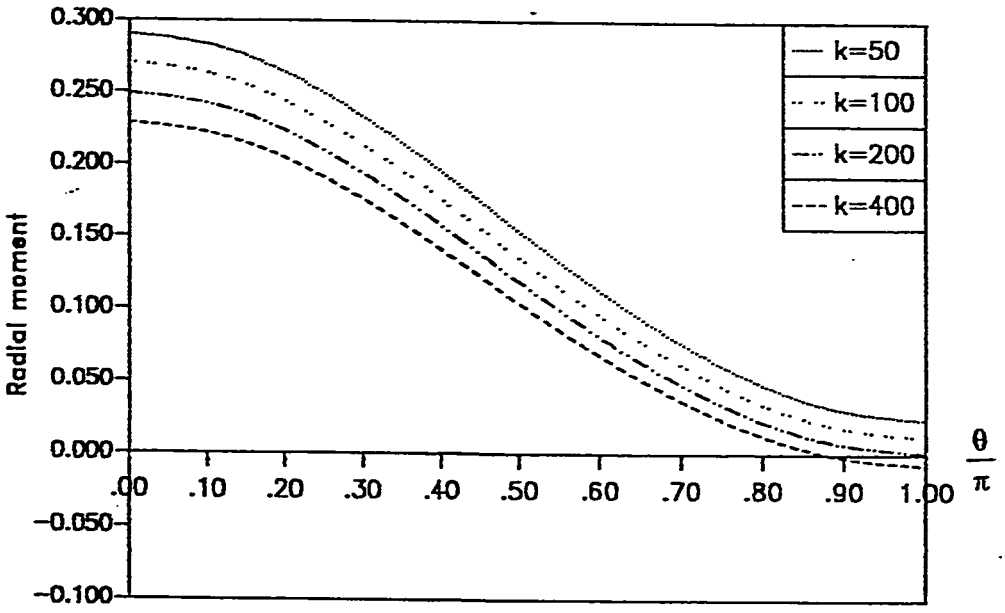

Figure 6.33: Distribution of the radial moment M_r^p of a cylinder-plate junction resting on tensionless Winkler subgrade subjected to point load P and a point moment M_0 for various subgrade stiffness, ($P = 1$, $M_0 = .2$, $r_i = .2$, $r_0 = 1$,).

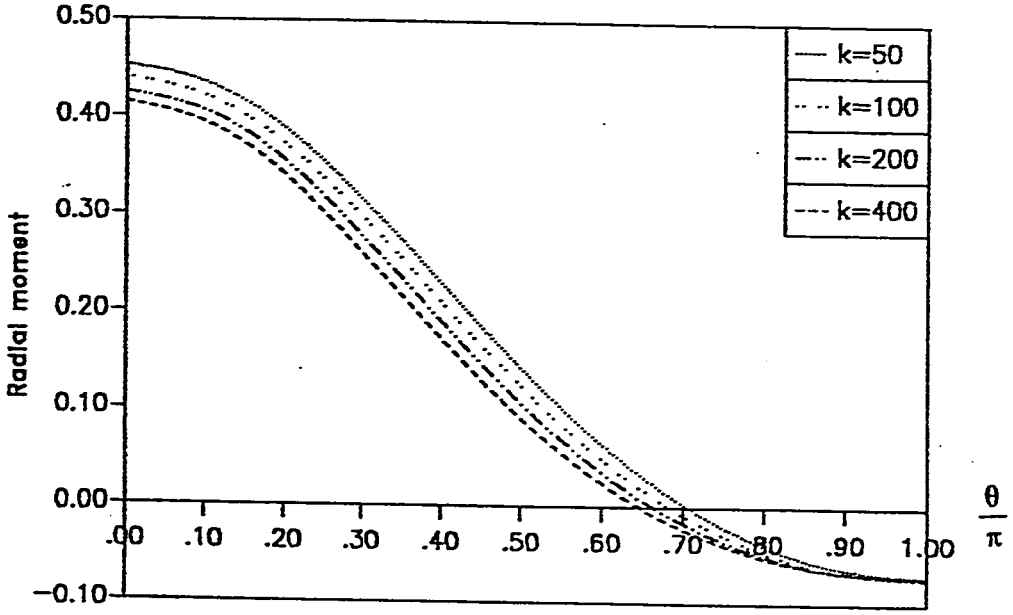

Figure 6.34: Distribution of the radial moment M_r^P of a cylinder-plate junction resting on tensionless Winkler subgrade subjected to point load P and a point moment M_0 for various subgrade stiffness, ($P=1$, $M_0=.4$, $r_i=.2$, $r_0=1$,).

6.3.2.3 The effect of the cylinder stiffness

Figure (6.35.a) shows the contact curves of the plate for different values of the thickness ratio T^*, for the case when k=200. It indicates that the contact zone increase as the cylinder becomes stiffer, which is in agreement with the axisymmetric case. Figure (6.35.b) shows the displacement along the symmetry axis of the plate. It shows the significant effect of a stiffer cylinder on reducing the displacement in the plate especially in the uplifted zone.

Figures (6.36.a,b) show the equivalent results when k=50. Figures (6.37) and (6.38) show the distribution of the radial moment in the plate M^p_r for k=200 and k=50 for different thickness ratios T^*.

To have a general idea about the effect of the different parameters on the non-axisymmetric problem, figure (6.39) shows plots of the ratio of the maximum radial moment M^p_r at the junction at $\theta=0$ over the maximum moment which occur at a very low subgrade stiffness for various values of subgrade stiffness and eccentricity. This ratio will be defined as M^*_{max}. The figure shows that the ratio M^*_{max} increases with increasing the eccentricity e. By examining the results for the different eccentricities, one may conclude that for very weak subgrades, the subgrade stiffness does not affect the moment in the plate. However, in the case of stiffer subgrades, the value of k plays a significant role especially for small eccentricities.

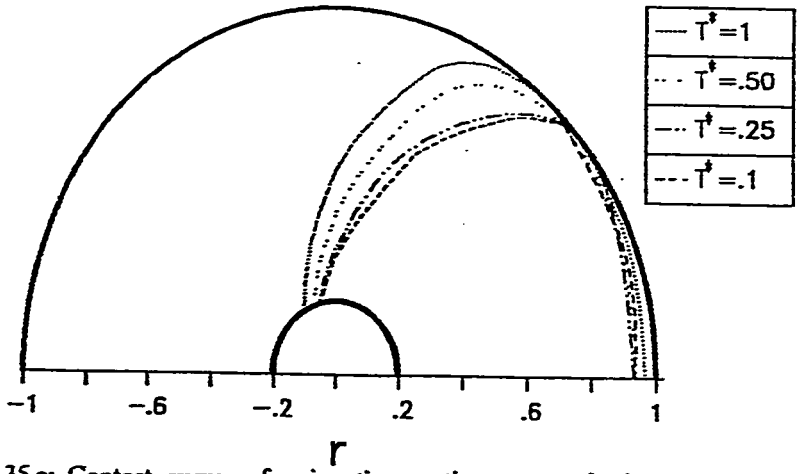

Figure 6.35.a: Contact curves of a junction resting on tensionless Winkler subgrade subjected to point load P and point moment M_0 for various thickness ratio T^*, ($P=1$, $M_0=.4$, $r_i=.2$, $r_0=1$, $k=200$)

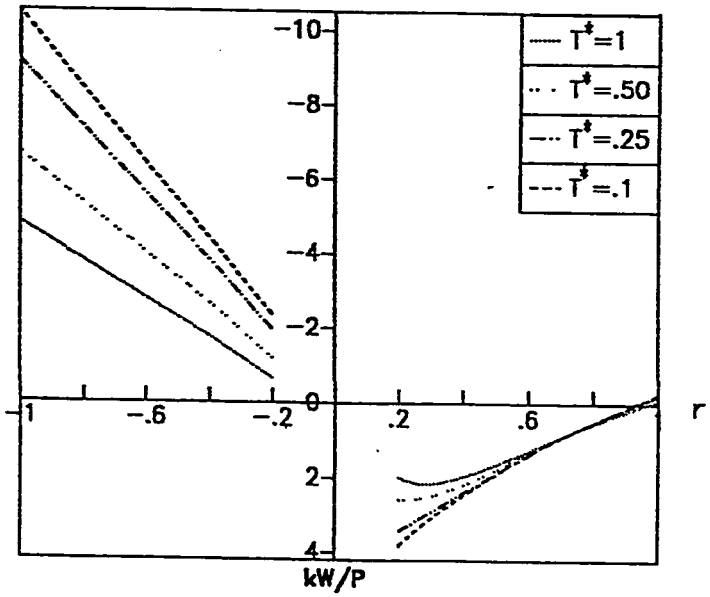

Figure 6.35.b: Displacement curves along symmetry axis of a junction resting on tensionless Winkler subgrade subjected to point load P and point moment M_0 for various thickness ratio T^*, ($P=1$, $M_0=.4$, $r_i=.2$, $r_0=1$, $k=200$)

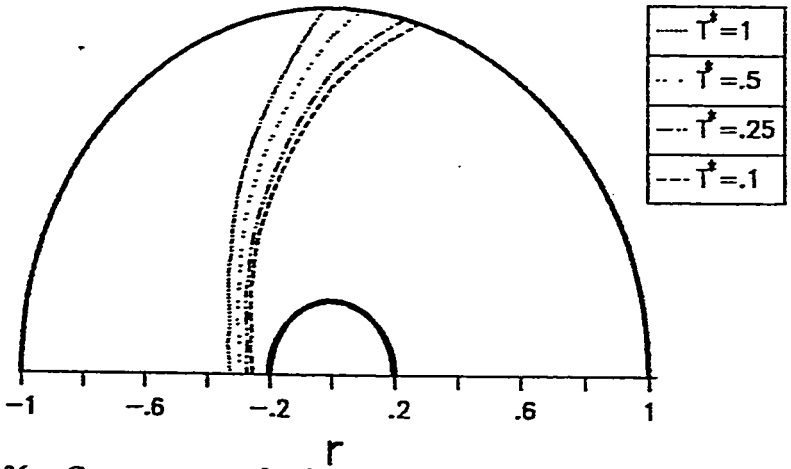

Figure 6.36.a: Contact curves of a junction resting on tensionless Winkler subgrade subjected to point load P and point moment M_0 for various thickness ratio T*, (P = 1, M_0 = .4, r_i = .2, r_0 = 1, k = 50)

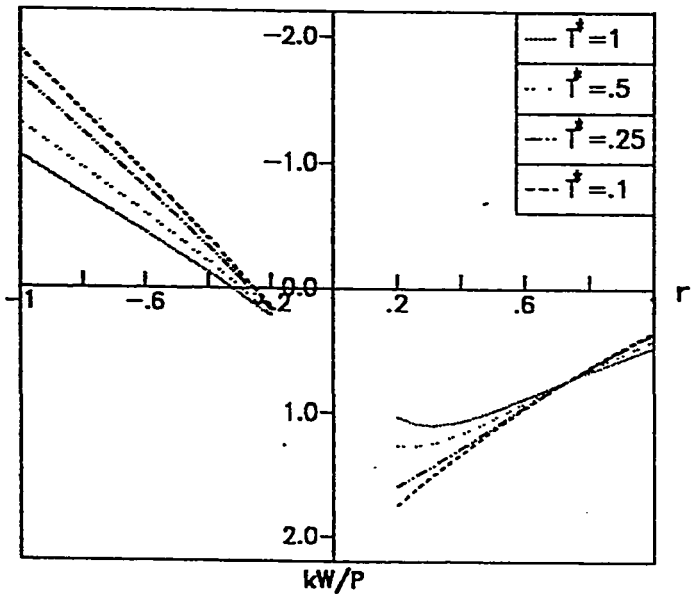

Figure 6.36.b: Displacement curves along symmetry axis of a junction resting on tensionless Winkler subgrade subjected to point load P and point moment M_0 for various thickness ratio T*, (P = 1, M_0 = .4, r_i = .2, r_0 = 1, k = 50)

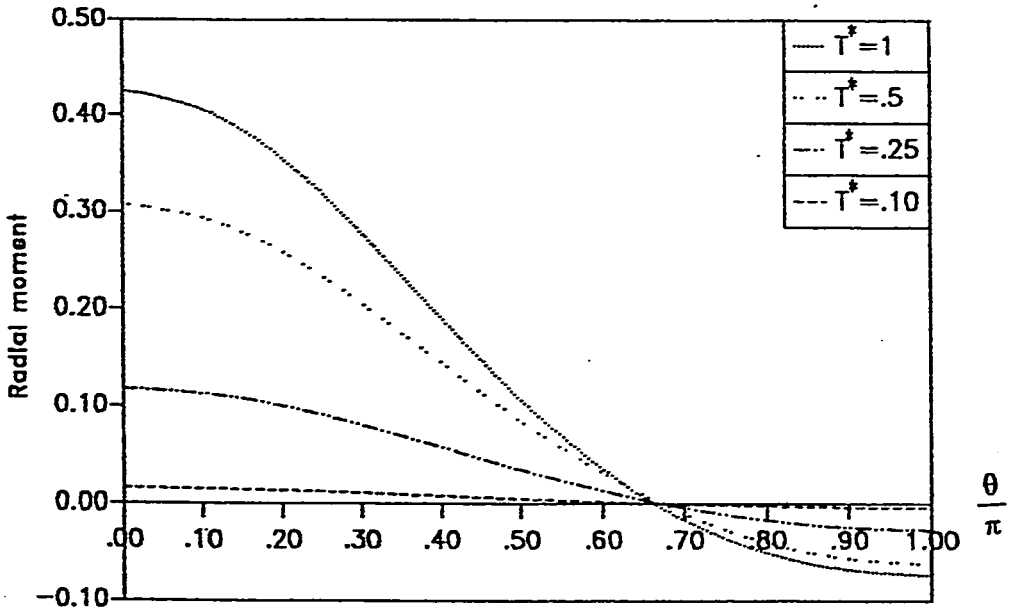

Figure 6.37: Distribution of the radial moment M_r^p at the interface of cylinder-plate junction resting on tensionless Winkler subgrade subjected to point load P and point moment M_0 for various thickness ratio T^*, (P = 1, M_0 = .4, r_i = .2, r_0 = 1, k = 200).

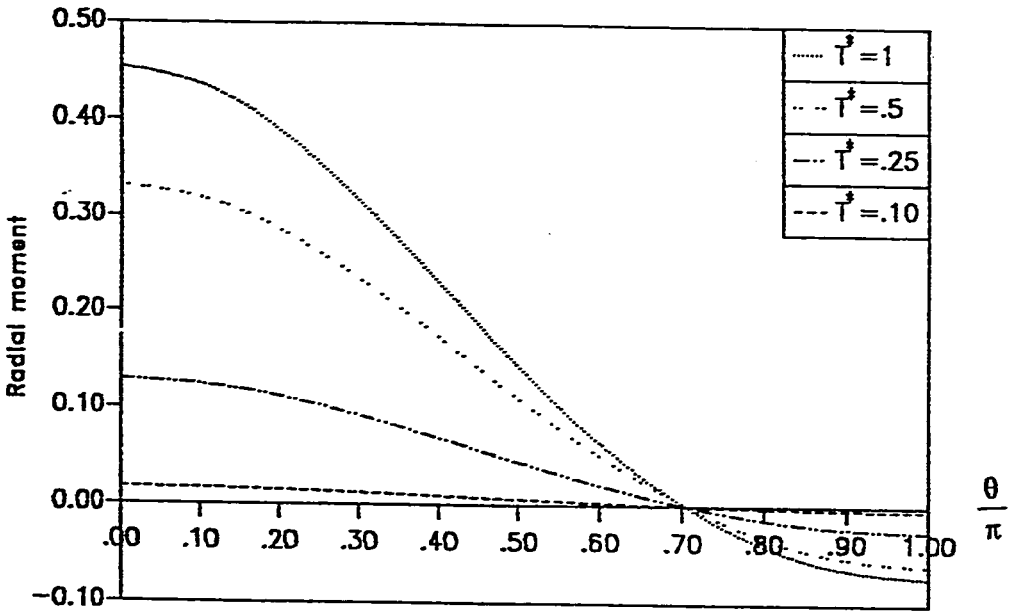

Figure 6.38: Distribution of the radial moment M_r^p of a cylinder-plate junction resting on tensionless Winkler subgrade subjected to point load P and point moment M_o for various thickness ratio T^*, ($P=1$, $M_o=.4$, $r_i=.2$, $r_o=1$, $k=50$).

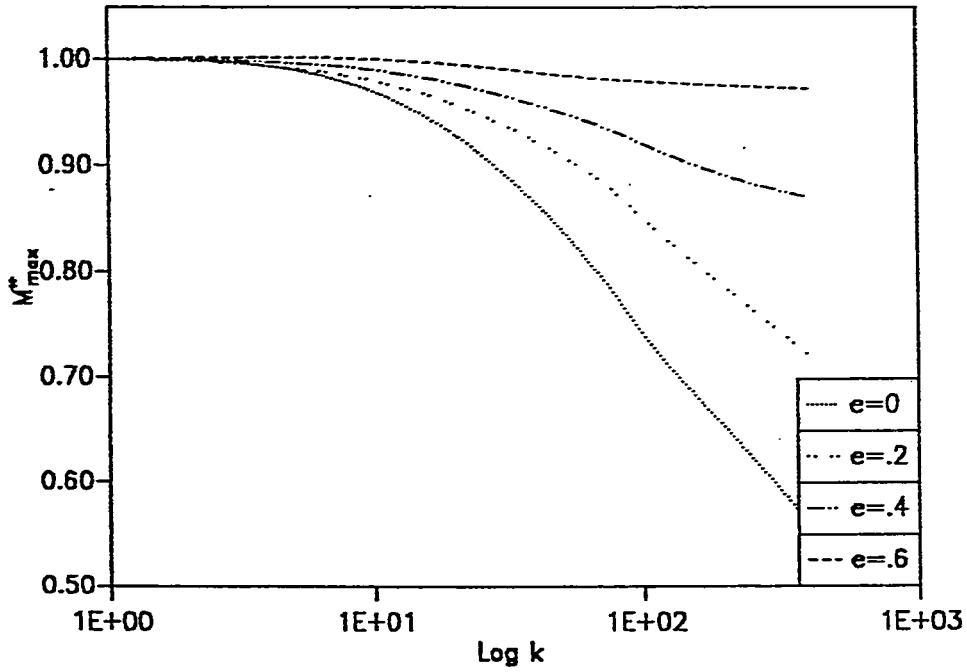

Figure 6.39: Ratio of the relative maximum radial moment M^*_{max} of a cylinder-plate junction resting on tensionless Winkler subgrade subjected to point load P and point moment M_0 for various subgrade stiffness and various levels of the applied moment M_0, ($P = 1$, $r_i = .2, r_e = 1$).

To summarize the effect of the system parameters on the nonlinear behavior of the problem, figure (6.40) shows plots for the edge displacement, kW_e/P, of the plate for various subgrade stiffness k and eccentricity e. It shows that the problem exhibits a linear behavior for small eccentricities and weak subgrade where the plate is in full contact with the subgrade. However, the behavior is nonlinear for most of the values of the subgrade stiffness k and and the eccentricity e.

Figure (6.41) shows plots for the ratio of the area of the contact zone to that of the plate domain, A^*, for different subgrade stiffness k and eccentricity e. It indicates that the relative area, A^*, becomes smaller for higher eccentricities. This behavior may explain the reason that higher eccentricities ($e>0.7$) can not be handled through the numerical analysis of this research.

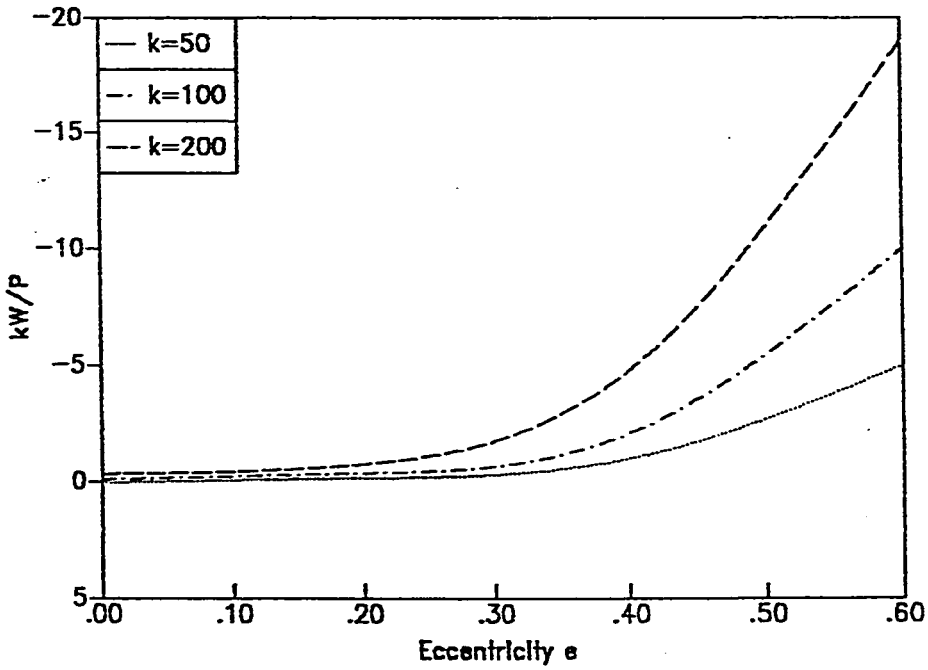

Figure 6.40: Maximum edge displacement kW_e/P of the plate of a cylinder-plate junction resting on tensionless Winkler subgrade subjected to point load P and point moment M_0 for various subgrade stiffness and various levels of the applied moment M_0, ($P = 1$, $r_1 = .2$, $r_0 = 1$).

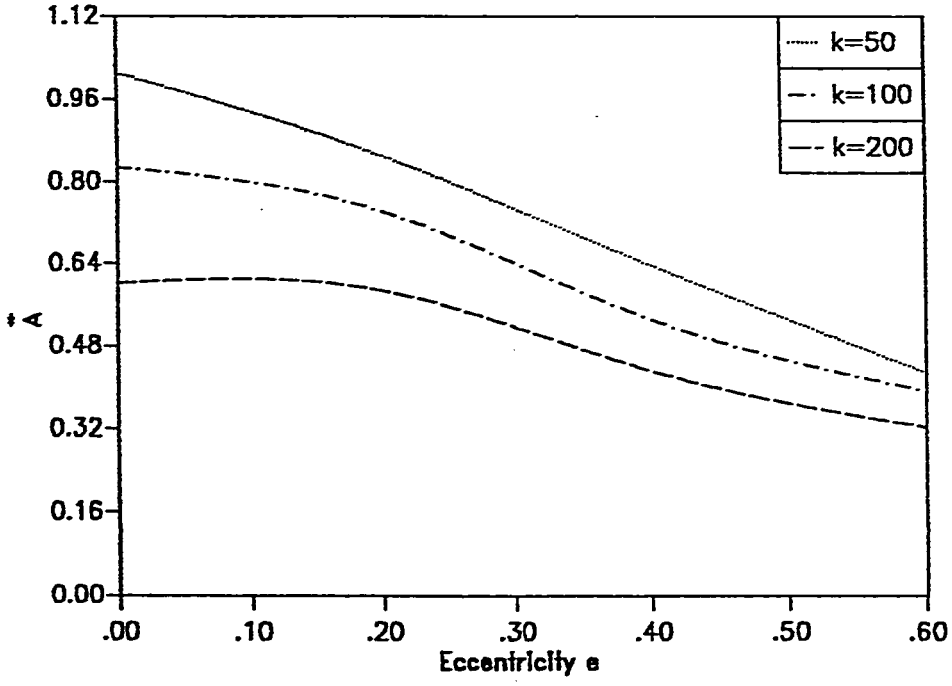

Figure 6.41: Ratio of the relative area A^* of a cylinder-plate junction resting on tensionless Winkler subgrade subjected to point load P and point moment M_0 for various subgrade stiffness and various levels of the applied moment M_0, ($P = 1$, $r_i = .2$, $r_0 = 1$).

Chapter 7

SUMMARY AND CONCLUSIONS

7.1 Summary

The proposed work investigated the problem of a cylinder-plate junction resting on tensionless elastic subgrade and subjected to a point load and a point moment that act at the top edge of the cylinder.

An energy minimization technique was utilized to analyze the plate-subgrade system. A displacement function for the plate was assumed in terms of generalized Bessel functions in the radial direction and Fourier series in the angular direction. The solution for a thin circular cylinder was obtained according to the equations derived by Flugge for this problem. The solution of the cylinder-plate junction was accomplished by achieving the continuity conditions at the cylinder-plate interface for the displacements and the edge forces.

A computer program was developed to solve the derived equations iteratively, but efficiently. The program has the capability to investigate the effect of a wide range of the system parameters. However, there are certain limitations on the largest values for eccentricity or aspect ratio to ensure convergence.

Numerical results have been presented to show the validity of the approach through comparisons with other existing solutions. This was followed by the investigation of several problems to study the nonlinear behavior of the problem and its dependency on the main parameters.

7.2 Conclusions

Based on the derivations and the obtained numerical results, the following conclusions can be made

1- For the axisymmetric plate problem, the present solution is in excellent agreement with the exact solution for the contact radius and the central displacement and more accurate than other existing approximate techniques.

2- For the axisymmetric plate problem, it has been observed that the size of the contact zone does not depend on the magnitude of the applied load, an observation also made by other investigators.

3- The convergence of the problem is rather fast, and guaranteed for a wide range of the system parameters, but can not be achieved when the eccentricity ($e = M_0/P$) exceeds 0.70. This is due to the significant reduction in the area of the contact zone between the plate and the subgrade. In addition, convergence can not be ensured when the ratio of the inner to outer radius exceeds 0.30.

4- The problem exhibited a nonlinear behavior for most of the values for the relative subgrade stiffness and eccentricity.

5- It has been observed that the different values of the eccentricity had a

significant effect on the overall junction behavior, and specifically on the contact zone and the displacements of the plate.

6- It has been observed that the stiffness of the subgrade has a bigger effect on the behavior of the problem for lower and moderate values of the eccentricity. For the axisymmetric junction problem, the maximum radial moment at the junction occurs at low subgrade stiffness ($k < 50$), with the radial moment decreasing significantly with increasing k. A similar behavior was observed for the non-axisymmetric problem with eccentricity $e < 0.4$. For higher eccentricities, the subgrade stiffness has a minor effect on the behavior of the problem with the radial moment remaining almost constant for any value of k.

7- In general, increasing the relative bending stiffness of the cylinder to that of the plate ($D^* = D_p/D_c$) increased the contact between the plate and the subgrade. The cylinder stiffness has a significant effect on the maximum displacement in the plate. For an axisymmetric junction problem, the radial moment at the junction becomes constant when D^* exceeds 1.25. In addition, for a non-axisymmetric junction problem, the behavior of the problem becomes constant when D^* exceeds 2.0.

7.3 Recommendations

It is believed that the presented work represents a starting point for other studies that may utilize the approach and expand its capabilities and applications. The following points represent the possible directions for expanding this work:

1- To investigate the effect of using different subgrade models like Pasternak model or elastic half-space.

2- To use the large-deformation theory for the analysis of the plate-subgrade system.

3- To incorporate the vibration effect in the solution of either the plate-subgrade problem or the plate-cylinder problem.

Finally, it should be pointed out that the finite element method represents an alternative approach for handling these problems and other ones that might include irregular geometries or material nonlinearities.

APPENDIX A

The Kelvin functions and Bessel functions and their first derivatives [21], in addition to the derived second and third derivatives that were used in the analysis of the plate problem can be obtained as follows

The Psi function is defined as

$$\Psi(n) = -\gamma + \sum_{k=1}^{n-1} k^{-1}, \qquad n \geq 2 \tag{A.a}$$

where

$$\gamma = 0.5772 \tag{A.b}$$

The Kelvin functions are defined as

$$ber_n x = \left(\frac{1}{2}x\right)^n \sum_{k=0}^{\infty} \frac{\cos\{(\frac{3}{4}n+\frac{1}{2}k)\pi\}}{k!\Gamma(n+k+1)}\left(\frac{1}{4}x^2\right)^k \tag{A.1}$$

$$bei_n x = \left(\frac{1}{2}x\right)^n \sum_{k=0}^{\infty} \frac{\sin\{(\frac{3}{4}n+\frac{1}{2}k)\pi\}}{k!\Gamma(n+k+1)}\left(\frac{1}{4}x^2\right)^k \tag{A.2}$$

$$\begin{aligned} \ker_n x = {} & \frac{1}{2}\left(\frac{1}{2}x\right)^{-n} \sum_{k=0}^{n-1} \cos\{(\frac{3}{4}n+\frac{1}{2}k)\pi\} \times \frac{(n-k-1)!}{k!}\left(\frac{1}{4}x^2\right)^k \\ & - \ln\left(\frac{1}{2}x\right) ber_n x + \frac{1}{4}\pi bei_n x \\ & + \frac{1}{2}\left(\frac{1}{2}x\right)^n \sum_{k=0}^{\infty} \cos\{(\frac{3}{4}n+\frac{1}{2}k)\pi\} \times \frac{\{\psi(k+1)+\psi(n+k+1)\}}{k!(n+k)!}\left(\frac{1}{4}x^2\right)^k \end{aligned} \tag{A.3}$$

$$kei_n x = -\frac{1}{2}\left(\frac{1}{2}x\right)^{-n}\sum_{k=0}^{n-1}\sin\{(\frac{3}{4}n+\frac{1}{2}k)\pi\}\times\frac{(n-k-1)!}{k!}\left(\frac{1}{4}x^2\right)^k -$$

$$\ln\left(\frac{1}{2}x\right)bei_n x - \frac{1}{4}\pi ber_n x$$

$$+\frac{1}{2}\left(\frac{1}{2}x\right)^n\sum_{k=0}^{\infty}\sin\{(\frac{3}{4}n+\frac{1}{2}k)\pi\}\times\frac{\{\psi(k+1)+\psi(n+k+1)\}}{k!(n+k)!}\left(\frac{1}{4}x^2\right)^k \quad \text{(A.4)}$$

The derivatives of Kelvin functions are

First derivatives

$$ber'_n x = \frac{n}{x}ber_n x + \frac{1}{\sqrt{2}}(ber_{n+1}x + bei_{n+1}x) \quad \text{(A.5)}$$

$$bei'_n x = \frac{n}{x}bei_n x + \frac{1}{\sqrt{2}}(bei_{n+1}x - ber_{n+1}x) \quad \text{(A.6)}$$

$$\ker'_n x = \frac{n}{x}\ker_n x + \frac{1}{\sqrt{2}}(\ker_{n+1}x + kei_{n+1}x) \quad \text{(A.7)}$$

$$kei'_n x = \frac{n}{x}kei_n x + \frac{1}{\sqrt{2}}(kei_{n+1}x - \ker_{n+1}x) \quad \text{(A.8)}$$

Second derivatives

$$ber''_n x = \left(\frac{-n}{x^2}+\frac{n^2}{x^2}\right)ber_n x - bei_n x - \frac{1}{x\sqrt{2}}(ber_{n+1}x + bei_{n+1}x) \quad \text{(A.9)}$$

$$bei''_n x = \left(\frac{-n}{x^2}+\frac{n^2}{x^2}\right)bei_n x + ber_n x - \frac{1}{x\sqrt{2}}(bei_{n+1}x - ber_{n+1}x) \quad \text{(A.10)}$$

$$\ker''_n x = \left(\frac{-n}{x^2}+\frac{n^2}{x^2}\right)\ker_n x - kei_n x - \frac{1}{x\sqrt{2}}(\ker_{n+1}x + kei_{n+1}x) \quad \text{(A.11)}$$

$$kei''_n x = \left(\frac{-n}{x^2}+\frac{n^2}{x^2}\right)kei_n x + \ker_n x - \frac{1}{x\sqrt{2}}(kei_{n+1}x - \ker_{n+1}x) \quad \text{(A.12)}$$

Third derivatives

$$ber''' _n x = \frac{ber_n x}{x^3}(n)(n\text{-}1)(n\text{-}2) + bei_n \frac{x}{x}(1\text{-}n) + (ber_{n+1}x + bei_{n+1}x)\frac{(n^2+2)}{\sqrt{2}\,x^2}$$

$$+ \frac{1}{\sqrt{2}}(ber_{n+1}x - bei_{n+1}x) \qquad \text{(A.13)}$$

$$bei''' _n x = \frac{bei_n x}{x^3}(n)(n\text{-}1)(n\text{-}2) - ber_n \frac{x}{x}(1\text{-}n) + (bei_{n+1}x - ber_{n+1}x)\frac{(n^2+2)}{\sqrt{2}\,x^2}$$

$$+ \frac{1}{\sqrt{2}}(bei_{n+1}x + ber_{n+1}x) \qquad \text{(A.14)}$$

$$\ker''' _n x = \frac{\ker_n x}{x^3}(n)(n\text{-}1)(n\text{-}2) + kei_n \frac{x}{x}(1\text{-}n) + (ker_{n+1}x + kei_{n+1}x)\frac{(n^2+2)}{\sqrt{2}\,x^2}$$

$$+ \frac{1}{\sqrt{2}}(\ker_{n+1}x - kei_{n+1}x) \qquad \text{(A.15)}$$

$$kei''' _n x = \frac{kei_n x}{x^3}(n)(n\text{-}1)(n\text{-}2) - \ker_n \frac{x}{x}(1\text{-}n) + (kei_{n+1}x - \ker_{n+1}x)\frac{(n^2+2)}{\sqrt{2}\,x^2}$$

$$+ \frac{1}{\sqrt{2}}(kei_{n+1}x + \ker_{n+1}x) \qquad \text{(A.16)}$$

The Bessel functions are defined as follows

$$J_n x = (\frac{1}{2}x)^n \sum_{k=0}^{\infty} \frac{(-\frac{1}{4}x^2)^k}{k!\Gamma(n+k+1)} \qquad \text{(A.17)}$$

$$I_n x = (\frac{1}{2}x)^n \sum_{k=0}^{\infty} \frac{(\frac{1}{4}x^2)^k}{k!\Gamma(n+k+1)} \qquad \text{(A.18)}$$

$$Y_n x = -\frac{(\frac{1}{2}x)^{-n}}{\pi} \sum_{k=0}^{n-1} \frac{(n\text{-}k\text{-}1)!}{k!}(\frac{1}{4}x^2)^k + \frac{2}{\pi}\ln(\frac{1}{2}x).J_n x$$

$$-\frac{(\frac{1}{2}x)^n}{\pi}\sum_{k=0}^{\infty}\frac{\{\psi(k+1)+\psi(n+k+1)\}}{k!(n+k)!}(-\frac{1}{4}x^2)^k \qquad \text{(A.19)}$$

$$K_n x=\frac{1}{2}(\frac{1}{2}x)^{-n}\sum_{k=0}^{n-1}\frac{(n-k-1)!}{k!}(-\frac{1}{4}x^2)^k+(-)^{n+1}\ln(\frac{1}{2}x)I_n x+(-)^n\frac{1}{2}$$

$$(\frac{1}{2}x)^n\sum_{k=0}^{\infty}\frac{\{\psi(k+1)+\psi(n+k+1)\}}{k!(n+k)!}(\frac{1}{4}x^2)^k \qquad \text{(A.20)}$$

The derivatives of Bessel functions are

First derivatives

$$J_n'x=\frac{nJ_n x}{x}-J_{n+1}x \qquad \text{(A.21)}$$

$$I_n'x=\frac{nI_n x}{x}+I_{n+1}x \qquad \text{(A.22)}$$

$$Y_n'x=\frac{nY_n x}{x}-Y_{n+1}x \qquad \text{(A.23)}$$

$$K_n'x=\frac{nK_n x}{x}-K_{n+1}x \qquad \text{(A.24)}$$

Second derivatives

$$J''_n x=J_n x\,\frac{(n^2}{x^2}-\frac{n}{x^2}-1)+\frac{J_{n+1}}{x} \qquad \text{(A.25)}$$

$$I''_n x=I_n x\,(\frac{n^2}{x^2}-\frac{n}{x^2}+1)-\frac{I_{n+1}}{x} \qquad \text{(A.26)}$$

$$Y''_n x=Y_n x\,\frac{(n^2}{x^2}-\frac{n}{x^2}-1)+\frac{Y_{n+1}}{x} \qquad \text{(A.27)}$$

$$K''_n x=K_n x\,(\frac{n^2}{x^2}-\frac{n}{x^2}+1)+\frac{K_{n+1}}{x} \qquad \text{(A.28)}$$

Third derivatives

$$J'''_n x = J_n x\left(\frac{1}{x^3}\{+n^3-3n^2+2n+n^3\} + \frac{1}{x}(-n+1)\right)$$

$$+ J_{n+1}x\left\{\frac{1}{x^2}(-n^2-2)+1\right\} \qquad \text{(A.29)}$$

$$I'''_n x = I_n x\left(\frac{1}{x^3}\{+n^3-3n^2+2n\} + \frac{1}{x}(n-1)\right)$$

$$+ I_{n+1}x\left\{\frac{1}{x^2}(n^2+2)+1\right\} \qquad \text{(A.30)}$$

$$Y'''_n x = Y_n x\left(\frac{1}{x^3}\{+n^3-3n^2+2n+n^3\} + \frac{1}{x}(-n+1)\right)$$

$$+ Y_{n+1}x\left\{\frac{1}{x^2}(-n^2-2)+1\right\} \qquad \text{(A.31)}$$

$$K'''_n x = K_n x\left(\frac{1}{x^3}\{+n^3-3n^2+2n\} + \frac{1}{x}(n-1)\right)$$

$$+ K_{n+1}x\left\{\frac{1}{x^2}(-n^2-2)-1\right\} \qquad \text{(A.32)}$$

APPENDIX B

The elements of the boundary conditions matrix [B] which was defined in chapter 3, equation (3.14), are obtained as follows

a) Using Kelvin functions

$$B(1,1) = \lambda_n^2\, ber_n''(\lambda_n r_i) + \nu \frac{\lambda_n}{r_i}\, ber_n'(\lambda_n r_i) - \frac{\nu n^2}{r_i^2}\, ber_n(\lambda_n r_i) \qquad \text{(B.1)}$$

$$B(1,2) = \lambda_n^2\, bei_n''(\lambda_n r_i) + \nu \frac{\lambda_n}{r_i}\, bei_n'(\lambda_n r_i) - \frac{\nu n^2}{r_i^2}\, bei_n(\lambda_n r_i) \qquad \text{(B.2)}$$

$$B(1,3) = \lambda_n^2\, ker_n''(\lambda_n r_i) + \nu \frac{\lambda_n}{r_i}\, ker_n'(\lambda_n r_i) - \frac{\nu n^2}{r_i^2}\, ker_n(\lambda_n r_i) \qquad \text{(B.3)}$$

$$B(1,4) = \lambda_n^2\, kei_n''(\lambda_n r_i) + \nu \frac{\lambda_n}{r_i}\, kei_n'(\lambda_n r_i) - \frac{\nu n^2}{r_i^2}\, kei_n(\lambda_n r_i) \qquad \text{(B.4)}$$

$$B(2,1) = \lambda^3{}_n\, ber_n'''(\lambda_n r_i) + \frac{\lambda_n^2}{r_i}\, ber''{}_n(\lambda_n r_i) - \frac{\lambda_n}{r_i^2}\, ber'(\lambda_n r_i) - \frac{n^2\lambda_n}{r_i^2}\, ber'(\lambda_n r_i)$$
$$+ \frac{2n^2}{r^3}\, ber_n(\lambda_n r_i) - \frac{(1-\nu)n^2}{r_i^2}\{\lambda_n ber'{}_n(\lambda_n r_i) - \frac{ber_n(\lambda_n r_i)}{r_i}\} \qquad \text{(B.5)}$$

$$B(2,2) = \lambda^3{}_n\, bei_n'''(\lambda_n r_i) + \frac{\lambda_n^2}{r_i}\, bei''{}_n(\lambda_n r_i) - \frac{\lambda_n}{r_i^2}\, bei'(\lambda_n r_i) - \frac{n^2\lambda_n}{r_i^2}\, bei'(\lambda_n r_i)$$
$$+ \frac{2n^2}{r^3}\, bei_n(\lambda_n r_i) - \frac{(1-\nu)n^2}{r_i^2}\{\lambda_n bei'{}_n(\lambda_n r_i) - \frac{bei_n(\lambda_n r_i)}{r_i}\} \qquad \text{(B.6)}$$

$$B(2,3) = \lambda^3_n \ker''_n(\lambda_n r_i) + \frac{\lambda_n^2}{r_i} \ker''_n(\lambda_n r_i) - \frac{\lambda_n}{r_i^2} \ker'(\lambda_n r_i) - \frac{n^2\lambda_n}{r_i^2} \ker'(\lambda_n r_i)$$

$$+ \frac{2n^2}{r^3} \ker_n(\lambda_n r_i) - \frac{(1-\nu)n^2}{r_i^2}\{\lambda_n \ker'_n(\lambda_n r_i) - \frac{\ker_n(\lambda_n r_i)}{r_i}\} \quad \text{(B.7)}$$

$$B(2,4) = \lambda^3_n kei''_n(\lambda_n r_i) + \frac{\lambda_n^2}{r_i} kei''_n(\lambda_n r_i) - \frac{\lambda_n}{r_i^2} kei'(\lambda_n r_i) - \frac{n^2\lambda_n}{r_i^2} kei'(\lambda_n r_i)$$

$$+ \frac{2n^2}{r^3} kei_n(\lambda_n r_i) - \frac{(1-\nu)n^2}{r_i^2}\{\lambda_n kei'_n(\lambda_n r_i) - \frac{kei_n(\lambda_n r_i)}{r_i}\} \quad \text{(B.8)}$$

$$B(3,1) = \lambda_n^2 ber''_n(\lambda_n r_0) + \nu \frac{\lambda_n}{r_0} ber_n(\lambda_n r_0) - \frac{\nu n^2}{r_0^2} ber_n(\lambda_n r_0) \quad \text{(B.9)}$$

$$B(3,2) = \lambda_n^2 bei''_n(\lambda_n r_0) + \nu \frac{\lambda_n}{r_0} bei_n(\lambda_n r_0) - \frac{\nu n^2}{r_0^2} bei_n(\lambda_n r_0) \quad \text{(B.10)}$$

$$B(3,3) = \lambda_n^2 \ker''_n(\lambda_n r_0) + \nu \frac{\lambda_n}{r_0} \ker_n(\lambda_n r_0) - \frac{\nu n^2}{r_0^2} \ker_n(\lambda_n r_0) \quad \text{(B.11)}$$

$$B(3,4) = \lambda_n^2 kei''_n(\lambda_n r_0) + \nu \frac{\lambda_n}{r_0} kei_n(\lambda_n r_0) - \frac{\nu n^2}{r_0^2} kei_n(\lambda_n r_0) \quad \text{(B.12)}$$

$$B(4,1) = \lambda^3_n ber''_n(\lambda_n r_0) + \frac{\lambda_n^2}{r_0} ber''_n(\lambda_n r_0) - \frac{\lambda_n}{r_0^2} ber'(\lambda_n r_0) - \frac{n^2\lambda_n}{r_0^2} ber'(\lambda_n r_0)$$

$$+ \frac{2n^2}{r^3} ber_n(\lambda_n r_0) - \frac{(1-\nu)n^2}{r_0^2}\{\lambda_n ber'_n(\lambda_n r_0)$$

$$- \frac{ber_n(\lambda_n r_0)}{r_0}\} \quad \text{(B.13)}$$

$$B(4,2) = \lambda^3_n bei''_n(\lambda_n r_0) + \frac{\lambda_n^2}{r_0} bei''_n(\lambda_n r_0) - \frac{\lambda_n}{r_0^2} bei'(\lambda_n r_0) - \frac{n^2\lambda_n}{r_0^2} bei'(\lambda_n r_0)$$

$$+ \frac{2n^2}{r^3} bei_n(\lambda_n r_0) - \frac{(1-\nu)n^2}{r_0^2}\{\lambda_n bei'_n(\lambda_n r_0)$$

$$- \frac{bei_n(\lambda_n r_0)}{r_0}\} \qquad \text{(B.14)}$$

$$B(4,3) = \lambda^3{}_n \, \mathrm{ker}'''_n(\lambda_n r_0) + \frac{\lambda_n^2}{r_0} \mathrm{ker}''_n(\lambda_n r_0) - \frac{\lambda_n}{r_0^2} \mathrm{ker}'(\lambda_n r_0) - \frac{n^2\lambda_n}{r_0^2} \mathrm{ker}'(\lambda_n r_0)$$

$$+ \frac{2n^2}{r^3} \mathrm{ker}_n(\lambda_n r_0) - \frac{(1-\nu)n^2}{r_0^2}\{\lambda_n \mathrm{ker}'_n(\lambda_n r_0)$$

$$- \frac{\mathrm{ker}_n(\lambda_n r_0)}{r_0}\} \qquad \text{(B.15)}$$

$$B(4,4) = \lambda^3{}_n \, kei'''_n(\lambda_n r_0) + \frac{\lambda_n^2}{r_0} kei''_n(\lambda_n r_0) - \frac{\lambda_n}{r_0^2} kei'(\lambda_n r_0) - \frac{n^2\lambda_n}{r_0^2} kei'(\lambda_n r_0)$$

$$+ \frac{2n^2}{r^3} kei_n(\lambda_n r_0) - \frac{(1-\nu)n^2}{r_0^2}\{\lambda_n kei'_n(\lambda_n r_0)$$

$$- \frac{kei_n(\lambda_n r_0)}{r_0}\} \qquad \text{(B.16)}$$

b) Using Bessel functions

$$B(1,1) = \lambda_n^2 J''_n(\lambda_n r_i) + \nu \frac{\lambda_n}{r_i} J_n(\lambda_n r_i) - \frac{\nu n^2}{r_i^2} J_n(\lambda_n r_i) \qquad \text{(B.17)}$$

$$B(1,2) = \lambda_n^2 I''_n(\lambda_n r_i) + \nu \frac{\lambda_n}{r_i} I_n(\lambda_n r_i) - \frac{\nu n^2}{r_i^2} I_n(\lambda_n r_i) \qquad \text{(B.18)}$$

$$B(1,3) = \lambda_n^2 Y''_n(\lambda_n r_i) + \nu \frac{\lambda_n}{r_i} Y_n(\lambda_n r_i) - \frac{\nu n^2}{r_i^2} Y_n(\lambda_n r_i) \qquad \text{(B.19)}$$

$$B(1,4) = \lambda_n^2 K_n''(\lambda_n r_i) + \nu \frac{\lambda_n}{r_i} K_n(\lambda_n r_i) - \frac{\nu n^2}{r_i^2} K_n(\lambda_n r_i) \qquad \text{(B.20)}$$

$$B(2,1) = \lambda^3{}_n J_n'''(\lambda_n r_i) + \frac{\lambda_n^2}{r_i} J''{}_n(\lambda_n r_i) - \frac{\lambda_n}{r_i^2} J'(\lambda_n r_i) - \frac{n^2\lambda_n}{r_i^2} J'(\lambda_n r_i)$$

$$+ \frac{2n^2}{r^3} J_n(\lambda_n r_i) - \frac{(1-\nu)n^2}{r_i^2}\{\lambda_n J'{}_n(\lambda_n r_i) - \frac{J_n(\lambda_n r_i)}{r_i}\} \qquad \text{(B.21)}$$

$$B(2,2) = \lambda^3{}_n I_n'''(\lambda_n r_i) + \frac{\lambda_n^2}{r_i} I''{}_n(\lambda_n r_i) - \frac{\lambda_n}{r_i^2} I'(\lambda_n r_i) - \frac{n^2\lambda_n}{r_i^2} I'(\lambda_n r_i)$$

$$+ \frac{2n^2}{r^3} I_n(\lambda_n r_i) - \frac{(1-\nu)n^2}{r_i^2}\{\lambda_n I'{}_n(\lambda_n r_i) - \frac{I_n(\lambda_n r_i)}{r_i}\} \qquad \text{(B.22)}$$

$$B(2,3) = \lambda^3{}_n Y_n'''(\lambda_n r_i) + \frac{\lambda_n^2}{r_i} Y''{}_n(\lambda_n r_i) - \frac{\lambda_n}{r_i^2} Y'(\lambda_n r_i) - \frac{n^2\lambda_n}{r_i^2} Y'(\lambda_n r_i)$$

$$+ \frac{2n^2}{r^3} Y_n(\lambda_n r_i) - \frac{(1-\nu)n^2}{r_i^2}\{\lambda_n Y'{}_n(\lambda_n r_i) - \frac{Y_n(\lambda_n r_i)}{r_i}\} \qquad \text{(B.23)}$$

$$B(2,4) = \lambda^3{}_n K_n'''(\lambda_n r_i) + \frac{\lambda_n^2}{r_i} K''{}_n(\lambda_n r_i) - \frac{\lambda_n}{r_i^2} K'(\lambda_n r_i) - \frac{n^2\lambda_n}{r_i^2} K'(\lambda_n r_i)$$

$$+ \frac{2n^2}{r^3} K_n(\lambda_n r_i) - \frac{(1-\nu)n^2}{r_i^2}\{\lambda_n K'{}_n(\lambda_n r_i) - \frac{K_n(\lambda_n r_i)}{r_i}\} \qquad \text{(B.24)}$$

$$B(3,1) = \lambda_n^2 J_n''(\lambda_n r_0) + \nu \frac{\lambda_n}{r_0} J_n(\lambda_n r_0) - \frac{\nu n^2}{r_0^2} J_n(\lambda_n r_0) \qquad \text{(B.25)}$$

$$B(3,2) = \lambda_n^2 I_n''(\lambda_n r_0) + \nu \frac{\lambda_n}{r_0} I_n(\lambda_n r_0) - \frac{\nu n^2}{r_0^2} I_n(\lambda_n r_0) \qquad \text{(B.26)}$$

$$B(3,3) = \lambda_n^2 Y_n''(\lambda_n r_0) + \nu \frac{\lambda_n}{r_0} Y_n(\lambda_n r_0) - \frac{\nu n^2}{r_0^2} Y_n(\lambda_n r_0) \qquad \text{(B.27)}$$

$$B(3,4) = \lambda_n^2 K_n''(\lambda_n r_0) + \nu \frac{\lambda_n}{r_0} K_n(\lambda_n r_0) - \frac{\nu n^2}{r_0^2} K_n(\lambda_n r_0) \qquad \text{(B.28)}$$

$$B(4,1) = \lambda^3{}_n J_n'''(\lambda_n r_0) + \frac{\lambda_n^2}{r_0} J''{}_n(\lambda_n r_0) - \frac{\lambda_n}{r_0^2} J'(\lambda_n r_0) - \frac{n^2\lambda_n}{r_0^2} J'(\lambda_n r_0)$$

$$+ \frac{2n^2}{r^3} J_n(\lambda_n r_0) - \frac{(1-\nu)n^2}{r_0^2}\{\lambda_n J'_n(\lambda_n r_0) - \frac{J_n(\lambda_n r_0)}{r_0}\} \qquad \text{(B.29)}$$

$$B(4,2) = \lambda^3{}_n I_n'''(\lambda_n r_0) + \frac{\lambda_n^2}{r_0} I''{}_n(\lambda_n r_0) - \frac{\lambda_n}{r_0^2} I'(\lambda_n r_0) - \frac{n^2\lambda_n}{r_0^2} I'(\lambda_n r_0)$$

$$+ \frac{2n^2}{r^3} I_n(\lambda_n r_0) - \frac{(1-\nu)n^2}{r_0^2}\{\lambda_n I'_n(\lambda_n r_0) - \frac{I_n(\lambda_n r_0)}{r_0}\} \qquad \text{(B.30)}$$

$$B(4,3) = \lambda^3{}_n Y_n'''(\lambda_n r_0) + \frac{\lambda_n^2}{r_0} Y''{}_n(\lambda_n r_0) - \frac{\lambda_n}{r_0^2} Y'(\lambda_n r_0) - \frac{n^2\lambda_n}{r_0^2} Y'(\lambda_n r_0)$$

$$+ \frac{2n^2}{r^3} Y_n(\lambda_n r_0) - \frac{(1-\nu)n^2}{r_0^2}\{\lambda_n Y'_n(\lambda_n r_0) - \frac{Y_n(\lambda_n r_0)}{r_0}\} \qquad \text{(B.31)}$$

$$B(4,4) = \lambda^3{}_n K_n'''(\lambda_n r_0) + \frac{\lambda_n^2}{r_0} K''{}_n(\lambda_n r_0) - \frac{\lambda_n}{r_0^2} K'(\lambda_n r_0) - \frac{n^2\lambda_n}{r_0^2} K'(\lambda_n r_0)$$

$$+ \frac{2n^2}{r^3} K_n(\lambda_n r_0) - \frac{(1-\nu)n^2}{r_0^2}\{\lambda_n K'_n(\lambda_n r_0) - \frac{K_n(\lambda_n r_0)}{r_0}\} \qquad \text{(B.32)}$$

REFERENCES

1- Timoshenko, S.P., and Woinowsky-Kreiger, S. (1959). "Theory of plates and shells." McGraw-Hill Book Co., New York, N.Y.

2- Kastikadelis, J.T. and Kallivokas, L.E. (1986). " Clamped plates on Pasternak-type elastic foundation by the boundary element method." J. of Applied Mechanics, Vol. 53, 909-917.

3- Bezine, G. (1988). "A new boundary element method for bending of plates on elastic foundation." Int. J. Solids & Structures, Vol. 24, 557-565.

4- Kastikadelis, J.T. and Armenakas, A.E. (1984). " Analysis of clamped plates on elastic foundation by the boundary integral equation method." J. of Applied Mechanics, Vol. 51, 574-580.

5- Weitsman, Y. (1969). "On the unbounded contact between plates and an elastic half space." J. of Applied Mechanics, Vol. 36, 198-202.

6- Keer, L.M., Dundurs,J., and Tsai, K.C. (1972). "Problems involving receding contact between a layer and a half space." J. of Applied Mechanics, VOL.39, 1115-1120.

7- Weitsman, Y. (1970). "On foundations that react in compression only." J. of Applied Mechanics, Vol.37, 1019-1030.

8- Gladwell, G. M. L., and Iyer, K. R. P. (1974)."Unbonded contact between a circular plate and an elastic half-space." Journal of

Elasticity, Vol. 4, No. 2, 115-130.

9- Villaggio, P. (1983). "A free boundary value problem in plate theory." J. of Applied Mechanics, Vol.50(2), 297-302.

10- Ascione, L., Grimaldi, A. (1984). "Unilateral contact between a plate and an elastic foundation." Journal de Meccanica. Vol 19, 223-233.

11- Selvadurai, A. P. S. (1984). "A contact problem for a Reissner plate and an isotropic elastic half-space." Journal de Mecanique Theoritque et Appliquee. Vol 3, No 2, 181-196.

12- Li, H., and Dempsey, J.P. (1988). "Unbonded contact between a square plate on an elastic half-space or winkler foundation." J. of Applied Mechanics, Vol.55, 430-436.

13- Celep, Z. (1988). "Circular plates on tensionless Winkler foundation " J. Engineering Mechanics Division, ASCE, 104(10), 1723-1739.

14- Celep, Z. (1988). "Rectangular plates resting on tensionless elastic foundation." J. Engineering Mechanics, ASCE, Vol. 114, No. 12, 2083-2092.

15- Celep, Z., Turhan, D. and Al-Zaid, R.Z. (1988). " Circular elastic plates on elastic unilateral edge supports." J. of Applied Mechanics, Vol.55, 624-628.

16- Celep, Z. (1990). "Axisymmetric vibration of circular plates on elastic foundation." J. of Applied Mechanics, Vol.57, 677-681.

17- Hulbert, L., E., Hopper, A., T., and Rybicki, E., F.(1971). "The stress analysis of plates with single and clustered nozzles by the boundary point least squares method." Journal of Engineering for Industry, No. 71,929-934.

18- Van Campen, D.H. (1971). "On the stress distribution in an arbitrarily loaded nozzle-flat plate connection." Numerical Engineering and Design, vol. 11, 495-516.

19- Redecop, D. (1977). "Three dimensional analysis of an elastic cylinder-plate intersection by the boundary-point-least-squares technique." Journal of Pressure Vessel and Technology, 76-PVP-34.

20- Flugge,W. (1973). "Stresses in shells." Springer-Verlag

21- Abramowitz, M., and Stegun, I. (1970). " Handbook of mathematical functions." Dover Publication, New York, N.Y.

22- Watson, G., N. (1966). "Theory of Bessel functions." Cambridge Press, New York, N.Y.

23- Ugural, A., C. (1981). "Stresses in plates and shells." McGraw- Hill Book Co., New York.

24- Griffiths, D.,V., and Smith, I.,M.(1991). "Numerical methods for engineers." Black Well Scientific Publications, Oxford.

25- Little, R.W. (1973). "Elasticity." Black Well Scientific Publications, Oxford.